University of Alberta

Effects of strain rate of prior deformation on corrosive wear of materials

by

Songbo Yin ©

A thesis submitted to the Faculty of Graduate Studies and Research in partial
fulfillment of the requirements for the degree of Doctor of Philosophy

in

Materials Engineering

Department of Chemical and Materials Engineering

Edmonton, Alberta

Spring 2008

Library and
Archives Canada

Published Heritage
Branch

395 Wellington Street
Ottawa ON K1A 0N4
Canada

Bibliothèque et
Archives Canada

Direction du
Patrimoine de l'édition

395, rue Wellington
Ottawa ON K1A 0N4
Canada

Your file Votre référence
ISBN: 978-0-494-45633-0
Our file Notre référence
ISBN: 978-0-494-45633-0

NOTICE:
The author has granted a non-exclusive license allowing Library and Archives Canada to reproduce, publish, archive, preserve, conserve, communicate to the public by telecommunication or on the Internet, loan, distribute and sell theses worldwide, for commercial or non-commercial purposes, in microform, paper, electronic and/or any other formats.

The author retains copyright ownership and moral rights in this thesis. Neither the thesis nor substantial extracts from it may be printed or otherwise reproduced without the author's permission.

AVIS:
L'auteur a accordé une licence non exclusive permettant à la Bibliothèque et Archives Canada de reproduire, publier, archiver, sauvegarder, conserver, transmettre au public par télécommunication ou par l'Internet, prêter, distribuer et vendre des thèses partout dans le monde, à des fins commerciales ou autres, sur support microforme, papier, électronique et/ou autres formats.

L'auteur conserve la propriété du droit d'auteur et des droits moraux qui protège cette thèse. Ni la thèse ni des extraits substantiels de celle-ci ne doivent être imprimés ou autrement reproduits sans son autorisation.

In compliance with the Canadian Privacy Act some supporting forms may have been removed from this thesis.

While these forms may be included in the document page count, their removal does not represent any loss of content from the thesis.

Conformément à la loi canadienne sur la protection de la vie privée, quelques formulaires secondaires ont été enlevés de cette thèse.

Bien que ces formulaires aient inclus dans la pagination, il n'y aura aucun contenu manquant.

Canada

Abstract

In many industries, such as mining, mineral processing, chemical processing, and energy production, facilities and machinery are often subject to combined attacks of corrosion, impact and wear. The combined action of these processes, i.e., corrosive impact wear, often results in mutual enhancement, leading to a significant increase in total material loss.

In this study, research was conducted to investigate effects of strain rate of prior deformation on corrosive wear behavior of materials with focus on carbon steel. In order to understand the role of strain rate in corrosive impact wear processes, studies of 1) effects of prior deformation on the corrosion and corrosive wear of copper respectively with and without passivation involved; 2) effects of the loading speed on corrosion and corrosive wear of impact-fractured and slow bending-fractured surface layers of AISI 1045 steel; 3) effects of strain rate of prior deformation on corrosion and corrosive wear of AISI 1045 steel were conducted more systematically using electrochemical test and corrosive sliding wear tests, respectively. In order to understand the mechanism responsible for the strain rate - corrosive wear behavior relationship, SEM fractography, X-ray line profile analysis and micro-hardness testing were employed to investigate changes in microstructure and corresponding mechanical properties with respect to the strain rate. During the studies, a modified experimental tribo-corrosion technique was developed to quantitatively investigate the corrosion-wear synergy for the materials.

Acknowledgements

I wish to express my deepest gratitude to my supervisor, Dr. Dongyang Li, for his valuable guidance encouragement and patience throughout the course of this work.

I also would like to acknowledge the financial support provided by Alberta Energy Research Institute (AERI / COURSE PROGRAM) and the Natural Science and Engineering research council of Canada (NSERC).

Table of Contents

Chapter 1 Introduction and Literature Review

Chapter 2 Effects of prior cold work on corrosion and corrosive wear of copper in HNO_3 and NaCl solutions

Chapter 3 Corrosion and corrosive wear of annealed, impact-fractured and slow bending-fractured surface layers of AISI 1045 steel in a 3.5% NaCl Solution

Chapter 4 Effects of strain rate of prior deformation on corrosion and corrosive wear of AISI 1045 steel in a 3.5% NaCl solution

Chapter 5 Development of a modified technique for investigating wear-corrosion synergy

Chapter 6 Investigation of Effects of the strain rate of prior deformation on the wear-corrosion synergy of carbon steel

Chapter 7 Summary and Future Work

List of Tables

List of Figures

Chapter 1

Introduction and Literature Review

1.1 Introduction

Wear and corrosion are two major materials failure and degradation processes which involve a number of mechanical and electrochemical mechanisms. Many industrial processes involve combined attack of wear and corrosion. Corrosion accompanies wear to certain extent in all environments, except in vacuum or an inert atmosphere. The combined action of these two processes, i.e., corrosive wear, often results in mutual enhancement, leading to a significant increase in total material loss [1-3]. These phenomena impact all sectors in terms of material loss and associated equipment downtime for repair, replacement of worn and corroded components, costing the industries hundreds of billions of dollars annually.

In many industries, such as mining, mineral processing, chemical processing, and energy production, facilities and machinery are often subject to combined attacks of corrosion and wear. Typical examples are discussed as follows.

- Slurry Handling

A slurry can be described as a mixture of solid particles in a liquid which can be readily pumped. The movement of materials in the slurry such as oil sands is an efficient means of transportation that is used in many industries. However, the movement of a slurry could cause significant corrosive wear. Pumps, elbows, tee junctions, valves, flotation cells, and hydrocyclones used for slurry handling systems are generally subject to corrosive wear. The periodic replacement of worn parts can result in costly process downtime. Figure 1.1 illustrates the complex synergistic reaction of many factors in a slurry handling system [4].

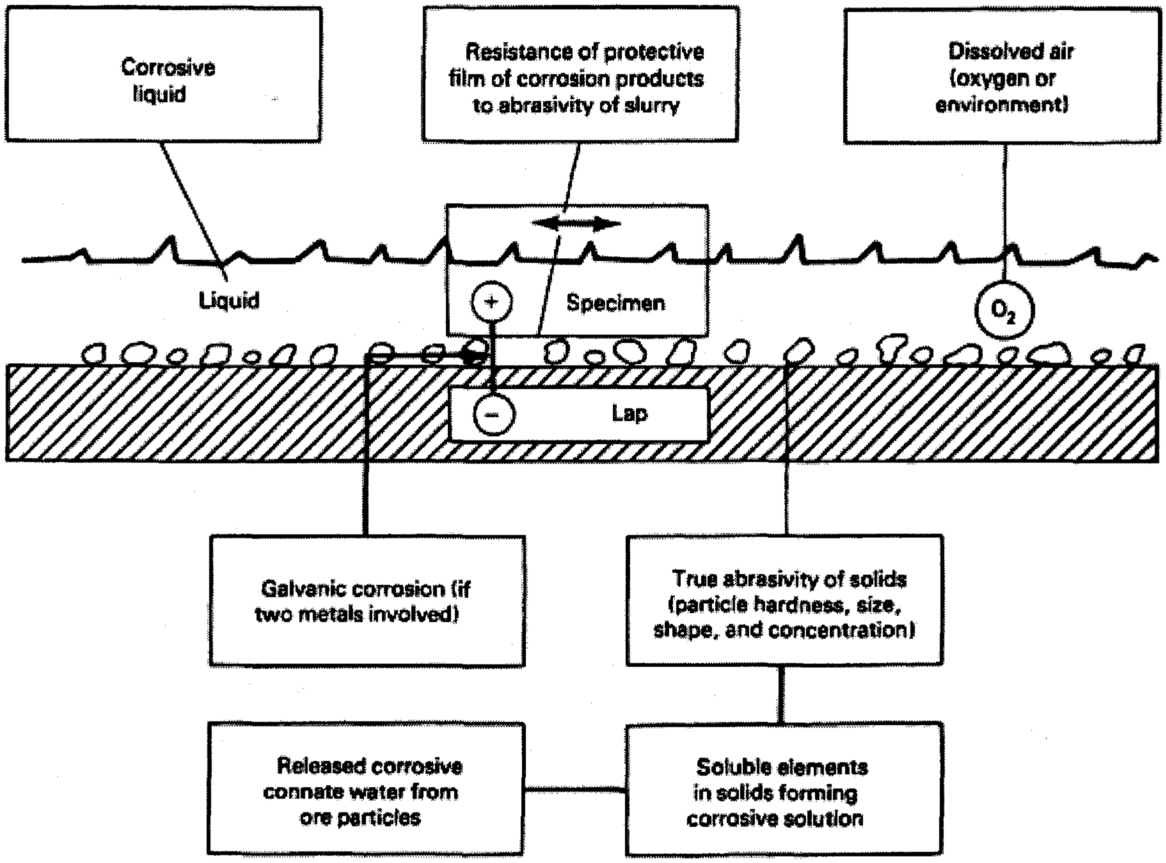

Fig. 1-1 Synergistic effects of seven factors in slurry handling

- Crushing and Grinding

Corrosive wear is prevalent in the grinding of mineral ores in mining and mineral processing industries. The annual cost of grinding media is very high in the mineral processing industry [5]. Corrosion and wear damage arising from comminution is equivalent to 12% of more than 30 billion kWh of energy consumed annually by U.S. industry for crushing and grinding purposes [6].

Collisions of mineral particles cause erosive damage to surfaces and removal of corrosion-resistant films, resulting in accelerated corrosion. Electrochemical interactions between minerals and grinding media can occur, causing galvanic coupling that leads to increased corrosive wear. Wear debris and corrosion products that are formed during comminution affect product quality and can adversely affect subsequent beneficiation by altering the chemical and electrochemical properties of the mineral systems. Corrosion and wear in grinding are also important in other industries, such as the pulp and paper industry, where physical processing steps such as the grinding of wood chips are increasingly being replaced by chemical processes in order to reduce water-treatment requirements and fulfill regulatory standards.

Power-generation

Power-generation plants utilize processes that occur without any particles and involve only the transport of solutions or steam. In the processes, liquid forces on the solid surfaces, resulting from turbulence or droplet impacts, mechanically remove surface reaction products, and thus expose more base material to corrosive action. An example of this type of process is the erosion-corrosion of steam turbines. Other systems may involve the failure of the protective oxide layer, because of a continual high-speed flow of liquid passing the turbine surface.

High-Temperature Processes

Many chemical processes take place at elevated temperatures and involve corrosive wear. Processes such as the coal gasification involve hot gases with entrained solid particles that impinge and erode the containment vessel surface. Many studies have been conducted to describe the wear-corrosion synergism that takes place during the oxide formation and subsequent removal by abrasive particles [7-8].

The above-mentioned cases demonstrate the wide involvement of corrosive wear and the need to better understand corrosive wear principles. Any strategy for minimizing the effect of wear-corrosion synergy requires fundamental understanding of the mechanisms involved, the way in which they interact, and their importance in specific environments. In recent years, the synergy between wear and corrosion has become an important research area and a number of investigations have been reported [1-54].

1.2 Review of experimental measurement of wear-corrosion synergy

The wear-corrosion synergy needs to be quantified, which may help guide a design engineer to select the best material for lowering overall material loss in a particular environment. A number of experimental methods have been proposed to quantify the wear-corrosion synergy in recent decades [9-19].

Madsen [9] developed a method for determining the synergy between wear and corrosion, which has been adopted as ASTM Standard. As suggested (ASTM G119 – 93), the total material loss, T, is related to the synergy:

$$T = W_0 + C_0 + S \quad (1.1)$$

Where W_0 is the wear rate in the absence of corrosion, C_0 is the corrosion rate in the absence of wear, and S is the synergistic component which results from the interaction of corrosion and wear processes.

The synergistic component, S, can be further resolved into two components: the change in corrosion rate due to wear (ΔCw) and the change in wear rate due to corrosion (ΔWc).

$$S = \Delta Cw + \Delta Wc \quad (1.2)$$

The experiments for determining wear-corrosion synergy, as suggested (ASTM G119 – 93), consist of four tests conducted using appropriate experimental apparatus that allow measurements of corrosion (C_0), wear (W_0) and concurrent wear and corrosion (S). T can be determined by performing wear test in a specific corrosive medium, while W_0 can be determined in the same way but under cathodic protection (the corrosion component eliminated). In order to determine corrosion related contribution, two sets of corrosion measurements are needed, in which the wear specimen is used as a working electrode in a typical three electrode system. In order to measure the corrosion rate, one needs to determine the polarization resistance, Rp, according to ASTM Practice G59 and to generate a potentiodynamic curve to obtain tafel constants using the ASTM Test Method G5.

The corrosion current density (icorr) is then calculated using the following equation: (ASTM standard G3-89):

$$i_{corr} = \frac{b_a b_c}{2.303(b_a + b_c)R_p} \qquad (1.3)$$

where i_{corr} = corrosion current density,
ba = anodic Tafel slope,
bc = cathodic Tafel slope,
R_p = linear polarization resistance

The icorr (the corrosion current density) value can be converted to a materials loss rate C or C_0 (mm^3 / mm^2 year) according to ASTM Practice G102.

One set of corrosion tests are run with the wear component to obtain corrosion rate in the presence of wear (C); The second set of corrosion tests are conducted so that the mechanical component of the degradation process is eliminated, thereby obtaining the pure corrosion(C_0). The additional corrosion due to wear (ΔCw) can be determined as:

$$\Delta Cw = C - C_0 \qquad (1.4)$$

According to equations (1) and (2), if the additional corrosion due to wear (ΔCw) is determined, the additional wear due to corrosion (ΔWc) can thus be calculated:

$$\Delta Wc = S - \Delta Cw = [T - (W_0 + C_0)] - \Delta Cw \qquad (1.5)$$

Quantitative measurements of corrosion (C_0), mechanical wear (W_0), and wear-corrosion synergy (S) have been made using various experiments. Basically these experimental techniques fall into two categories: slurry particle impingement system and experiments that simulate ore-grinding environments. Examples that show how these measurements have been made are described below [10-17].

Slurry Particle Impingement Systems

Various types of slurry wear tests designed to measure corrosive wear are reported in the literature. Madsen [10, 11] utilized a slurry pot that was capable of using either recycled or flow-through slurries. Pitt and Chang [12,13] conducted experiments with a jet-impingement apparatus, and Postlethwaite *et al.* [14] used electrodes in a closed-loop pipeline to measure both wear and corrosion rates.

Slurry Pot Experiments. A slurry wear test developed by the US Bureau of Mines [10, 11] was used to measure both wear and corrosion rates during slurry wear in order to establish the synergy between wear and corrosion of metal-alloy specimens. Figure 1.2 illustrates the slurry wear apparatus.

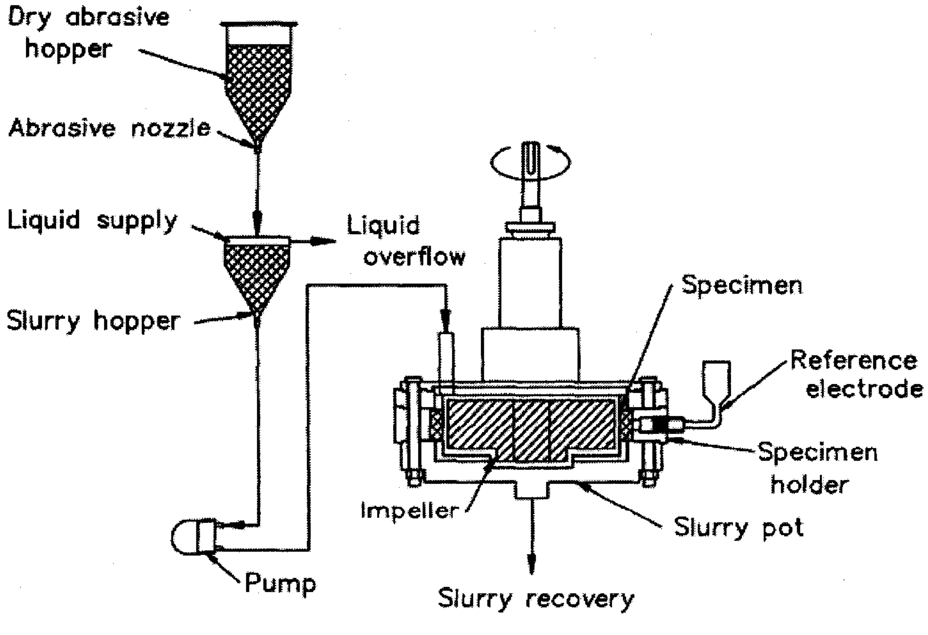

Fig.1-2 Flow-through slurry wear apparatus. Ref [10].

Three types of tests are needed to determine T, W_0, C_0, S, ΔCw, Δ Wc. The total material loss, *T*, is determined by performing the slurry test at open circuit. The wear rate of pure mechanical wear is determined under cathodic protection to eliminate corrosion.

These experiments showed that mechanical wear significantly affected the polarization curves of passive alloys, such as stainless steels. Figure 1.3 shows the polarization plots of 316 stainless steel that was exposed to a silica sand slurry at various slurry concentrations and impeller velocities. It is noted that the anodic current density increases with increases in the amount of solid particles and speed, indicating that the passive film is damaged and such damage was enhanced as the frequency of particle impacts was increased.

Jet-impingement Experiments. Pitt and Chang [12, 13] used an electrochemically instrumented jet slurry apparatus to study the wear-corrosion synergy. A hardened stainless steel nozzle with a 3.81 mm (0.15 in.) diam orifice delivered a slurry jet stream that impinged on the working electrode, which was 3 mm (0.12 in.) away from the orifice. The corrosion currents were determined according to Eq. 3 by using the polarization resistance technique. The total weight loss (T) was directly measured during corrosive wear. W_0 was determined from experiment in which the working electrode was cathodically protected at a potential of -1.5 V versus the saturated calomel electrode. This system used a recycled slurry that was replenished with fresh slurry periodically to minimize the effect of slurry particle rounding on wear loss. The synergistic effect accounted for 8.3% to 54.9% of the total material loss. The wear-corrosion synergy was enhanced when larger particles and higher jet velocities were used.

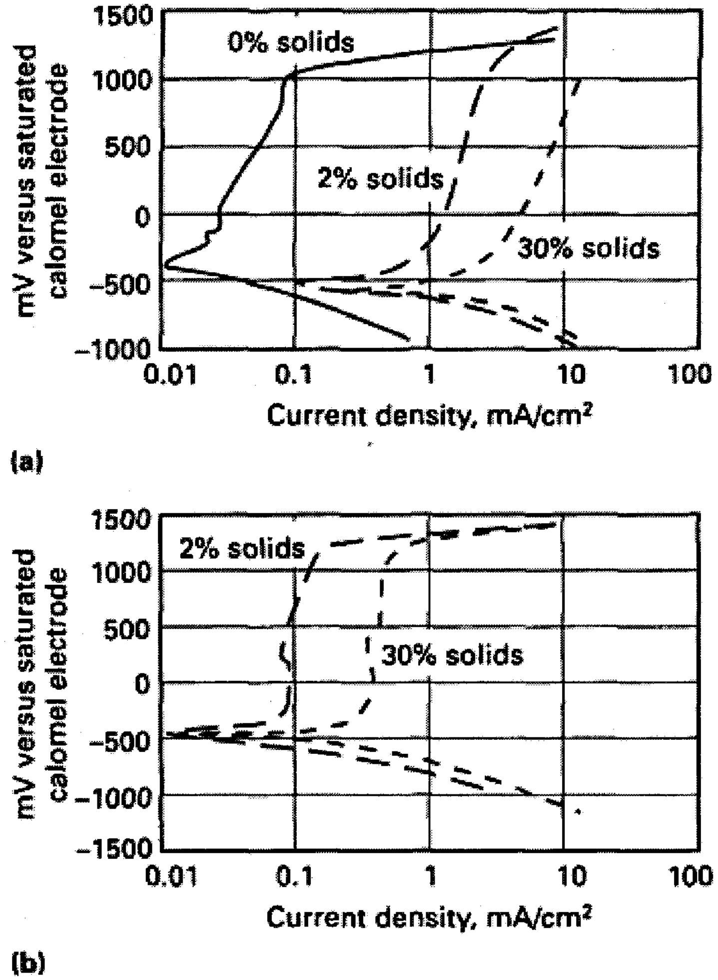

Fig. 1-3 Polarization curves for 316 stainless steel showing the effect of percent solids and impeller speed in a silica sand slurry. (a) Impeller velocity, 15.6 m/s. (b) Impeller velocity, 5.8 m/s. Ref [11].

Closed-Loop Pipeline Experiments. Postlethwaite et al. [14] measured the electrochemical corrosion rate of steels in a closed-loop pipeline experimental apparatus. Electrode specimens flush was mounted with the pipe wall. The test section of pipe was a 38 mm diameter vertical leg of the test loop. The vertical orientation of the pipe eliminated the effect of gravity on the solid concentration in the pipe. The total wear loss (T) was obtained by measuring the weight loss whereas corrosion rate was obtained using the polarization resistance technique. It was demonstrated the mechanical wear W_0 (under cathodic protection) was less than 5% of the total material loss, and S varied between 2.8 and 40.9% of the total material loss. Most of the material loss from a commercial carbon steel pipe were due to electrochemical corrosion. Depending on the slurry flow rate, corrosion rate in the presence of wear, Cw, varied from 56 to 92% of the T. It was shown that the erosive effect prevented the formation of a rust film that normally stifles the diffusion of oxygen to the corroding surface.

Grinding Wear Systems

The abrasive wear in grinding is different from that experienced in slurry particle impingement systems, because the abrasive particles from the crushed ore participate in three-body abrasion between two solid surfaces.

Rotating Cylinder / Anvil Experiments. Kotlyar, Pitt, and Wadsworth [15] used a rotating cylinder/anvil apparatus to measure the corrosive wear of a HCLA steel. The apparatus consisted of a rotating cylindrical wear specimen and two counterbody anvils made of either the tested material or quartz rods. This apparatus possessed the components of an electrochemical cell so that anodic and cathodic polarization curves could be recorded. Values of *T* were determined by weighing the specimens before and after a testing. To estimate W_0, cathodic protection was applied to the sample with a fixed voltage of -1.7 V versus a saturated calomel electrode (SCE). The electrochemical corrosion rate was determined using a linear polarization technique. In experiments using HCLA steel rotating cylinders in a 15 wt% quartz slurry (pH = 9), total material losses were higher by a factor of four when quartz, rather than HCLA, anvils were used.

Rotating Ball-on-Electrode Experiments. In investigations of the electrochemistry of complex sulfide-grinding systems, the galvanic currents of pyrite, pyrrhotite, and mild steel electrodes were determined in short-circuit connections under abrasive and nonabrasive conditions [16,17]. The device shown in Figure 1.4 was developed for the tests performed under abrasive conditions. It consisted of a porcelain ball rotating against three fixed electrodes of pyrite, pyrrhotite, and mild steel. Quartz slurries prepared with mild steel balls were used, and the galvanic current for each electrode was separately and alternately monitored via a switch with a zero-resistance ammeter.

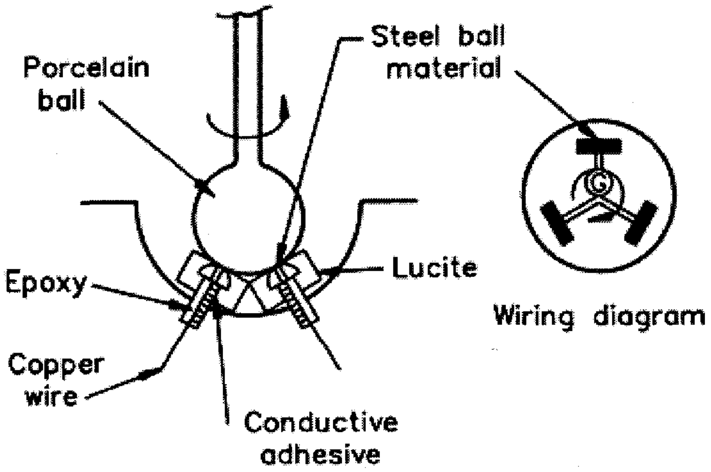

Fig.1-4 Experimental ball-on-electrode device to measure galvanic currents between minerals and alloys

Electrochemical scratch technique

An Electrochemical scratch technique was recently proposed by Wang and Li to separate individual contributions of corrosion and wear to the total material loss caused by corrosive wear [18, 19]. During the test, a target surface was scratched by a diamond tip under a certain normal load, and corresponding changes in the corrosion current were recorded using a potentiostatic method. The change in corrosion rate (mass loss) due to wear, (ΔCw), was calculated using the Faraday Law and the recorded changes in the corrosion current. Once the additional corrosion due to wear (ΔCw) is determined, the additional wear due to corrosion (ΔWc) can thus be calculated according to Eq. 1.5. It was observed that in most cases the current increased rapidly when the scratch was started and then decreased when scratch was ended, indicating the additional material dissolution caused by wear.

1.3 Mechanisms of wear-corrosion synergy

1.3.1 General

Extensive researches have been conducted to investigate the mechanism of wear-corrosion synergy in recent years. Early in 1980s, Dunn [3] has identified a number of possible synergistic relationships between wear and corrosion. Other mechanisms have also been proposed in recent decades [11-24]. These mechanisms are briefly reviewed in this section.

Wear can accelerate corrosion rate. Such accelerating effects include:

- Continuous removal of protective metal oxides and passive films by abrasive, thus exposing the unoxidized metal to a corrosive environment [11, 20];
- The plastic deformation by high-stress metal-mineral contact makes the target materials more anodic with higher susceptibility to chemical attack [15,21];
- Localized electrochemical cells between strained and unstrained regions result in preferential anodic sites for material dissolution and promote pitting [15, 21];
- Formed microscopic grooves and dents serve as sites for concentration cell corrosion. This can happen to many alloys, including HCLA steels, in which the formation of microgrooves and partial removal of oxide films lead to the initiation of pits that affect the total material losses[21];
- The surface area exposed to corrosion is increased by surface roughening , thus increasing the corrosion current [3];

Corrosion significantly accelerates wear as well. The synergistic effect during corrosive wear can be considerable even when the corrosion rate is very low [12, 15]. Possible accelerating effects of corrosion on wear include:

- Material degradation by corrosion facilitates the removal of materials by wear;
- Produced pits can be precursors to microcracking, which invites hydraulic splitting during impact[3];
- Roughening of target surfaces increases the stress concentration and enhances the surface attack;
- Selectively attack grain boundaries and less-noble phases of multiphase microstructure, weakening adjacent metal. This is especially true for white cast irons, where corrosion attacks the chromium-depleted zones that surround the hard carbides in the structure. This corrosion eventually promotes the premature removal of the harder carbide phases, thus accelerating material removal[22,23];
- Produced hydrogen by corrosion process can embrittle the metal and lead to surface cracking[24];

1.3.2 Forms of wear-corrosion synergy and advances in relevant research

Wear phenomena may involve many different kinds of processes, ranging from dry sliding to solid particle erosion, abrasion, rolling contact, cavitation, fretting and fatigue wear. When any of these types of wear occurs in a corrosive environment, corrosion will have an effect on the tribological process resulting in a certain form of corrosive wear, e.g.

erosion-corrosion, abrasion-corrosion, etc. Figure 1.5 illustrates several typical examples of wear-corrosion phenomena and resultant materials loss mechanisms [1].

In real practice, equipment is often subject to attacks from a combination of these wear modes. Figure 1.6 illustrates the complexity in a slurry erosion process, in which a number of wear-corrosion modes are involved [25]. These wear-corrosion modes are briefly discussed as follows.

Abrasion-corrosion wear is the result of any metal-to-metal rubbing in the presence of abrasive solids in a corrosive liquid. This is the most destructive mode encountered when handling slurry, aside from high-velocity erosion. Typical parts of reciprocating pumps that are involved are: metal-to-metal valves and seats (upon each closure), metal piston parts that rub on metal liners and plungers, or piston rods that rub against metal stuffing box parts or trim. In the case of parts of different metals exposed to slurry, electrolytic effects are included in this mode.

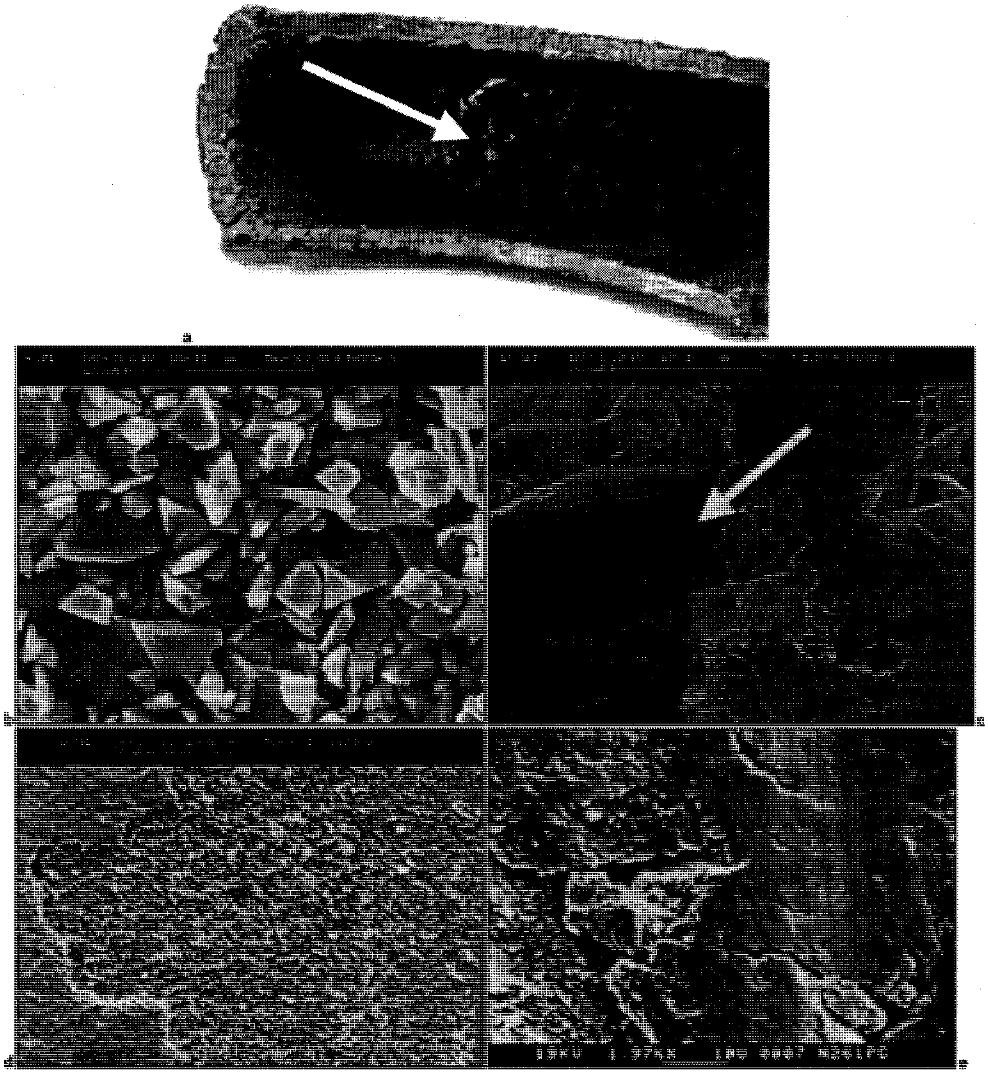

Fig. 1-5 Micrographs of typical tribo-corrosion phenomena. Ref. [1].

a) The interior surface of a pipe suffered by slurry **erosion-corrosion**, the arrow indicates where erosion-corrosion has led to significant material wastage; b) silicon carbide particles commonly used in laboratory simulation of erosion and **abrasion-corrosion**, note angular shape of particles; c) a Ni–Cr/WC lasercarb coating damaged by **micro-abrasion-corrosion** of surface at 5 N at 2200 mV with particles as in b and in a carbonate/bicarbonate solution (pH 9.7); the arrow indicates where WC particle has been removed from the coating owing to tribo-corrosion action; d) a Cr/NbN superlattice PVD coating (2 μm in thickness) damaged by **erosion-corrosion** at 90° and at 3 m/s at -400 mV in a carbonate/bicarbonate slurry solution containing alumina particles; e) Nimonic N80 exposed to sliding wear at 250°C in air.

Scouring wear is encountered with elastomer-to-metal rubbing. Abrasive solid particles become embedded in the softer elastomer, or rubber, as in the case of pistons, packing, and valve inserts.

Crushing and grinding occur in abrasive metal-to-metal contact. An example is a valve that repeatedly closes with great force against solid particles that are trapped between the valve and seat at closure.

High-velocity erosion can be very destructive, which is often encountered in reciprocating pumps for slurry transport. High velocity is usually considered to be greater than 6 to 9 m/s. When a valve seat or a piston is worn to the extent that a slight leak develops, the extremely high velocity of slurry leakage through the small gap can result in catastrophic and rapid failure of the system. Slurry-throttling valves and parts also experience this type of rapid wear.

Low-velocity erosion occurs when there is a flow of slurry at low velocities. In a pipeline with laminar flow, the velocity profile (in the shape of a parabola) is such that the velocity near the wall of the pipe is nearly zero, and minimum wear takes place. The impellers and cut-water mechanism of centrifugal pumps are sometimes subjected to this mode.

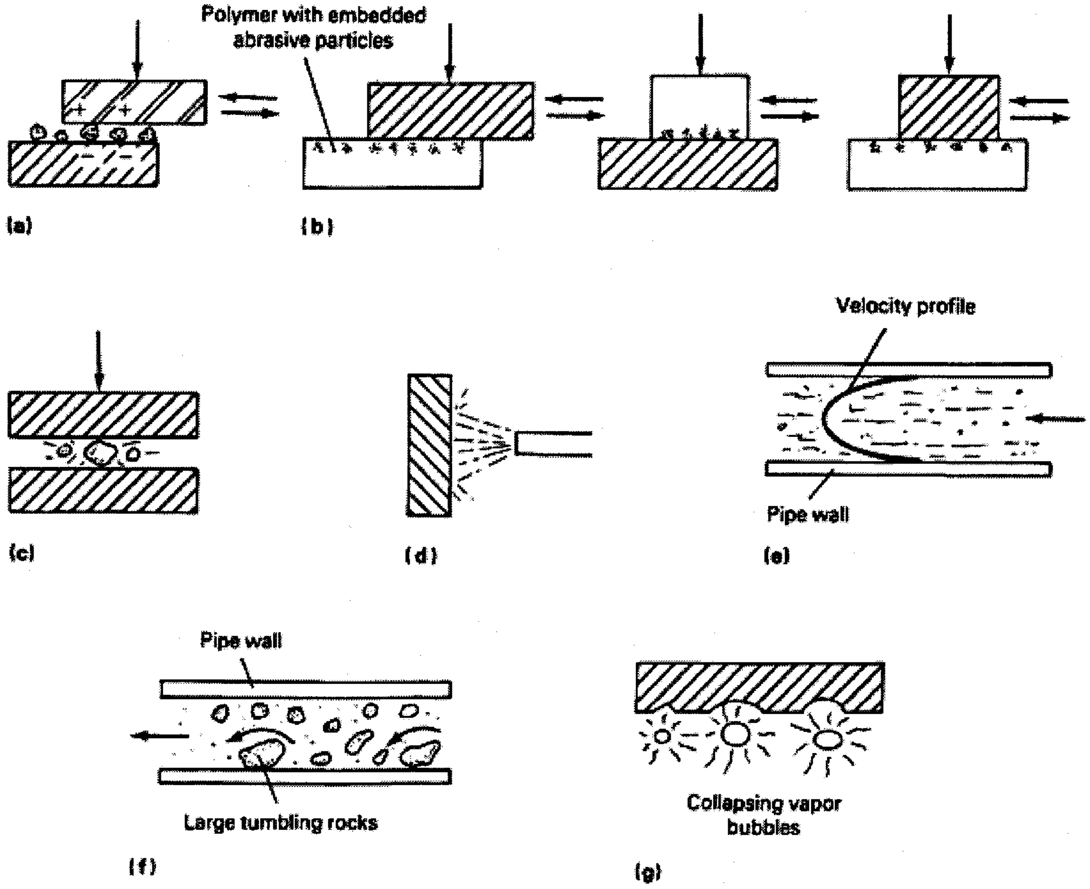

Fig.1-6 Various wear modes involed in slurry erosion. (a) Abrasion-corrosion. (b) Scouring wear, with wear areas equal (left) and unequal (center and right). (c) Crushing and grinding. (d) High-velocity erosion-corrosion. (e) Low-velocity erosion-corrosion. (f) Saltation erosion-corrosion. (g) Cavitation-corrosion Ref [25].

Saltation wear results from the transport of a sediment, where the particles are moved forward in a series of short intermittent bounces from a bottom surface. Rapid wear of this type occurs, for example, in pipelines that transport phosphate rock from slurry pit to the processing plant. The pipe requires frequent turning to distribute the wear.

Cavitation can result in damage to the metal in the liquid end of the pump. The parts of a reciprocating pump can also sustain damage from the microscopic, but intense, liquid pressure blasts against the metal near the cavitation area, following the repeated collapse of the vapor bubbles.

Progress in the understanding of typical corrosive wear modes is briefly reviewed in this section.

Erosion-corrosion

Erosion is the loss of material that results from repeated impact of small solid particles [25]. Erosion-corrosion is an erosion process in a corrosive solution. In this general sense, discussion in this area should logically include erosion-corrosion synergy in slurry, cavitation, and liquid erosion, as well as gas-borne particle erosion [25]. Such a wear mode is of importance to several types of technical applications, including slurry piping, coal gasification or liquefaction, steam turbines, jet turbines, and in the in-bed evaporator tubes. Understanding of how surfaces erode in aqueous corrosive environments has advanced significantly in recent years [26-33]. Erosion can enhance corrosion as a result of removal (leading to subsequent reformation) of film from the surface. In some cases, it can be impeded by corrosion, e.g. when the film is sufficiently protective to resist impact.

Investigation by Burstein and colleagues [26, 27] on the erosion of aluminium in an impinging jet apparatus showed that the solution composition has a significant influence on the erosion-corrosion rate. In particular, in Na_2CO_3 solutions, flakes of oxides were observed on the aluminium surface after erosion-corrosion. The relatively high erosion-corrosion rates in such solutions are attributed to the poor erosion resistance of the oxide films. Other studies on aluminium in NaOH showed similar trends [28]. Pistorius and Burstein, who characterised the transition from 'stable' to 'metastable pitting' more than a decade ago [29], applied a similar analysis to erosion-pitting corrosion and showed that erosion events had a significant effect on such pitting transitions [30]. The importance of surface finish in providing initiation sites for pitting in erosion-pitting corrosion, particularly in the initial stages of erosion-corrosion, demonstrated with evidence that the pitting potential was significantly affected by surface roughening before erosion.

Other erosion-corrosion studies [31, 32] have shown that multiphase materials, such as cast irons, Stellite type materials or cermet based coatings, significant increases in the erosion rate were observed in the presence of corrosive media. It is thought that the corrosive media acts preferentially to dissolve materials at interfaces between the matrix material and the reinforcement, although the matrix and the reinforcement particles are also damaged. In erosion-corrosion of cast irons [31] the corrosive action significantly enhances the removal of materials through a preferential interfacial dissolution mechanism. Thus, composites [31, 32] could be eroded much faster in corrosive environments and synergistic effects are very marked.

Other work in erosion-corrosion has concentrated on additive and synergistic contributions to the weight loss. Precise electrochemical measurements on steel [33] showed that the synergistic effect was negligible in carbonate–bicarbonate solution, except at the corrosion potential where the active-to-passive corrosion transition took place. These results were interesting as earlier studies to quantitatively evaluate the relative contributions of corrosion and erosion to the overall weight loss, using electrochemical techniques. It is suggested that the enhanced synergy at the corrosion potential is attributed to intergranular fracture; the fact that stress corrosion cracking is also prone to occur at such potentials has led the investigators to conclude that erosion-corrosion is largely affected by stress corrosion cracking may be analogous.

Sliding wear in aqueous environments

Sliding wear refer to a type of wear generated by the sliding of one solid surface on another surface [34]. There have been significant advances in the understanding of wear-corrosion mechanisms during sliding contact in aqueous corrosive environments. Several studies have shown acceleration in the sliding wear rate in the presence of corrosive media. Watson et al. [35] defined a basis for distinguishing between synergistic and additive wear-corrosion effects. Other studies by this team identified a significant increase in wear-corrosion synergy of cast irons [23, 31]. The extent of sliding wear in aqueous conditions has been shown to be a complex function of materials properties and the corrosivity of the environment. Studies have also shown the importance of keeping the counter-body inert in order to assess the 'true' electrochemical response of the target surface [36].

Much recent work on sliding wear has concentrated on precise measurements of the corrosion contribution to the weight loss during sliding [37]. The concept of the 'active wear' track has been proposed by Celis as a means of calculating the corrosion contribution to the wear rate. In such cases, the corrosion rate (in passive conditions) is essentially the re-passivation rate over the active wear track and is calculated from the Faradaic conversion of the anodic current density.

Mischler and co-workers conducted research on sliding processes in aqueous conditions [38-40]. In a study of wear of an alumina pin against various pure metals, the relative importance of mechanical and electrochemical removal was evaluated through applying an anodic potential in various solutions, e.g. sulphuric acid and sodium sulphate. A theoretical model was developed to describe the tribo-corrosion behaviour, taking account multiple asperity contact and material dependent parameters such as hardness and passivation behavior [39].

In studies of coatings such as TiN in a borate solution [40], it was shown that the sliding wear-corrosion depended critically on the electrochemical condition particularly on the applied potential. It was suggested that the potential dependence of the mechanical wear was largely influenced by the lubricating properties of the thin surface film formed in the passive potential range. The distinctive effect of increasing potential on erosion-corrosion of TiN coatings had also been observed in aqueous conditions. It was shown that above a critical velocity the coating endured erosion-corrosion through pin holes and defects in the coating [41].

Efforts were also made to investigate the effect of the contact configurations on the tribo-chemical interaction. For instance, three contact configurations were evaluated: a ceramic pin rubbing on a steel plate, a steel pin rubbing on a ceramic plate and a steel plate running on a steel plate in sulphuric acid solution [42]. The results indicated that the total wear volumes for the first two couples were comparable; however, for the metal on metal contact, the wear rates were significantly higher due to severe adhesive wear.

Abrasion-corrosion

Abrasion is due to hard particles or hard protuberances that are forced against and move on a solid surface [34]. Abrasion is typically categorized according to types of contact, as well as contact environment. Types of contact include two-body and three-body wear [34]. Two-body wear is caused by hard protuberances on the counterface, while in three-body wear hard particles are free to roll and slide between sliding surfaces. The effect of abrasion is particularly evident in the industrial areas of mining and mineral processing where dirt, rock, and minerals are handled in a moisture environment. Examples include ore loading / moving buckets, crushers, and dump truck beds. Extensive studies have been conducted in the past decades to investigate the synergy of abrasion and corrosion [6,11,15,16,17,21,43-45].

Much recent interest has concentrated on the micro-abrasion of materials (where the particles causing abrasion are typically less than 10μm in diameter) [46-48]. Various regimes of micro-abrasion, ranging from rolling to grooving wear, have been identified, resulting in the construction of micro-abrasion maps [46, 47]. Other work has suggested the possibility of oxidational micro-abrasion regimes, leading to additional information added to the wear maps [48]. Wherever micro-abrasion occurs in an aqueous medium with the abrasive particles entering and being trapped in the contact region, corrosion may have a significant effect on the micro-abrasion mechanism transitions. Recent results on WC–Co based cermets have shown significant enhancement of micro-abrasion rate in corrosive environments [49]. Microscopy of the worn surfaces showed the surfaces to be abraded uniformly; however, the micro-abrasion rate in acidic environments was significantly higher than that at high pH values. Considerable work is still required to characterize the micro-abrasion–corrosion interaction for various materials in a range of corrosive environments.

Other forms of wear-corrosion synergy

There are other forms of wear-corrosion synergy which are also of technical importance and have attracted considerable research interests, e.g. corrosive fretting wear[50-52], corrosive cavitation wear[53-54], etc.

1.4 Impact wear in corrosive environments

1.4.1 Phenomena

Previous corrosive wear studies mainly dealt with abrasion, erosion, sliding or rolling contact in corrosive environments. However, in some industrial corrosive wear processes, particularly in mineral processing operations, repetitive high-energy impacts are involved thus introducing a variety of material loss mechanisms that combine impact, wear and corrosion. The high-energy impacts occur in ore-ore, ore-metal, and metal-metal collisions in ore, liners, and grinding media in crushing and grinding equipment. During an impact event, there are both transfer and dissipation of kinetic energy. The kinetic energy that is not transferred to other bodies is dissipated by generating heat, fracturing ore, and damaging metal components of the system. The damage resulting from absorption of energy takes the following forms [3]:

1) cracking
2) plastic deformation
3) cutting and removal of metal fragments
4) transformation of austenite to martensite
5) twinning of metal crystals
6) adiabatic heating and recrystallization of subsurface metal
7) adiabatic pressurization of fluids, trapped in contact area

It has been estimated that as little as 10-20% of the energy applied to grinding processes is absorbed in fracture of ore [55]. The remaining energy is consumed by accelerating bodies within the system, heating them, and damaging them. Experimentation and theoretical calculations indicate that impact forces and related energy levels in these impact events are large. Grinding ball impacts in relatively small 2.9 m ball mills have been measured and found to produce an average stress of 2290 MPa during collisions [56]. T. E. Norman [57] has shown that the ball wear rate is of a function of grinding intensity, i.e. mill energy per unit of ball surface area. Increasing mill diameter increase the grinding intensity expressed as watts/cm^2. Wear rates of grinding balls increase rapidly as mill size increases, supporting the theory that increased impact energy accelerates the wear loss.

Since large stresses with high strain rates are often encountered in this wear mode, changes in surface microstructure and defect configuration caused by such impact could result in considerable variations in electrochemical and mechanical properties of target surface and thus affect the subsequent corrosive wear behavior of the materials. Therefore, mechanisms responsible for corrosive impact wear could be very different from those for corrosive abrasive or sliding contacts.

D. J. Dunn has suggested some possible mechanisms on how impact could affect wear-corrosion synergy [3]:

- Plastic deformation makes materials more susceptible to corrosion
- Crack brittle constituents and tear apart ductile constituents to form sites for crevice corrosion and hydraulic splitting

- Supply the kinetic energy to drive the abrasion mechanism, thus accelerating the abrasive component of wear. In ore processing, some minerals are driven into the softer steel grinding media, promoting the formation of galvanic corrosion cells
- Pressurize mill water to cause splitting, cavitation, and jet erosion of metal and protective oxidized material
- Heat grinding media, mill liners, ore, and fluids to increase corrosive effects

However, there is no solid experimental support for these assumptions. The study of corrosive wear involving impact is rather limited. In attempting to understand the impact wear in corrosive environment, it is worth investigating the following issues:

1) Material failure mechanisms for impact wear in the dry condition;
2) Effect of prior deformation on corrosion and corrosive wear
3) Effect of high strain rate on changes in material microstructure, defects configuration, and mechanical properties.

Previous investigation in these three areas is briefly reviewed below.

1.4.2 Impact wear in the dry condition

Impact wear may be defined as the wear of a solid surface resulting from repeated percussion, or repetitive exposure to dynamic contact with another solid body [25]. In other words, impact wear is the wear of surfaces under impacting conditions, when two surfaces contact with high relative velocities normal to their interface [58]. Impact energies are typically several orders of magnitude higher than the energies involved in other types of wear, e.g. in erosive wear.

Impact wear may also involve other wear mechanisms, such as adhesive, abrasive, erosive, surface fatigue and thermal wear [25]. There are two typical modes of impact wear: 1) Normal impact wear occurs when the relative approach of the impacting bodies contains no tangential or rotational elements; 2) when a shear component is added, either when normal impact occurs with a component of sliding or the bodies impact the target surface at a acute angle, the term compound impact wear is used [59]. Most impact situations involve impact with a small amount of sliding. The compound impact wear has been shown to lead to much higher wear rates than normal impact alone [59]. This is thought to be due to enhanced removal of wear debris that occurs with the introduction of a shear component.

Considerable effort has been made to understand the mechanism of impact wear. Early in 1970s, N.P. Suh [60-63] proposed a delamination theory of wear, which was primarily concerned with deformation below the surface during the impact wear process. Under repetitive impacts, severe plastic shear deformation is introduced and voids form in the subsurface layer. When voids coalesce, cracks are generated below the surface. Crack nucleation near the very surface is not favored because of a triaxial state of highly compressive stress which exists below the contact regions. Once cracks are present, further impact loading and deformation causes cracks to propagate, joining neighboring ones. Delamination could result from the crack propagating in the surface layer.

In recent years, considerable attention has been paid to the role which white layer (WL) plays in impact wear [64-71]. High stresses under impact loading cause severe plastic deformation and work-hardening in the subsurface layer, resulting in a special deformation or transformation zone which shows a bright color after etching under optical microscope. There is strong evidence of crack and void formation inside and around the WL, suggesting its role as a precursor to fracture or delamination. Some researchers proposed that WLs were related to the adiabatic shear band formed under heavy impact load [64, 65]. Others considered that the WLs resulted from martensite transformation, since the concentrated frictional heat and subsequent fast cooling may lead to martensitic transformation [66, 67]. It has also been reported that oxygen, nitrogen, or carbon elements can be diffused to subsurface or chemically reacted with counter-face to form oxide, nitride or carbide [68, 69]. Dynamic recrystallizaton is also considered to be a possible mechanism for white layer formation [70]. Two models were proposed in Ref [71] to explain the failure mechanism of impact wear by WL formation: One is a delamination model, in which the microcracks inside the WL propagate along the interface between WL and the deformed zone below WL, thus resulting in delamination of the WL. The other is a spalling model, where the cracks inside the WL propagate through the deformed zone along an acute angle to the surface, and result in a spalling.

However, the impact wear in a corrosive environment was not addressed by these previous investigations.

1.4.3 Effect of prior deformation on corrosion and corrosive wear

1.4.3.1 Effect of prior deformation on corrosion

Plastic deformation generated by heavy impact could make materials more susceptible to corrosion, since plastic deformation renders materials more anodic. Such an effect is called mechanochemical effect [72], which has been reported in many alloy systems during past decades. In this section, the mechanochemical behaviors of various metals and alloys are reviewed.

- General corrosion

It was found [73] that when a wire made of 18Cr-8Ni stainless steel was deformed in a boiling $MgCl_2$ solution, more than 104 fold increase in the anodic current density in comparison with an undeformed counterpart was measured, manifesting the mechanochemical effect.

E.M. Gutman [74] studied the mechanochemical effect on Type 316L stainless steel. It was shown that both passive and transpassive current densities increased with plastic strain.

Haanappel [75] obtained a different result when investigating AISI 304 stainless steel. Large differences in corrosion rates were found between zones with different degrees of deformation. An increase in deformation resulted in a decrease in the corrosion current density, whereas after cyclic polarization the number of pits increased.

Ocampo [76] investigated the mechanochemical behavior of carbon steel samples (0.098wt% C), which were cold reduced to attain 27%, 42%, 50% thickness reduction, respectively. Corrosion tests in aerated solutions based on polarization curves revealed that the cold reduction led to significant improvements in corrosion resistance, compared to undeformed samples. However, corrosion tests in deaerated solutions revealed that the cold reduction didn't significantly influence corrosion resistance when compared with the undeformed counterparts. This behavior was attributed to low dissolved oxygen, which made oxygen reduction more difficult and slowed down the steel dissolution, thus making the corrosion rate independent of material stress condition.

A.O. Surendranathan [77] studied the corrosion behavior of ductile iron (DI) in natural sea water, 5 % H_2SO_4 and 5% NaOH. Samples were tested in the as cast, annealed and cold worked conditions at 300K, 325K and 340K. It was found that annealed material showed slightly improved corrosion resistance compared with the as-cast condition. Small amount of cold working (less than 14%), which was proposed to remove the casting surface irregularities and reduce the porosity, is also beneficial for the corrosion resistance. High degree of cold working is detrimental with respect to corrosion resistance as it increases the stored energy and dislocation density in the material thereby enhancing the kinetics of corrosion reactions.

R.B. Leggat [78] studied the effect of micron-scale surface deformation on the corrosion behavior of coated aluminum alloy 5182. The results showed that the micron-scale substrate deformation (dimples) produced on precoated AA5182 sheet during manufacturing resulted in increased corrosion susceptibility at these sites. It was suspected that precipitation of an anodic second phase around dislocations during subsequent processing and oxide damage was responsible for the increased corrosion susceptibility.

M. Kh. Rabinovich [79] investigated the influence of superplastic deformation on the corrosion resistance of aluminum alloys. It was established that superplastic deformation of aluminum alloys reduced their resistance to intercrystalline corrosion due to the decrease in electrode potential of near boundary PFZs(precipitate free boundary zones).

T. M. Yue reported [80] the effects of surface machining on corrosion behavior of aluminum 2009/SiC composite. The aluminum 2009 matrix was reinforced with 20vol% of silicon carbide, having its nominal particle size equal to 3.5 μm. It was shown that the surface finish condition had a major effect on the corrosion behavior of MMCs, and in a sense this could be more significant than the potential problem of chemical instability that exists at the Al/SiC interface.

Effects of prior deformation on other forms of corrosion, such as pitting, intergranular corrosion, and stress corrosion cracking, can also be found in literature [81-88].

- Pitting

Pitting corrosion resistance of stainless steel is significantly affected by cold work. Several investigations carried out in past decades have reported unclear role of cold working on the localized corrosion resistance [81-83]. The susceptibility of cold worked 18Cr-10Ni-2Mo steel to pitting corrosion in a NaCl solution was reported to be higher with the number and size of pits generally increasing with the amount of cold work [81]. Forchhammer et al. [82] studied the effect of cold work on the pitting potential of different austenitic stainless steels. It was found that in a 30% NaCl solution the pitting potential was not significantly affected by cold work; it appeared that the cold worked specimens had a large number of pits but the size of the pits was smaller. According to Randak [83], the quasimartensite produced in 18Cr-8Ni steels by cold working does not change the pitting potential value in chloride solution, but an increase in the pitting density with increasing cold work was observed.

- Intergranular corrosion

It is well known that intergranular corrosion (IGC) can occur in austenitic stainless steel when sensitized by welding or improper heat treatment. The influence of plastic deformation on IGC of SS has been extensively studied [84-86]. It is found that small deformation has a negative effect on the behavior of sensitized SS while greater deformations seem to have a beneficial effect.

- Stress corrosion cracking

The effects of prior cold work (CW) on the stress corrosion cracking (SCC) behaviour of Type 304 stainless steel in chloride solution were reported in chloride solutions [87]. The results indicated that the SCC behavior of the cold worked steel was essentially different from that of annealed steel. Intergranular stress corrosion cracking (IGSCC) of the annealed steel changed into a mixed mode or dominant transgranular stress-corrosion cracking (TGSCC) when the degree of CW was increased. J.H. Zheng [88] investigated the stress-corrosion cracking (SCC) behavior of cold-worked AISI type 316L stainless steel (SS) in a concentrated lithium salt solution at elevated temperatures. The results are very similar: Intergranular stress -corrosion cracking (IGSCC) of the annealed material changed into a mixed SCC mode, or a dominant transgranular SCC (TGSCC) with an increase in cold work to 20% and 40%. The susceptibility of cold-worked 316L SS to TGSCC increased with the extent of cold work.

1.4.3.2 Effect of dislocation on electron work function

As reported in the mechanochemical behavior of most alloys, the common effect of deformation on corrosion behavior is the shift of the steady (corrosion) potential to the disennobling direction and an increase in the corrosion rate with the amount of plastic deformation. In attempt to understand the effect of deformation on the corrosion behavior, the concept of electron work function (EWF) is very helpful [89-93].

The EWF refers to the minimum energy required to remove an electron from the interior of a solid to a position just outside the solid, which represents the ability of metal crystals to lose electrons. In general, the EWF φ is expressed as

$$\varphi = E_0 - E_F \qquad (1.6)$$

where E_0 is the energy of electron at infinity and E_F is the Fermi energy. The value of φ is approximately the depth of the potential well for electrons in the crystal lattice or the work required to move electrons to infinity from the highest electron state in a metal [89].

Attempts have been made to investigate the influence of deformation on the EWF [90-91]. It has been demonstrated that the EWF decreases with plastic deformation regardless if it is tensile or compressive [92]. This implies that dislocations render electrons more active, and thus, increase the driving force for electrochemical reactions. Such relationship between the EWF and plastic deformation has been well demonstrated using an electrostatic model [93].

1.4.3.3 Effect of deformation on corrosive wear behavior

X.C. Lu studied [94] the effects of surface deformation on corrosive wear of austenitic, ferritic and duplex stainless steel in sulfuric acid solution. The results indicated that the corrosive wear rate of duplex stainless steel (DSS) increased linearly with load while that of austenitic stainless steel (ASS) and ferritic stainless steel (FSS) increased exponentially with load. At high loads, the rank of corrosive wear rate was

ASS>FSS>DSS but it changed to ASS>DSS>FSS at low loads.

A laboratory study has been conducted on the corrosive wear behavior of AISI304 steel and Cr-Mn-N duplex stainless steel [95]. The removal rate of steel, the hardness of wear track and the relative wear resistance were measured. The Cr-Mn-N duplex stainless steel has stronger deformation strengthening and better wear resistance in dry sliding and corrosive environment. It was found that the deformation strengthening of alloy can be used to improve the corrosive wear resistance of the alloy.

However, research on the influence of plastic deformation on the corrosive wear performance is rather limited.

1.4.4 Deformation at high strain rates

The dynamic behavior of materials i.e. deformation at high strain rates has been a subject of many studies in recent decades, due to its significance to engineering practice [96, 97].

The high-strain-rate plastic deformation of materials is often described by constitutive equations that link stress with strain, strain rate, and often, temperature. In the meantime, since plastic deformation is an irreversible and path-dependent process, the response of a material at a certain (σ, ε) point is dependent on instantaneous deformation substructure, e.g. dislocation cells, which tend to be developed in materials having low stacking-fault free energies such as copper and nickel [96]. Since there are a variety of deformation substructures, affected by strain rate, temperature, and stress state, the "deformation history" has to be considered. Therefore, we may express the stress as

$$\sigma = f(\varepsilon, \dot{\varepsilon}, T, deformation - history) \tag{1.7}$$

where ε is the strain, $\dot{\varepsilon}$ is the strain rate, and T is the temperature.

There are a number of constitutive equations proposed and successfully used to describe the plastic behavior of materials as a function of strain rate and temperature [98-101]. Among these equations, the Johnson Cook equation is a useful constitutive model:

$$\sigma = (\sigma_0 + B\varepsilon^n)(1 + C\ln\frac{\dot{\varepsilon}}{\dot{\varepsilon}_0})[1 - (T^*)^m] \tag{1.8}$$

In order to understand the established constitutive equations, effects of applied stress on the dislocation velocity have been investigated for a number of materials [102-105]. Gilman and Johnston [102] measured the velocity of dislocations in LiF as a function of stress. The dislocation velocity was expressed as

$$v \propto \sigma^m e^{-E/kT} \tag{1.9}$$

where m varies between 15 and 25 when v is expressed in cm/s and σ in kg/mm^2.

It is also accepted generally that the flow stress of a material depends not only on the strain and strain rate, but also on its microstructure at the dislocation level. Many investigators have investigated the effects of strain rate on the dislocation substructure by means of transmission electron microscopy (TEM) [106-108]. In many cases, a cellular dislocation substructure develops, and the dislocation density increases with strain rate; while the dislocation cell size decreases with the strain rate. This is of great importance to the corrosive wear studies since the dislocation structure, particularly the dislocation density, can significantly affect the electrochemical and wear behavior of materials.

1.5 Objective of the research

As discussed above, extensive researches have been conducted to investigate the mechanisms of wear corrosion synergy in recent years. A number of synergistic relationships between wear and corrosion have been identified and proposed. However, previous corrosive wear studies mainly dealt with abrasion, erosion, sliding or rolling contact in corrosive environments, i.e. abrasion-corrosion, erosion-corrosion, etc. In many industrial corrosive wear processes, particularly in mining and mineral processing operations, the material surface is subjected to repetitive impact actions, followed by combined attacks of corrosion, abrasion or sliding wear. Investigating effects of the prior impact action on subsequent corrosion and corrosive wear would help to gain understanding of the failure mechanism responsible for impact wear in a corrosive environment. Unfortunately, to our knowledge, there are few studies addressing this issue. The present research was carried out to study how the prior impact action influenced subsequent corrosion and corrosive wear rather than the spontaneous corrosion-impact wear synergy. Such influence is worth studying, since the period of an impact event could be too short to allow electrochemical reactions to take place. However, the defects generated by impact, e.g., micro cracks and voids, strongly affect the synergistic effect of subsequent corrosion and wear on material loss.

In this study, we are going to investigate the effect of prior deformation at different strain rate on corrosion and corrosive wear. This work could be resolved into two steps:

1) Evaluate the influence of prior deformation on corrosion and corrosive wear of metallic materials;
2) Investigate effects of strain rate of prior deformation on dislocation density and defect configuration, and consequently its influences on corrosion and corrosive wear.

This thesis consists of seven chapters:

Chapter 1 is the literature review, which provides the information on previous and current studies in this field.

Chapter 2 reports a study of the effects of prior cold work on corrosion and corrosive wear behavior of copper in 0.1 M HNO_3 and 3.5% NaCl solutions, respectively. The objective of this study is to investigate how the prior plastic deformation affects corrosion and corrosive wear of materials respectively involving and without involving passivation.

Chapter 3 reports the study of the effects of the loading speed or strain rate on corrosion and corrosive wear of annealed, impact-fractured and slow bending-fractured surface layers of AISI 1045 steel in a 3.5% NaCl solution. Prior deformation was generated by Charpy impact test and slow bending test to achieve two different loading rates. This is a preliminary study of the effects of strain rate on microstructure, mechanical behavior, corrosion properties, wear and corrosive wear of the material.

Chapter 4 presents a systematic study on the effects of strain rate of prior deformation on corrosion and corrosive wear of AISI 1045 steel in a 3.5% NaCl solution. Prior deformation was generated by tensile test at various strain rates. Based on the effects of prior strain at different rates on surface microstructure and resultant changes in electrochemical and mechanical properties, the corresponding wear behavior of the steel in the 3.5% NaCl solution and relevant mechanisms are discussed.

Chapter 5 reports a new phenomenon in measuring the wear-accelerated corrosion. Accordingly, a modified experimental technique is proposed to quantitatively determine the corrosion-wear synergy. The objective of this study is to develop a reliable technique to evaluate corrosive wear and investigate responsible mechanisms.

In Chapter 6, the wear-corrosion synergy as presented in Chapter 4 is further quantified using the modified experimental technique presented in Chapter 5. The synergistic component, S, can be further divided into two components: the change in corrosion rate due to wear (ΔCw) and the change in wear rate due to corrosion (ΔWc). Effects of prior deformation strain rates on these two components were investigated in details.

In Chapter 7, the final chapter, main conclusions are presented and possible future work is discussed.

Chapter 2

Effects of prior cold work on corrosion and corrosive wear of copper in HNO_3 and NaCl solutions

In this chapter, effects of prior cold work on corrosion and corrosive wear behavior of copper in 0.1 M HNO_3 and 3.5% NaCl solutions, respectively, were investigated using electrochemical tests, electron work function measurements, and sliding corrosive wear tests with and without cathodic protection. Optical microscope and SEM were employed to examine the microstructure and worn surfaces. It was shown that, in general, the prior cold work raised the corrosion rate, but the effect differed in different corrosive media. In both the solutions, pure mechanical wear decreased with an increase in cold work. The prior cold work had a significant influence on the corrosive wear of copper, depending on the corrosive solution and the applied load. In the 0.1M HNO_3 solution, the ratio of the wear loss caused by corrosion-wear synergy to the total wear loss increased with the cold work and became saturated when the cold work reached a certain level. In the 3.5% NaCl solution, however, this ratio decreased initially and then became relatively stable with respect to the cold work. It was observed that wear of copper in the 3.5% NaCl solution was larger than that in 0.1M HNO_3 solution, although copper showed lower corrosion rate in the former solution. The experimental observations and the possible mechanisms involved are discussed.

The aim of this chapter is to investigate how the plastic deformation affects corrosion and corrosive wear of materials. Copper was selected as a sample material, since its electrochemical properties change with the corrosive solution, involving passivation or non-passivation. Consequently, we may gain understanding of general response of cold worked materials to corrosion and corrosive wear no matter whether they are passive or non-passive materials.

2.1 Experimental details

The material used in this study was commercially pure copper. Copper plates were fully annealed at 850°C for 2 hours. They were then cold rolled at 20°C to obtain 18%, 33%, 52%, 63%, and 77% reductions in thickness, respectively. Specimens cut from the plates had the following dimensions: 15mm × 15mm × 1~5 mm. The specimens were polished using 320#, 400#, and 600# SiC abrasive papers and finally a 6μm diamond paste. For optical micrography, electrochemical tests and electron work function measurements, the specimens were further polished using a 0.05 μm Al_2O_3 slurry to get mirror-finished surfaces.

Corrosive sliding wear tests were performed on a pin-on-disc tribometer (CSEM Instruments, Switzerland). A schematic drawing of the apparatus is shown in Fig. 2-1.

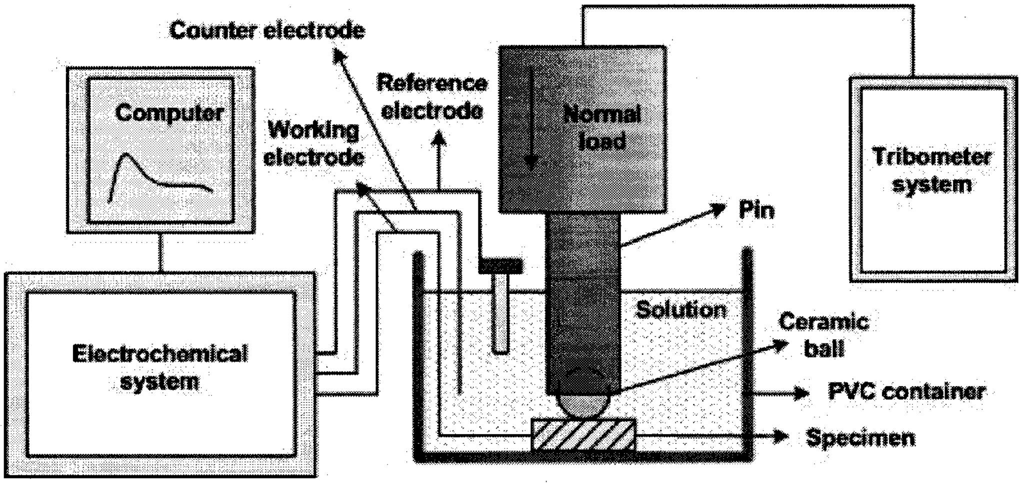

Fig.2-1 Schematic diagram of the apparatus for corrosive sliding wear tests

In this work, the pin was a ball made of silicon nitride (Si_3N_4) with a diameter of 6mm. During a wear test, the pin was pressed onto a rotating copper sample (plate: 15 × 15 × 1~5 mm) under an applied load. The apparatus was attached with an electrochemical system (connected to a Gamary PC4/750 electrochemical system), which allowed a wear test performed in a plastic cell that contained a corrosive solution under an applied potential. A saturated calomel electrode (SCE) was used as the reference electrode and a platinum plate was used as the counter electrode. 3.5% NaCl ($NaCl+H_2O$) and 0.1M HNO_3 (HNO_3+H_2O) solutions were used as the electrolytes.

The sliding wear tests were carried out under different loads (1N, 3N, 5N) over a sliding distance of 5.5 m at a sliding speed of 0.5cm/s. The wear rate, reported as the volume loss per unit length of wear track (mm^3/mm), of copper samples in 3.5 % NaCl and 0.1 M HNO_3 solutions respectively were measured. The wear rate was calculated using the following equation (ASTM Practice G99-04):

$$\text{Volume loss rate} = r^2 \sin^{-1}(d/2r) - (d/4)(4r^2 - d^2)^{1/2} \tag{2.1}$$

where r is the pin end radius and d the width of wear track. The pin end radius, r =3 mm, kept approximately constant, confirming by checking the pin end under an optical microscope. For each wear condition, at least 3 tests were performed. The width of wear track, d, was measured under the optical microscope and averaged over at least 10 measurements at different positions on the track.

Pure mechanical wear in a corrosive solution was evaluated by performing wear test in solution under full cathodic protection. In order to select an appropriate cathodic potential, variations in the wear rate with respect to applied cathodic potential were determined. The potential below which the wear rate became stable was selected for the cathodic protection.

The microstructure of the copper samples was characterized by standard optical metallography [Etchant: $K_2Cr_2O_7$ (10g) + H_2SO_4 (5ml) + H_2O (80ml)]. Vickers hardness tests were performed using a Mitutoyo AVK-C1 hardness tester under a load of 5 kg.

Electrochemical tests, including potentiodynamic polarization, linear polarization and Tafel plot measurements, were performed using the computerized Gamary PC4/750 electrochemical system. The potentiodynamic polarization curves were obtained at a scan rate of 0.33 mV/s.

At least three reproducible linear polarization tests were performed for each sample to measure its polarization resistance R_p, starting from 9.0 mV below OCP (open circuit potential) and ending at 9.0 mV above OCP. The scanning rate was 0.05 mV/s with a scanning increment of 0.1 mV.

At least three reproducible Tafel plot corrosion tests were carried out for each sample, starting from 100 mV below OCP and ending at 140 mV above OCP. The scanning rate was 0.1 mV/s with a scanning increment of 0.2mV.

The corrosion current density icorr was calculated based on the following relationship: (ASTM Practice G3-89):

$$i_{corr} = \frac{b_a b_c}{2.303(b_a + b_c)R_p} \qquad (2.2)$$

where i_{corr}=corrosion current density,

b_a= anodic Tafel slope,

b_c= cathodic Tafel slope,

R_p=polarization resistance

To confirm the corrosion behavior evaluated using electrochemical test, direct corrosion weight loss of copper in a 1M HNO_3 solution was also measured. Each sample was immersed in the nitric acid solution for 3 hours before the weight loss measurement. For each sample, at least 3 tests were performed.

To better understand the corrosion behavior of the copper samples, a scanning Kelvin probe (SKP) system (KP echnology Ltd., Caithness, UK) was used to investigate the influence of prior cold work on the electron work function (EWF) of copper. The KP system had three sub-systems (a digital oscillator, data acquisition, and sample translation) controlled by a host PC. A three-axis microstepper positioner permitted high-resolution sample positioning (0.4 μm per step) and the scanning area was 2mm ×2mm. A gold tip with diameter equal to 1mm was used. The oscillation frequency of the Kelvin Probe was 173Hz.

In order to examine the effect of surface oxide film on the deformation-electron work function relationship, two group of specimens were used. Before the EWF test, one group of specimens were first polished and then immersed to 3.5% NaCl solution for 40 minutes to form a surface oxide film. The other group of polished surfaces was etched with 0.1 M HNO_3 solution (HNO_3+H_2O) for 120s in order to remove the deformed layer caused by polishing along with possible surface oxide film formed in air.

2.2 Experimental results

2.2.1 Changes in microstructure and hardness caused by cold work

Microstructures of annealed and cold-rolled samples are shown in Fig.2-2. After the cold rolling, initial equal-axial grains were elongated along the rolling direction. The width of the grains decreased with an increase in the percent reduction in thickness.

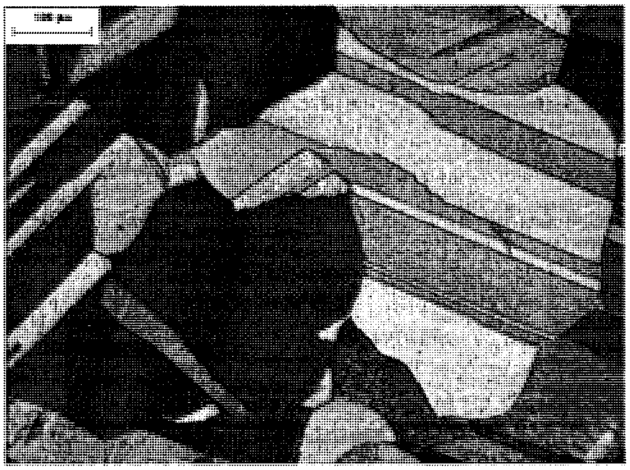

(a)

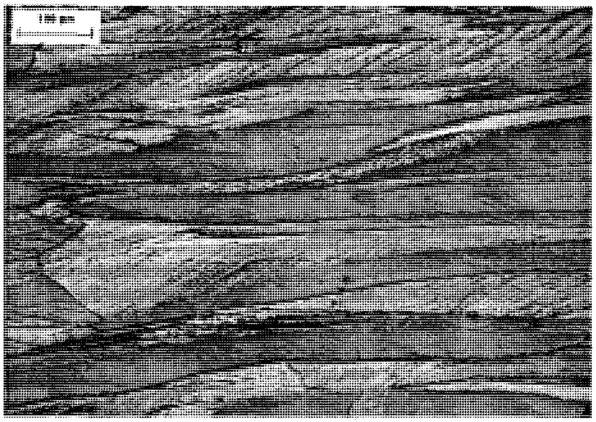

(b)

Fig.2-2 Metallographs of samples with
(a) 0% cold reduction (b) 77% cold reduction

Fig.2-3 illustrates variations in hardness with respect to the cold rolling reduction. As shown, the hardness increased with an increase in the percent reduction in thickness, which was attributed to the work-hardening effect. The increase in hardness should be attributed to increases in both the dislocation density and the grain boundary density caused by the cold work.

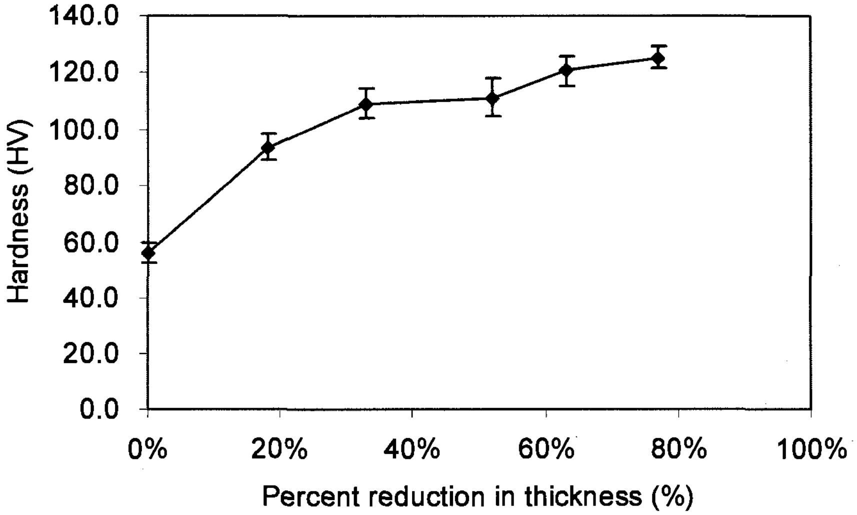

Fig.2-3 Variation in hardness (HV) as a function of percent reduction in thickness

2.2.2 Effects of prior cold work on corrosion

Fig.2-4 illustrates variations in the corrosion current density and the corrosion potential against the percent reduction in thickness, measured in the 0.1M HNO_3. As shown, the corrosion current density increased while the corrosion potential decreased with an increase in the cold work.

The influence of prior cold work on the corrosion rate of copper was also evaluated by the weight loss measurement. Fig.2-5 shows the weight loss rate (g/mm^2min) of copper after being immersed in a 1M HNO_3 solution for 3 hours. As demonstrated, the corrosion rate increased monotonically with the percent reduction in thickness. This result is consistent with the changes in the corrosion current density of copper in the 0.1M HNO_3 solution, as illustrated in Fig.2-4.

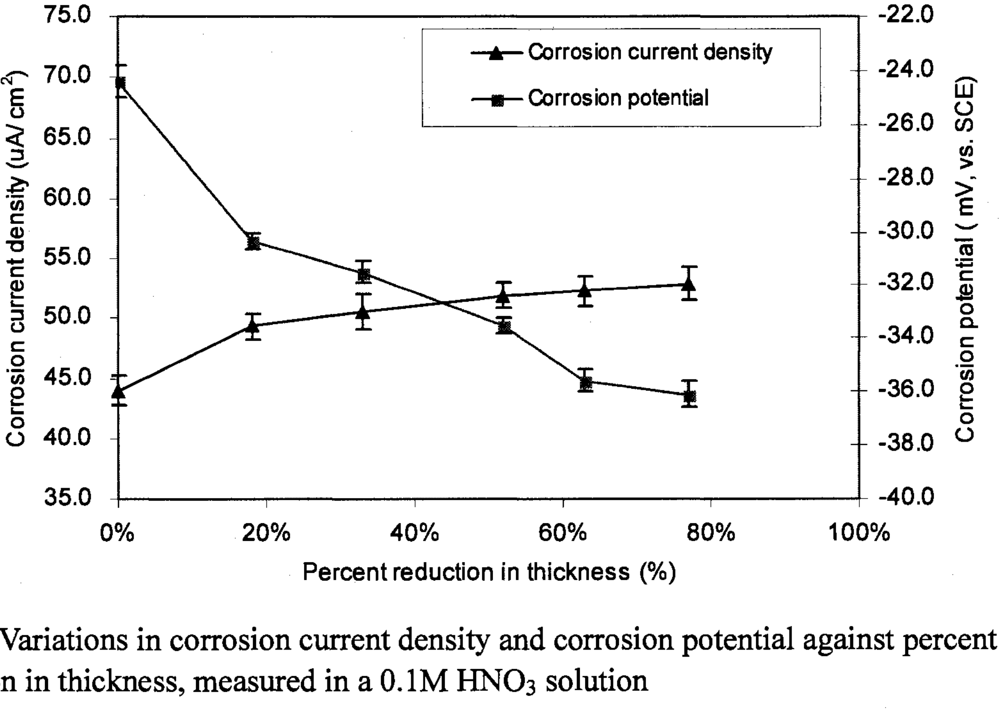

Fig.2-4 Variations in corrosion current density and corrosion potential against percent reduction in thickness, measured in a 0.1M HNO_3 solution

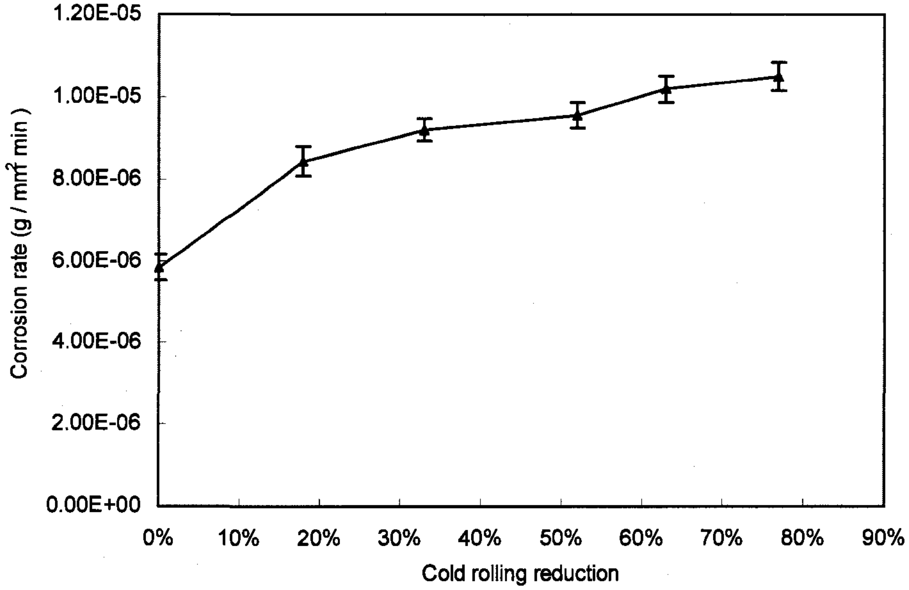

Fig.2-5 Corrosion weight loss in 1M HNO_3 solution as a function of percent reduction in thickness

The effect of cold work on corrosion of copper in the NaCl solution was different from that in the HNO_3 solution. Fig.2-6 illustrates the corrosion behavior of copper in the 3.5% NaCl solution. As shown, the corrosion current density initially increased with the cold work, but somehow decreased slightly as the percent reduction was further increased. Changes in the corrosion potential with the prior cold work were consistent with the changes in the corrosion current density. As illustrated, the corrosion potential decreased initially and then increased with further cold work.

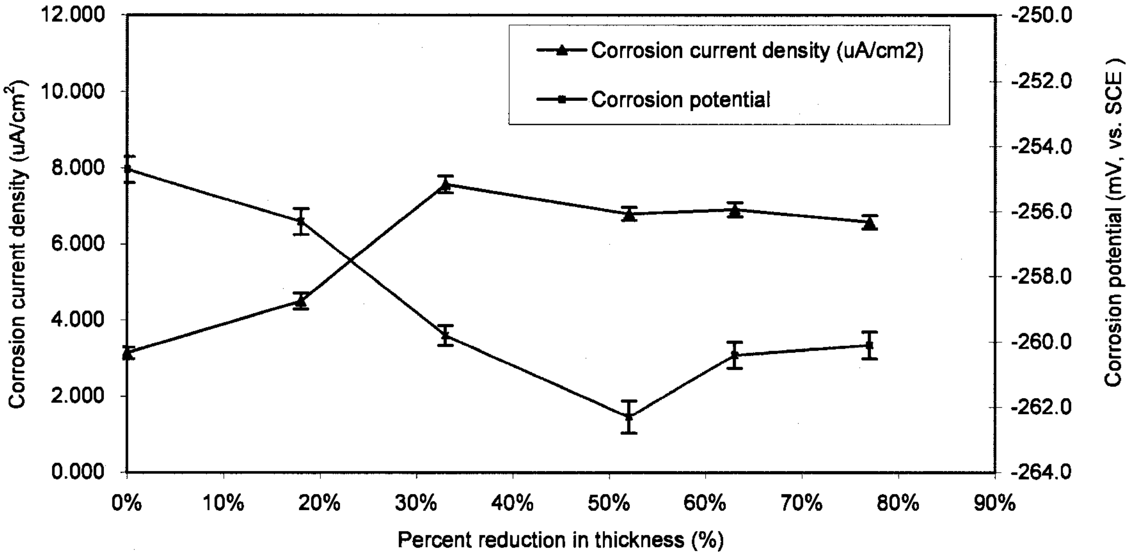

Fig.2-6 Variations in corrosion current density and corrosion potential against percent reduction in thickness, measured in 3.5% NaCl solution

The different responses of copper to the different solutions were further investigated by evaluating the polarization behavior of copper in the solutions, respectively. Fig.2-7. presents potentiodynamic polarization curves of copper specimens in 3.5% NaCl and 0.1M HNO_3 solutions, respectively. One may see that copper performed better in the 3.5% NaCl solution than in the 0.1M HNO_3 solution in terms of dissolution. It is worth noting that the corrosion current density i_{corr} of copper in the 0.1M HNO_3 solution (40~50 $\mu A/cm^2$) is almost one order of magnitude higher than that in 3.5% NaCl solution (1~5$\mu A/cm^2$). This means that copper dissolved much faster in the nitric acid solution.

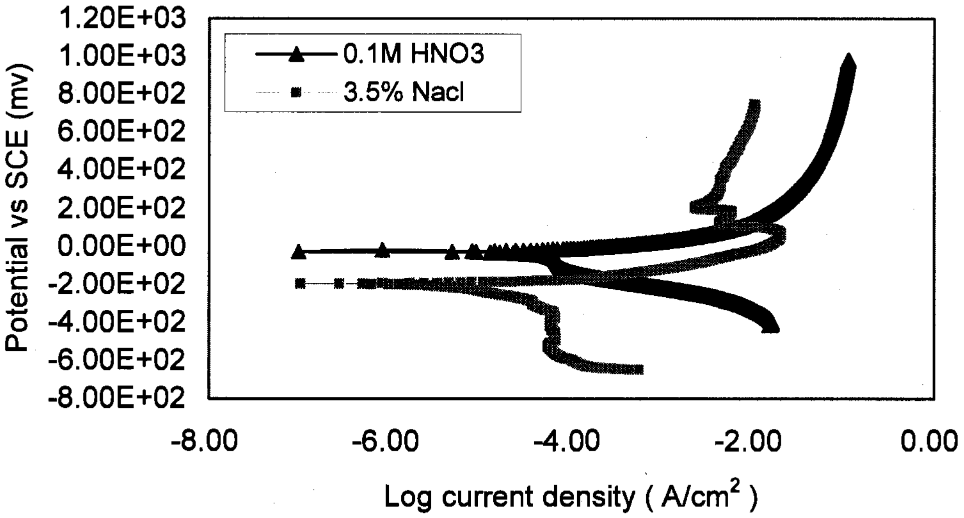

Fig.2-7 Polarization curves of copper in 3.5% NaCl and 0.1M HNO_3 solutions, respectively (samples in annealed state).

The electrochemical behavior of a metal is largely dependent on the electron activity, which may be evaluated by the electro work function, a minimum energy required to move electrons from inside the metal to its surface with zero kinetic energy [110]. The higher the EWF, the less active are the electrons. Fig.2-8 shows variations in the electron work function as a function of the percent reduction in thickness. For those samples etched by the 0.1M HNO_3 solution for 2 min, the electron work function decreased with an increase in cold work. Etching by the nitric acid solution could dissolve an additional deformed layer caused by polishing without forming a surface film that might affect the EWF measurements. Therefore, the measured results could mainly reflect the effect of plastic deformation on EWF. Electron work functions of annealed and cold-rolled copper specimens after being immersed in the 3.5% NaCl solution for 40 minutes were also illustrated in Fig.2-8. One may see that the electron work function increased slightly with the percent reduction in thickness in this solution.

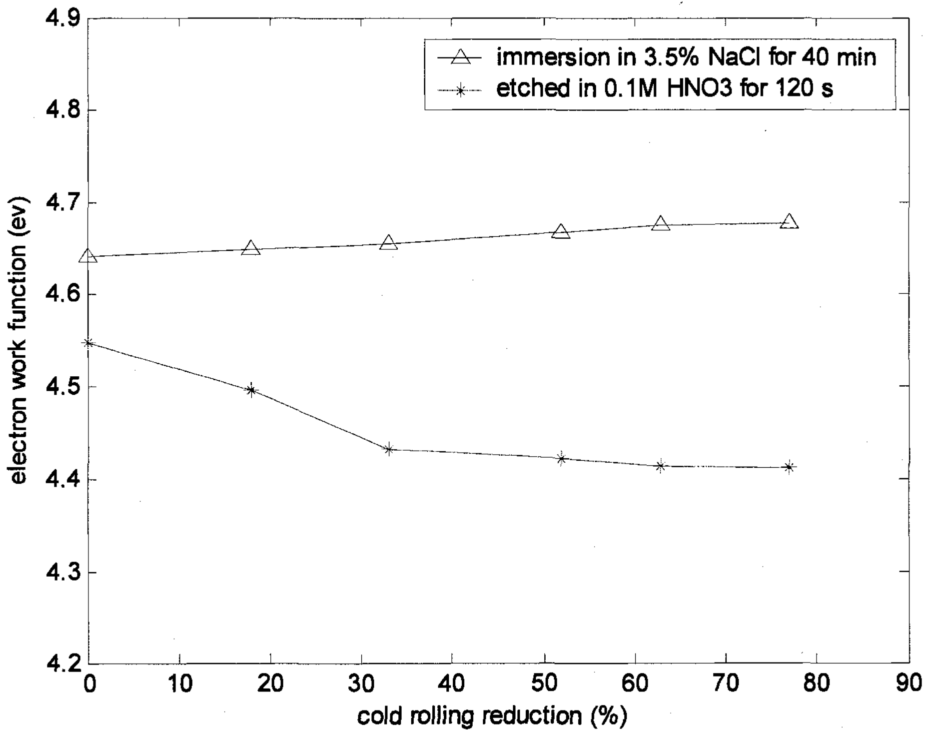

Fig.2-8 Variations in electron work function as a function of cold rolling reduction (For each data point, standard deviation varies between 0.06% ~1% of average)

2.2.3 Effect of prior cold work on corrosive wear

Pin-On-Disc sliding wear tests were performed in 3.5% NaCl and 0.1M HNO_3 solutions, respectively, to investigate effects of prior cold work on the corrosive wear behavior of copper in the two solutions. Three normal loads were used: 1N, 3N and 5N.

In this study, the wear loss caused by pure mechanical wear during corrosive wear was evaluated by means of corrosive wear test under full cathodic protection. Fig.2-9 and Fig.2-10 show variations in wear rate (volume loss per unit sliding distance) as a function of applied cathodic protection potential. As shown, the wear rates became stable (reached minima) at about –1000mV and –800 mV relative to the open circuit potential (OCP) for wear measured in 0.1M HNO_3 and 3.5% NaCl solutions, respectively. Therefore, the cathodic protection potentials for evaluating the contribution of pure mechanical wear to corrosive wear in these two solutions were chosen to be –1200mV and –1000 mV relative to the OCP, respectively.

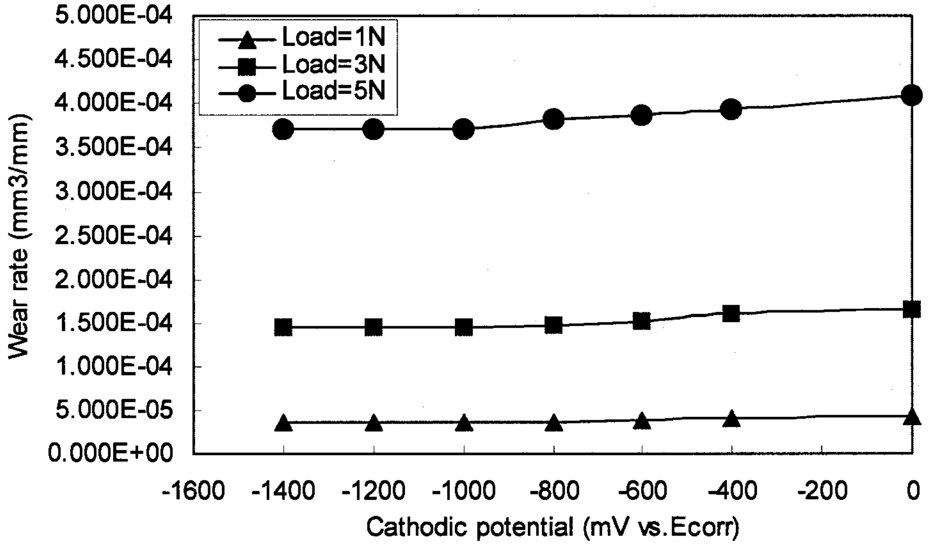

(a)

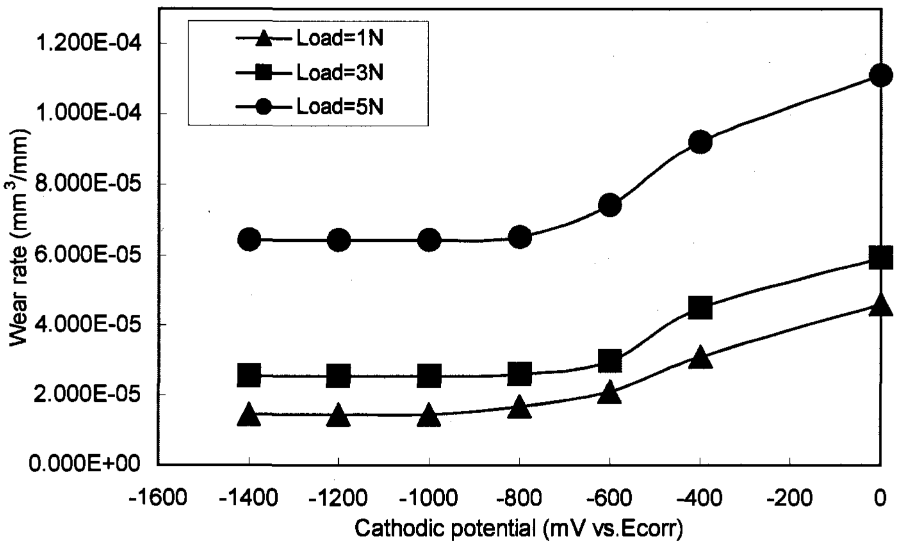

(b)

Fig.2-9 Variation of wear rates as a function of applied cathodic protection potential in 0.1M HNO_3 solution: (a) annealed sample; (b) 77% reduction sample (For each data point, standard deviation varies between 1% ~3% of average).

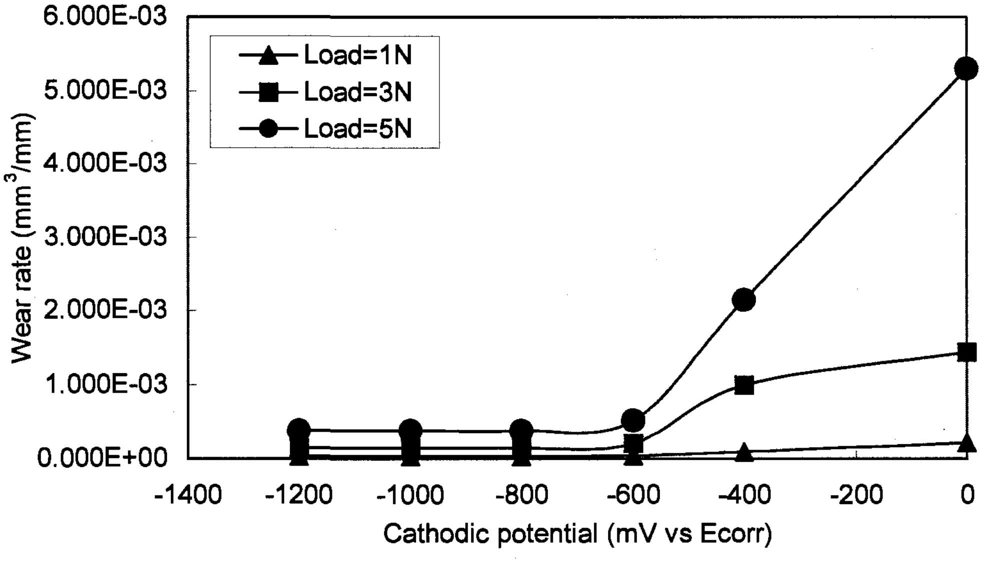

(a)

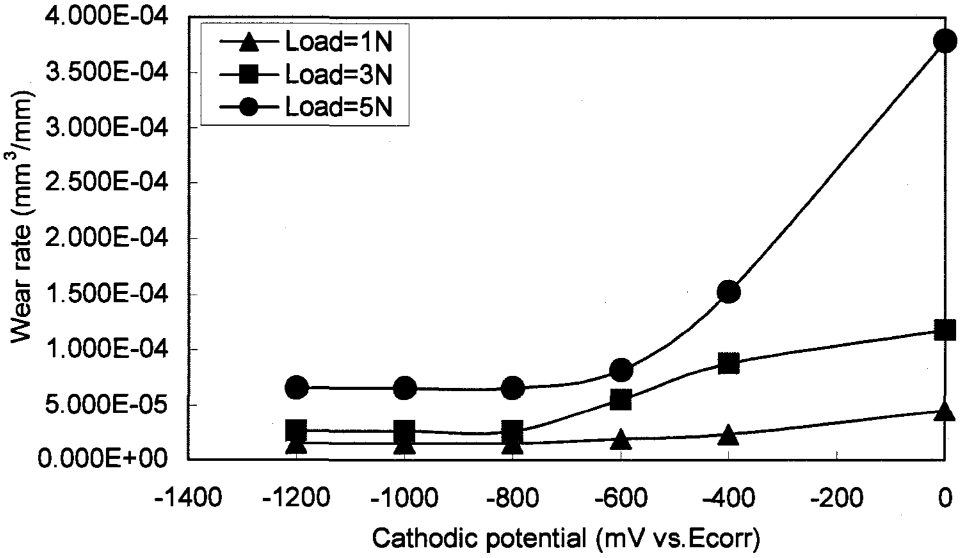

(b)

Fig.2-10 Variation of wear rates as a function of applied cathodic protection potential in 3.5% NaCl solution: (a) annealed sample; (b) 77% reduction sample (For each data point, standard deviation varies between 1% ~3% of average)

Fig.2-11 and Fig.2-12 illustrates the effect of prior cold work on total corrosive wear and pure mechanical wear of copper in 0.1M HNO_3 and 3.5% NaCl solutions, respectively. As shown, in both the solutions, the mechanical wear decreased with increasing the percent rolling-reduction in thickness. Under the same loads, mechanical wear losses in the different corrosive solutions were very close, which could be an indication that the corrosion process was effectively suppressed by the cathodic protection.

For the total corrosive wear rates, in the 0.1M HNO_3 solution, under a load of 1N, the wear rate was relatively stable with respect to the cold work. While under higher loads (3N and 5N), the wear rate decreased initially with the percent rolling reduction and became stable after the percent reduction reached 20%.

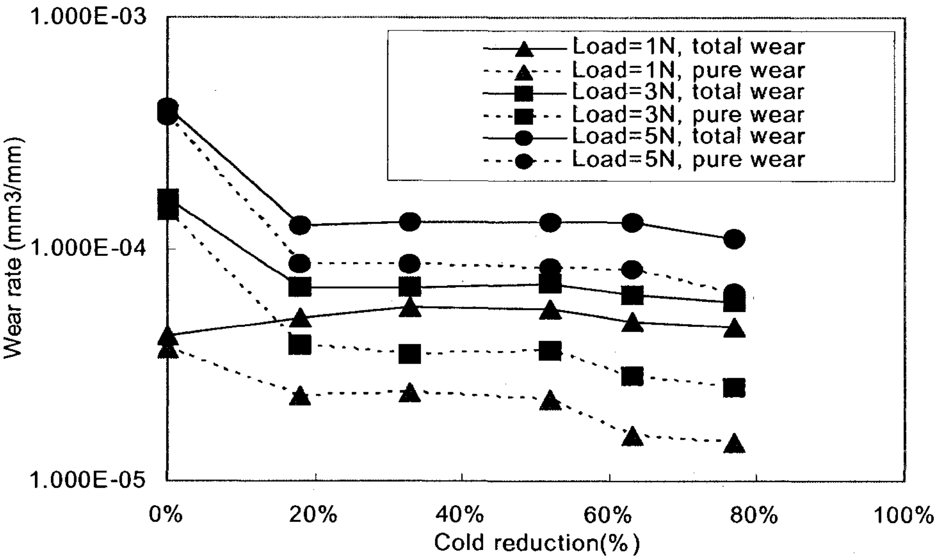

Fig. 2-11 Effect of prior cold work on total corrosive wear and pure mechanical wear in 0.1M HNO_3 (For each data point, standard deviation varies between 1% ~3% of average)

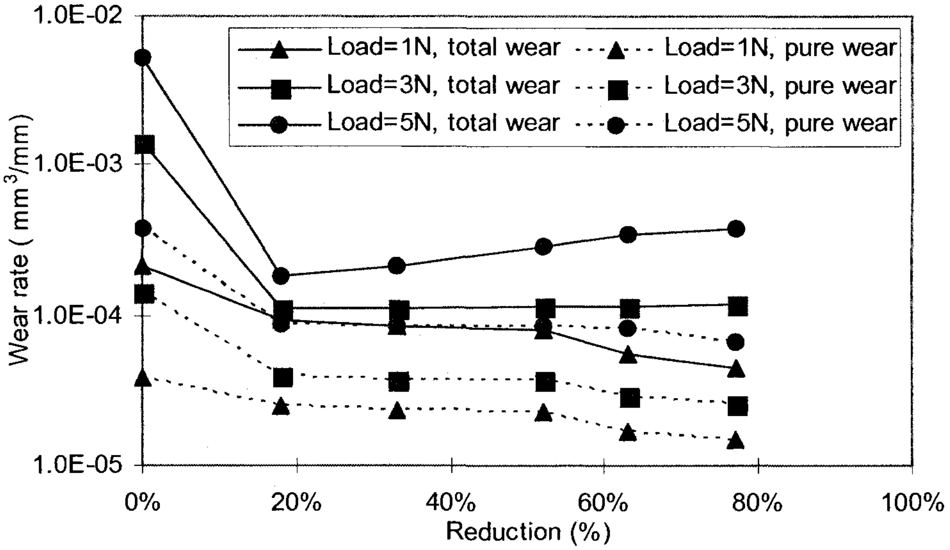

Fig. 2-12 Effect of prior cold work on total corrosive wear and pure mechanical wear in 3.5% NaCl solution (For each data point, standard deviation varies between 1% ~3% of average)

Wear of copper in the 3.5% NaCl solution was similar to that in the 0.1M HNO_3 solution. As shown in Fig.2-12, for all the loads, the wear rate was reduced by cold work and then became stable. However, under the highest load of 5N, the wear rate slightly rose after the percent reduction reached 20%.

In this study, effect of cold work on the wear loss caused by the corrosion-wear synergy (S) was also evaluated. The total material loss, T, is related to the synergy by (ASTM Practice G119-04):

$$T = W_0 + C_0 + S \qquad (2.3)$$

Where W_0 is the wear rate in the absence of corrosion, C_0 is the corrosion rate in the absence of wear, and S is the synergistic component which results from the interaction of corrosion and wear processes.

Fig. 2-13 and Fig.2-14 illustrate the effect of prior cold work on the synergy between wear and corrosion in 0.1M HNO_3 and 3.5% NaCl solutions, respectively. In the 0.1M HNO_3 solution, as shown in Fig. 2-13, the synergistic component or the wear loss (per unit sliding distance) caused by the corrosion-wear synergy increased with the percent reduction in thickness. The ratio of the synergistic component to the total wear loss was found to increase with the prior cold work and eventually became saturated when the cold work reached a certain level. Besides, this ratio decreased with the applied load. In the 3.5% NaCl solution (Fig.2-14), however, the synergistic component initially decreased with increasing the percent reduction and then became relatively stable under loads of 1N and 3N. While under the higher load of 5N, the synergistic component decreased initially and then increased with the percent reduction in thickness.

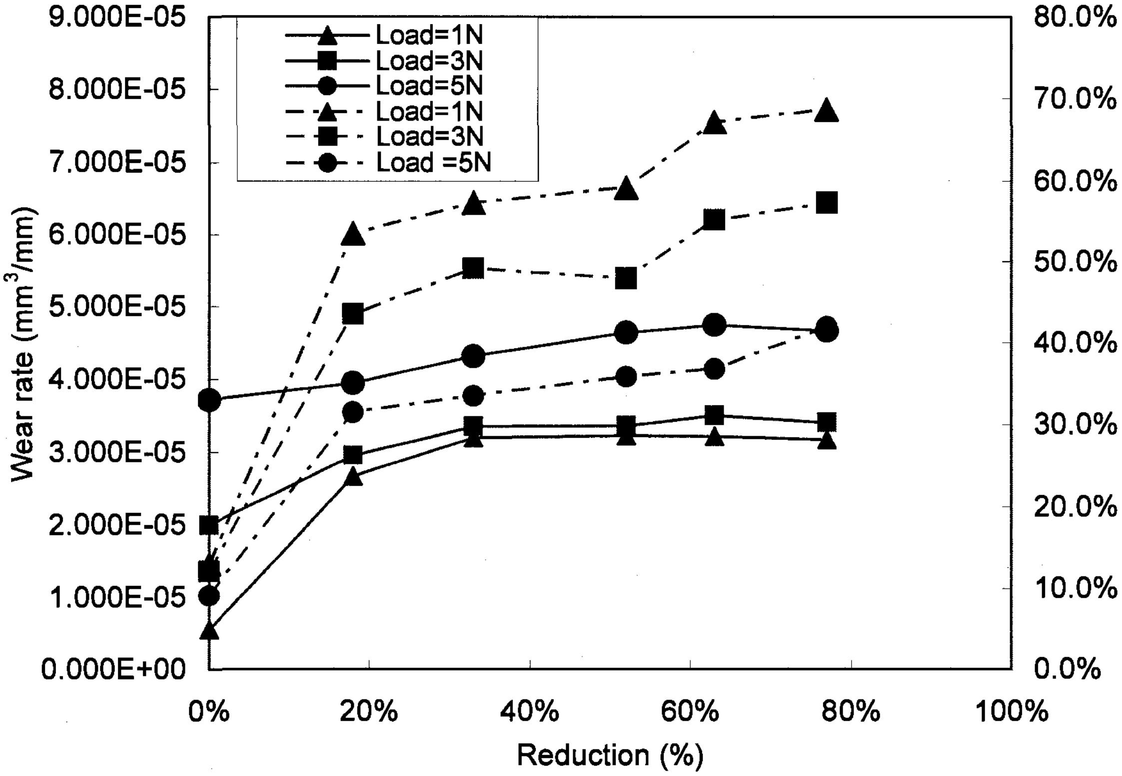

Fig. 2-13 effect of prior cold work on the synergy of wear and corrosion in 0.1M HNO_3 solution (solid line: synergy component; dashed line: the percentage of synergy component in total wear; For each data point, standard deviation varies between 1% ~3% of average)

Fig. 2-15 illustrates variations in friction coefficient as a function of the percent reduction in thickness in the different solutions. It was observed that the friction coeffecient of copper in the 3.5% NaCl solution was higher than that in the 0.1M HNO_3 solution.

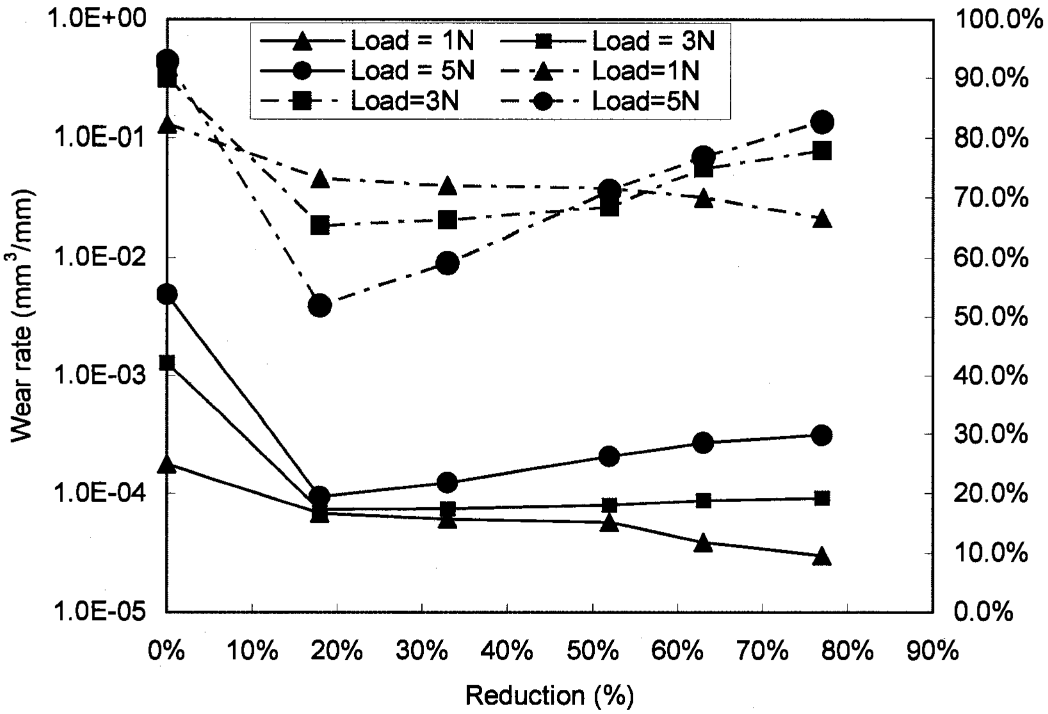

Fig. 2-14 effect of prior cold work on the synergy of wear and corrosion in 3.5% NaCl solution (solid line: synergy component; dashed line: the percentage of synergy component in total wear; For each data point, standard deviation varies between 1% ~3% of average)

The worn surfaces after the wear tests were examined by SEM. In the 0.1M HNO_3 solution, as shown in Fig.2-16 (a) and (b), the samples without cathodic protection displayed a uniform wear pattern with smooth worn surface and pitting corrosion. In the 3.5% NaCl solution, the wear pattern was different: for samples without cathodic protection, as shown in Fig.2-17 (a) and (b), microgrooves, ridges, surface flaking, pitting, corrosion products, and wear debris were all visible. For both the solutions, the samples under cathodic protection only displayed wear grooves without any visible pitting or corrosion product on the wear tracks (Figs. 16(c) and (d); Figs. 2-17(c) and (d)), which could imply that the cathodic protection was effective in suppressing corrosion for evaluating the contribution of pure mechanical wear to the total corrosive wear loss.

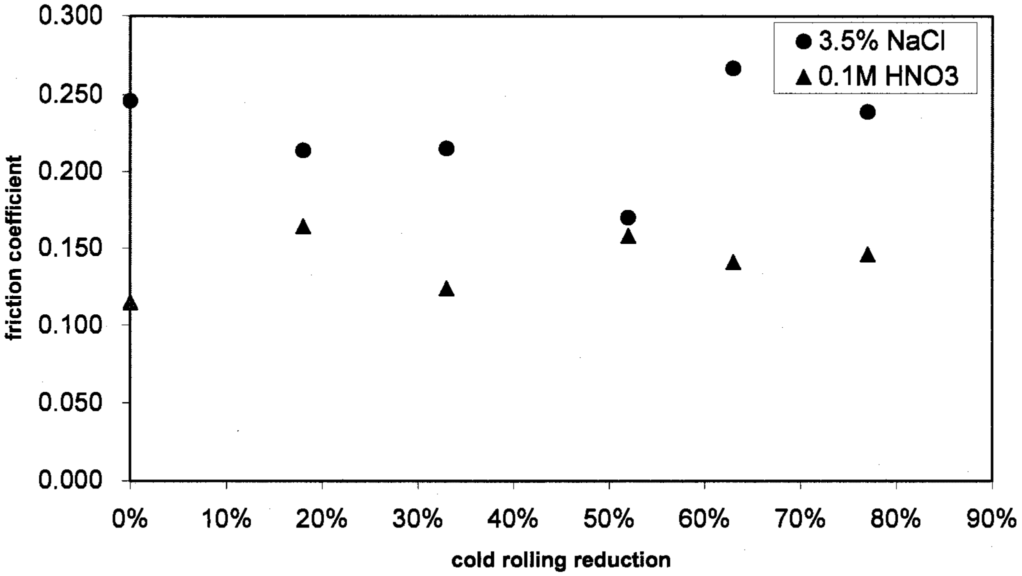

(a) load=1N

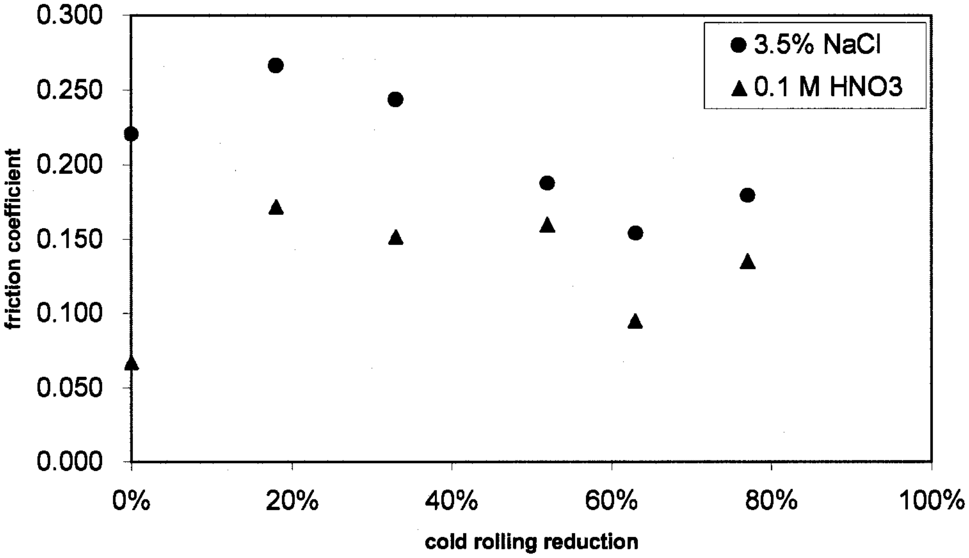

b) load =3N

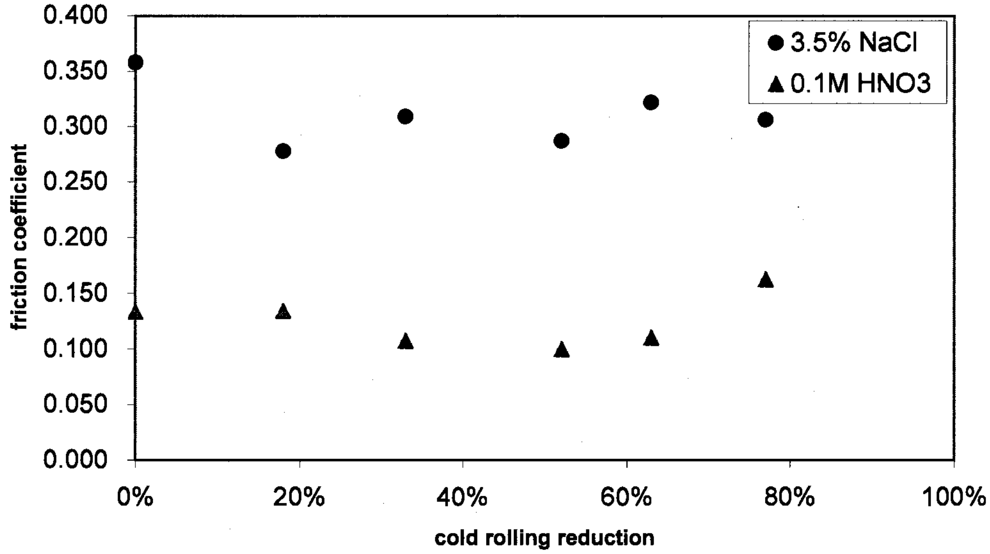

(c) load=5N

Fig. 2-15 Friction coefficients in different solutions as a function of percent reduction under various normal loads (For each data point, standard deviation varies between 1% ~2% of average)

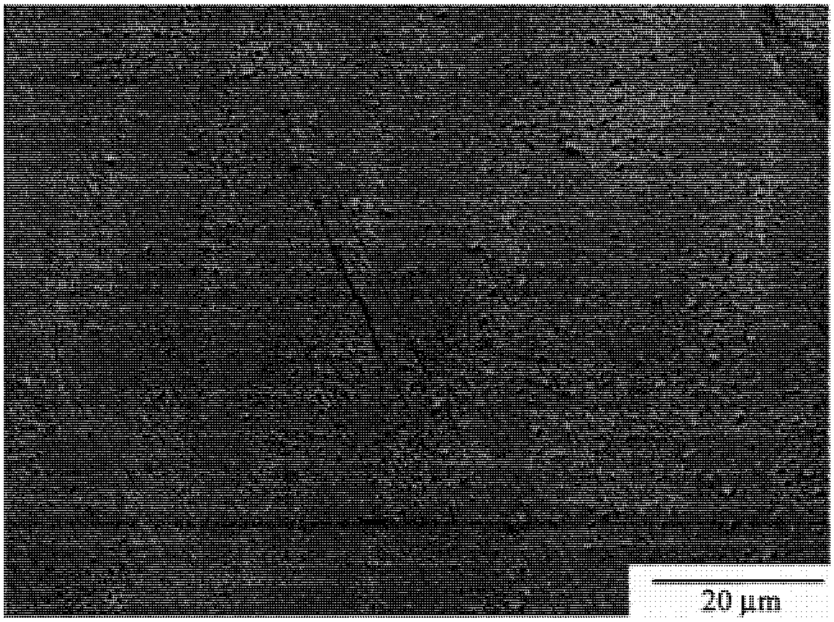

(a)

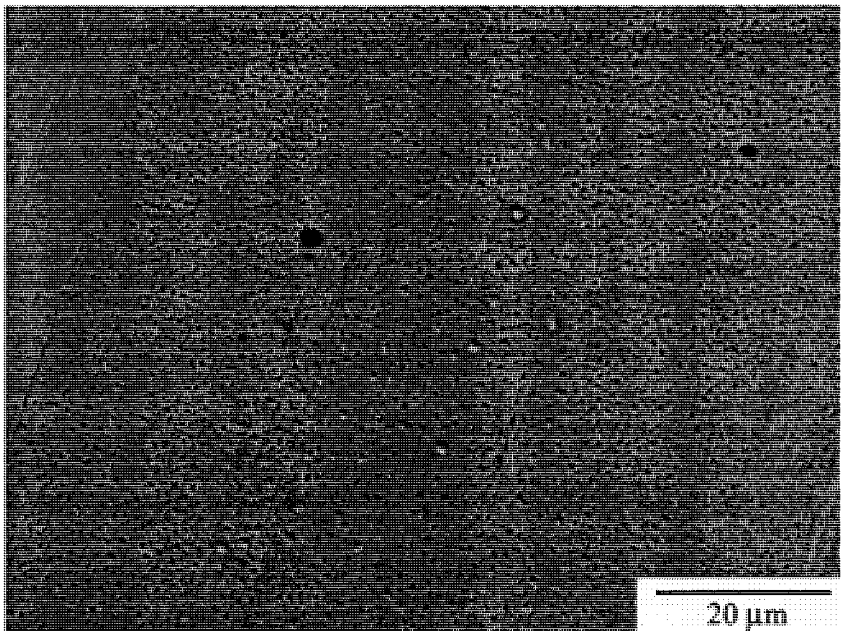

(b)

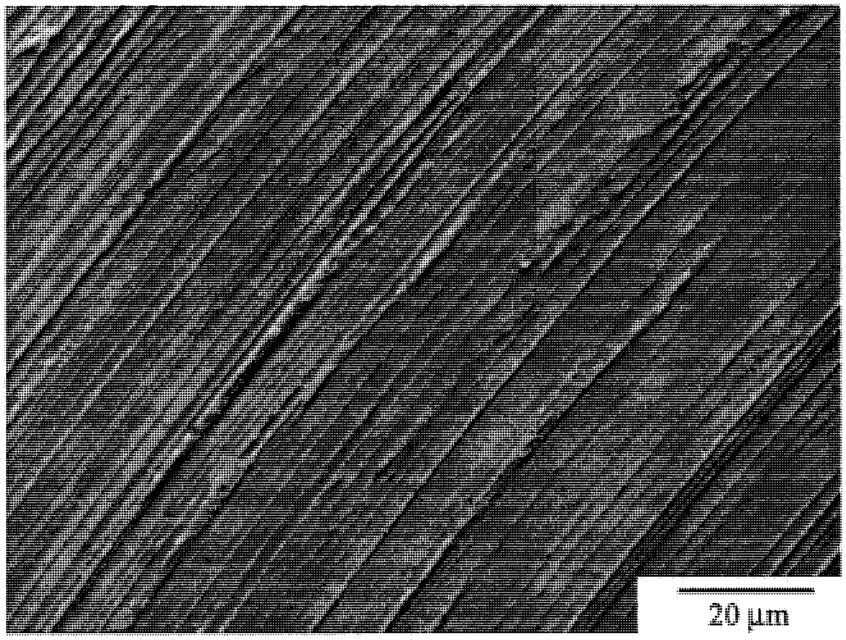

(c)

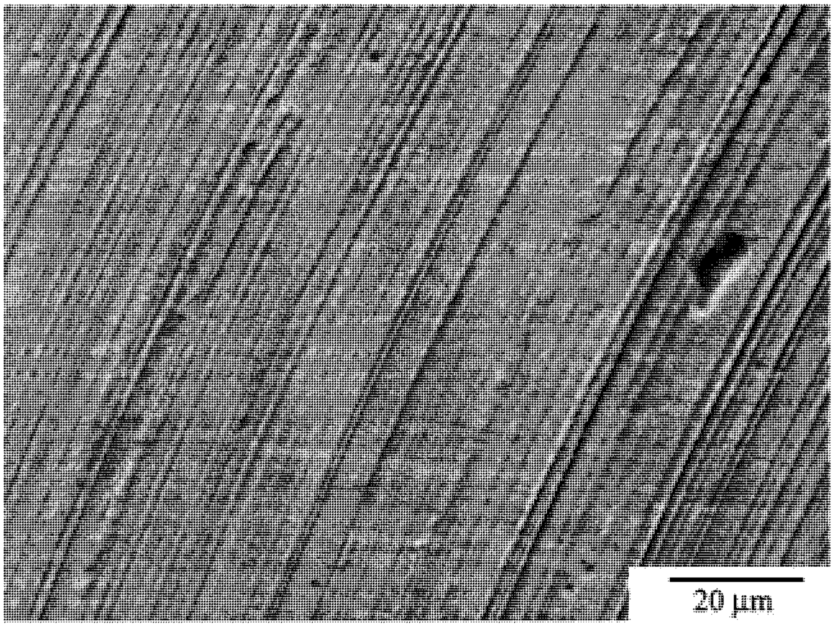

(d)

Fig. 2-16 SEM photograph of the wear track obtained in 0.1M HNO_3 solution
(a) annealed sample, without cathodic protection
(b) 77% reduction sample, without cathodic protection
(c) annealed sample, with full cathodic protection
(d) 77% reduction sample, with full cathodic protection

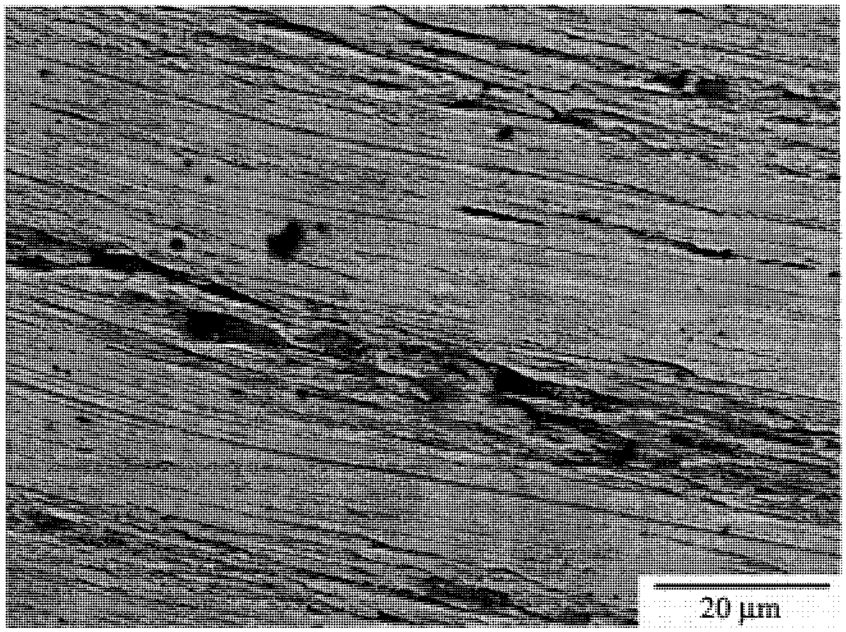

(a)

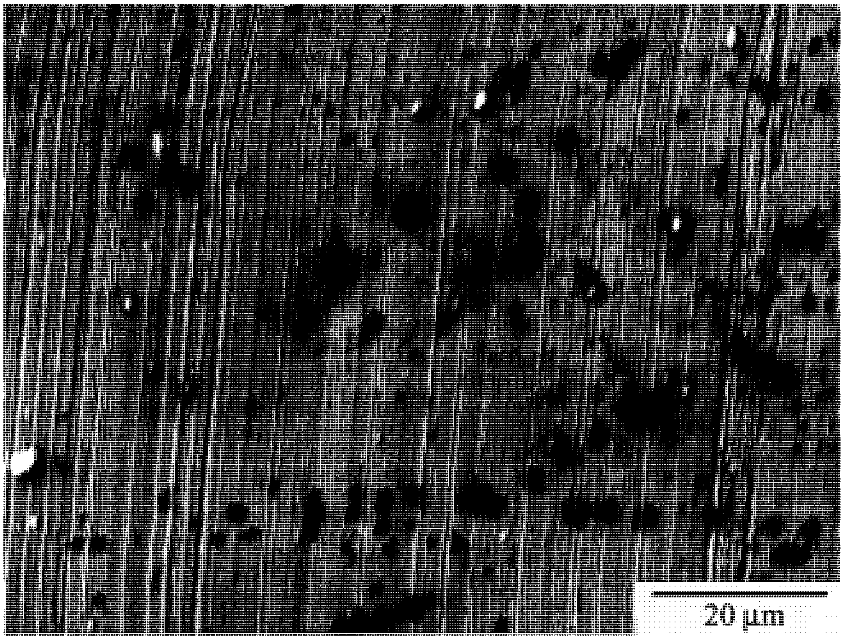

(b)

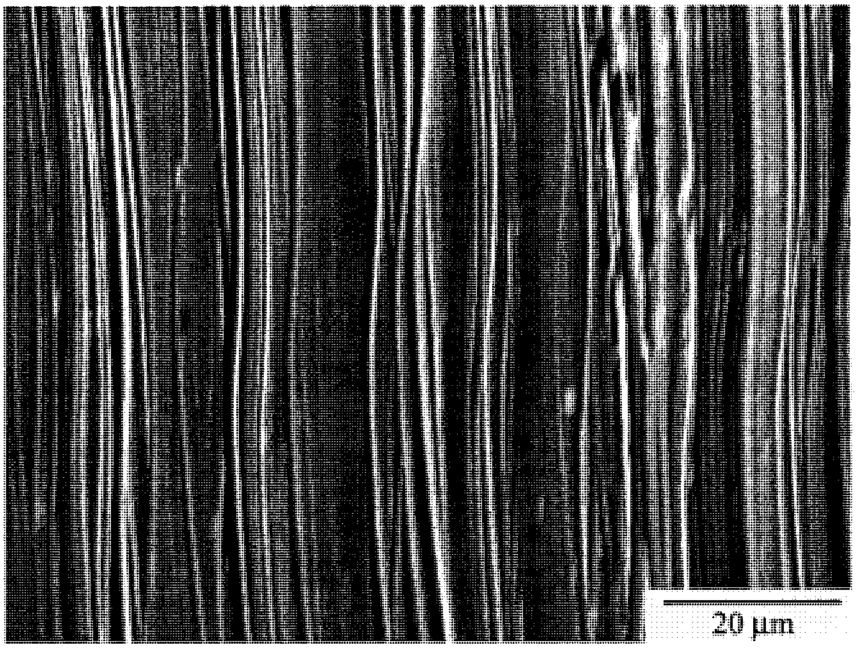

(c)

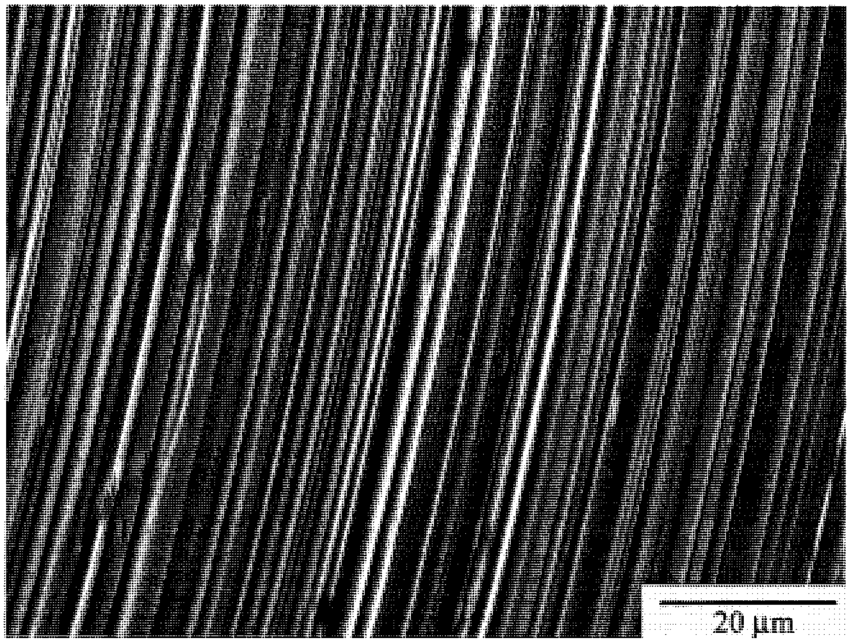

(d)

Fig. 2-17 SEM photograph of the wear track obtained in 3.5% NaCl solution
(a) annealed sample, without cathodic protection
(b) 77% cold-rolled sample, without cathodic protection
(c) annealed sample, with full cathodic protection
(d) 77% cold-rolled sample, with full cathodic protection

2.3 Discussion

2.3.1 The effect of prior cold work on the corrosion behavior

Figs. 2-4 and 2-5 clearly indicate that the prior cold work enhanced corrosion of copper in the HNO_3 solution. This may be explained as follows: The prior cold work increased the dislocation density and thus led to higher stored strain energy, which could increase the driving force for corrosion [111]. This may also be indicated by the electron work function measurement. As demonstrated in Fig.2-8 (for samples etched by the HNO_3 solution), the plastic deformation decreased the electron work function. Attempts have been made to investigate the influence of deformation on the electron work function [90, 91]. It has been demonstrated that the EWF decreases with plastic deformation regardless if it is tensile or compressive [92]. This implies that dislocations render electrons more active, and thus, increase the driving force for electrochemical reactions. Such a relationship between the EWF and plastic deformation has been well demonstrated using an electrostatic model [93].

In addition to the effect of dislocations on the electron activity, strain-induced micro-electrochemical heterogeneity, e.g., inhomogeneous dislocation distribution and microtexture, may also accelerate corrosion to some extent [72]. Such heterogeneity helps to form microelectrodes, which promote electrochemical reactions.

In the NaCl solution, copper showed different corrosion behavior. As illustrated in Fig.2-6, the corrosion current increased first and then decreased as the cold work was increased. This could be explained based on the different capabilities of forming a surface oxide film in the different solutions.

In seawater, a thin film of cuprite (Cu_2O) and clinoatacamite ($Cu_2(OH)_3Cl$) may form on the surface of copper [112]. Cu_2O is a p-type semiconductor which can protect copper from further corrosion, since copper ions and electrons have difficulty migrating through the Cu_2O oxide film [113]. As a result, copper has improved polarization behavior in the NaCl solution (Fig.2-7). This is also consistent with the EWF measurement, which shows a slight increase in EWF for copper samples etched by the NaCl solution (Fig.2-8). Since dislocations enhance atomic migration, plastic deformation may promote or accelerate the formation of surface oxide film. Therefore, after initial increase, the corrosion current of copper in the 3.5% NaCl solution decreased to some extent as the plastic strain was further increased as Fig.2-6 illustrates. However, the situation changed when copper was exposed to the dilute HNO_3 solution. According to a potential-pH diagram of Cu [114] (Fig.2-18), Cu_2O is stable only in solutions with pH over 3, which means that when copper specimens were immersed in 0.1M HNO_3 solution (pH<3), no stable Cu_2O film was present on its surface. Therefore, the copper was relatively active in this solution as shown in Fig.2-7. Under such circumstances, large plastic strains resulted in higher corrosion rates and lower EWF values as Fig.2-5 and Fig.2-8 illustrate, respectively.

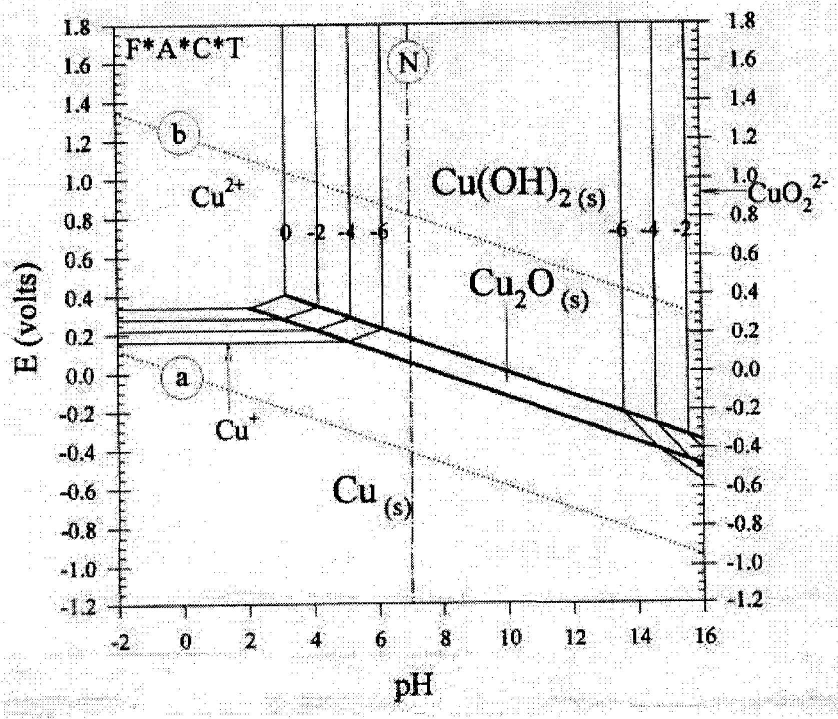

Fig.2-18 The Cu Pourbaix diagram at 298K

2.3.2 Pure mechanical wear

Wear test in corrosive medium under full cathodic protection is generally accepted as a method to separate pure mechanical wear from total corrosive wear [10,115]. However, when a material is sensitive to hydrogen embrittlement, the wear loss increases with increasing the magnitude of the cathodic potential after it exceeds a critical value, and the cathodic protection may not be appropriate to use [115]. In this study, since copper is not sensitive to hydrogen embrittlement [116], it may be adequate to use cathodic protection for evaluating pure mechanical wear. As shown in Figs. 2-9 and 2-10, the wear rates became almost constant as the applied cathodic potentials were below –1000mV and –800 mV for tests in 0.1M HNO_3 and 3.5% NaCl solutions, respectively. It was found that the pure mechanical wear rates measured in the two different solutions were close, indicating that corrosion could be effectively suppressed. The worn surface observations (Figs. 2-16 and 2-17) may also lead to the same conclusion. As shown, no trace of corrosion was observed on the worn surfaces under cathodic protection, compared those without cathodic protection.

Pure mechanical wear of copper measured in both 0.1M HNO_3 solution and 3.5% NaCl solution decreased with increased percent reduction in thickness, as evidenced in Fig.2-11 and Fig. 2-12. This effect can be attributed to the strain-hardening effect, i.e., the cold work hardened the material due to the increases in 1) the dislocation density and 2) the grain boundary density as shown in Fig.2-3. These two factors increased the strength of copper and consequently reduced the wear loss.

It should be pointed out that, theoretically, the ultimate tensile strength of a metal is not affected by prior tensile deformation associated with an increase in the dislocation density if the tensile stress is applied along the same direction. This implies that such an increase in the dislocation density may not benefit the resistance of the metal to tensile failure. However, during a wear process, the wearing stress varies all the time, including its magnitude and direction. As a result, the configuration of dislocations is much more complex than that under a uniaxial stress. The interaction between dislocations could therefore be stronger. Or in other words, the dislocations may pin each other more strongly. Consequently, in addition to the increase in the grain boundary density by cold work, the increase in the dislocation density should also be beneficial to the wear resistance.

2.3.3 Effects of prior cold work on corrosive wear

- The synergistic effect

Corrosive wear involves combined actions of wear and corrosion, which may promote each other. The corrosion-wear synergy resulted in additional wear loss and such extra wear loss largely depended on the corrosive solution, load, and the prior cold work. For instance, the wear loss caused by the corrosion-wear synergy under a load of 5N took 8% of total wear loss, i.e., S/T= 8%, for annealed sample in the 0.1M HNO_3 solution, while this ratio increased up to about 35% for deformed samples (Fig.2-13). However, the S/T ratio of copper in the 3.5% NaCl solution decreased from more than 90% down to

53% when annealed copper was deformed with a rolling reduction of 20% as Fig. 2-14 illustrates.

The different S/T ratios in the different solutions are understandable. In the NaCl solution, corrosion of copper was reduced by the formation of a passive film on surface. Therefore, a large S/T ratio can be expected when worn in this solution, since wear could destroy the passive film and thus considerably accelerate corrosion and promote the corrosion-wear synergy. While in the HNO_3 solution, wear may not result in a significant increase in corrosion, since the dissolution of copper in this solution is already severe and the resultant corrosion-wear synergy may not be as strong as that in the NaCl solution. As a result, the corresponding S/T ratio is smaller than that in the NaCl solution.

The prior cold work certainly affects the S/T ratio. In the HNO_3 solution, S/T increased with an increase in the amount of cold work. As discussed earlier, cold work introduced dislocations and made the surface electrons more active, leading to enhanced corrosion and thus promoted synergy between corrosion and wear. As a result, the S/T ratio increased, which, however, became saturated after the cold work was sufficiently large as Fig.2-13 illustrates.

The situation is more complicated when copper was worn in the NaCl solution due to the formation of a passive film on its surface. As shown in Fig.2-14, under higher loads of 5N and 3N, the S/T ratio decreased initially and then increased as the amount of cold work was increased. This could be explained as follows. When the cold work was small, dislocations accelerated passivation and repassivation, which helped to reduce corrosion and thus the corrosion-wear synergy. However, when the cold work was further increased, the interface between the passive film and the substrate could be less strong or less coherent due to the existence of higher-density dislocations at the passive film/substrate interface. This could make the passive film relatively easier to be removed by the wearing force. Consequently, corrosion and corrosive wear were enhanced as the cold work was increased. However, if the load was small, the damage to the passive film was less, which might not increase the S/T ratio. This could be a possible reason why the S/T ratio continuously decreased with respect to the cold work when the load was 1 N (Fig.2-14).

- Effect of prior cold work on the total wear loss

The effect of prior cold work on the total wear loss was different in the different solutions: in the 0.1M HNO_3 solution (Fig.2-11), under the load of 1N, the wear rate was relatively stable with respect to the cold work. This happened probably because the increase in corrosion due to cold work was compensated by accompanied strain-hardening effect that reduced wear. Under higher loads of 3N and 5N, however, the wear rate decreased with cold work but eventually became stable when the cold work was larger than 20%. Such a change is understandable, since under higher loads, the contribution of mechanical wear increased (see Fig.2-11). In this case, the increase in hardness by the cold work could play a more predominant role in resisting wear, although corrosion was also enhanced by the cold work. As a result, the cold work helped to reduce corrosive wear initially, and the wear rate became stable when the cold work reached a certain level (Fig.2-11) at which a stable balance between corrosion and wear was established.

In the case of wear in the 3.5% NaCl solution, due to the lower corrosion rate of copper in this type of solution, mechanical wear could be dominant. As a result, the wear rate was reduced by cold rolling (Fig.2-12). The slight increase in wear rate at larger cold work under the highest load of 5N could be attributed to larger damage to the surface passive film under more severe wear conditions.

It is worth noting that although the corrosion rate in the 0.1M HNO_3 solution was one order of magnitude higher than that in 3.5% NaCl solution, the corrosive wear rate was, however, higher in the 3.5% NaCl solution than in 0.1M HNO_3 solution. This implies that mechanical wear, including pure mechanical wear and additional mechanical wear due to the existence of corrosion, could play a predominant role in corrosive wear of copper. Fig. 2-15 illustrates variations in friction coefficient with the cold rolling reduction in different solutions. As shown, the friction coeffecient of copper in 3.5% NaCl solution was higher than that in 0.1M HNO_3 solution. The higher friction in the NaCl solution led to larger lateral force on the target surface, and thus, resulted in a larger wear loss. This could be a possible reason why copper had a larger loss when worn in NaCl solution.

2.4 Conclusion

Effects of prior cold work on corrosion and corrosive wear of copper in 0.1M HNO_3 and 3.5% NaCl solutions, respectively, were investigated. The following conclusions were drawn:

1. Prior cold work showed significant influence on the corrosion behavior of copper. In 0.1M and 1M HNO_3 solutions, the corrosion rate of copper increased with an increase in the percent cold-rolling reduction in thickness. However, in the 3.5% NaCl solution, the corrosion rate increased initially and then decreased as the cold work was increased.

2. Prior cold work had significant influence on the pure mechanical wear of copper. In both the solutions, the pure mechanical wear decreased with an increase in the percent reduction in thickness.

3. Prior cold work had significant influence on corrosive wear of copper. In the 0.1M HNO_3 solution, the ratio of the synergistic component to the total wear increased with the cold work and became saturated when the cold work reached a certain level. In the 3.5% NaCl solution, however, this ratio decreased initially and then became relatively stable with respect to the cold work.

4. Wear of copper in the 3.5% NaCl solution was larger than that in 0.1M HNO_3 solution, although in the former solution copper showed lower corrosion rate. This could be attributed to the higher frictional force when worn in the NaCl solution.

Chapter 3

Corrosion and corrosive wear of annealed, impact-fractured and slow bending-fractured surface layers of AISI 1045 steel in a 3.5% NaCl Solution

Previous studies have demonstrated that the wear-corrosion synergism can be markedly affected by the loading speed. In this study, effects of the loading speed or strain rate on corrosion and corrosive wear of annealed, impact-fractured and slow bending-fractured surface layers of AISI 1045 steel in a 3.5% NaCl solution were investigated using electrochemical, scanning Kelvin probing and electrochemical scratching techniques. In order to understand the mechanism responsible for the effects of loading speed on corrosion and corrosive wear, SEM fractography, X-ray line profile analysis and micro-hardness testing were employed to investigate changes in microstructure and corresponding mechanical properties with respect to the loading speed. Results of the experiments are explained in terms of the effect of strain rate on surface microstructure and corresponding electrochemical and mechanical properties, and consequently the corrosive wear behaviour of the steel.

3.1 Experimental details

AISI 1045 steel (0.43-0.50 wt% C, 0.60-0.90wt% Mn, maximum 0.04wt% P, maximum 0.05wt% S) was selected as a sample material. All samples were austenized at 810°C for 45 minutes and quickly cooled down to and maintained at 640°C for 30 minutes, followed by furnace cooling to room temperature. The microstructure of the sample was characterized by standard optical metallography (etchant: 2% NYTOL). Figure 3-1 shows the optical microstructure of the steel sample, which is a typical hypo-eutectoid structure: Ferrite + Pearlite.

Fig.3-1 Optical microstructure of the full-annealed 1045 steel

Samples for Charpy impact test were machined following the requirement specified in ASTM E 23 (Type A). The Charpy impact tests were performed at room temperature using a standard Charpy pendulum machine with a capacity of 360 J. Some of the Charpy samples were tested using a three-point-bending fixture in an Instron testing machine at a loading rate of 0.5mm/min. Charpy absorbed energy (CVN) and the slow-bending absorbed energy were determined. Fracture surfaces generated by both the tests were examined using SEM.

Micro-hardness of the fractured surface layer was evaluated using a Fischerscope H100C micro-mechanical probe (Fisher Technology Ltd., Winsor, CT, USA). A standard

Vickers diamond indenter was employed, which was pyramid-shaped and had an angle of 136° between faces. The indenter tip penetrated into the sample at a normal load that was increased continuously up to a designated level. The load was then gradually decreased back to zero. The entire loading and unloading processes were recorded automatically, resulting in a load-displacement curve. Hardness and elastic modulus could be determined from the curve, based on the attained stiffness of contact, contact depth and projected contact area. This system also incorporated a positioning device consisting of a microscope and a measuring stage, which allow precise location of the measurement point.

In order to qualitatively investigate the lattice distortions caused by deformation at different loading rates, residual microstrains in the fractured surface layers were determined through X-ray diffraction line profile analysis based on approximated profile shape-functions [117]. X-ray diffractograms of annealed, impact-fractured and slow bending-fractured surface layers were obtained using a Rigaku 3014 X-ray diffractometer with CuKα radiation, operated at 40 kV and 35mA in a continuous-scan mode. The scanning speed was 0.2 degree/min. A graphite crystal monochromator was used to obtain monochromatization. Kα1 lines were separated from the combined Kα1 and Kα2 lines using a computer program. The full-annealed sample was used as a reference sample. (110) and (220) peaks were selected for the line profile analysis.

Electrochemical tests, including potentiodynamic polarization, linear polarization and Tafel plot measurements, were performed using a computerized Gamry PC4/750 electrochemical system. For all the electrochemical experiments, a saturated calomel electrode (SCE) and a platinum (Pt) net were used as the reference electrode and the counter electrode, respectively. The electrolyte solution was 3.5% NaCl. All the experiments were performed at room temperature (~ 22 °C). The Potentiodynamic polarization experiments were performed at a scan rate of 0.33mV/s.

At least three linear polarization corrosion tests were performed for each sample to measure its polarization resistance Rp, starting from 9.0 mV below the open circuit potential (OCP) and ending at 9.0 mV above OCP. The scanning rate was 0.05 mV/s.

At least three Tafel plot corrosion tests were performed for each sample, starting from 100 mV below OCP and ending at 140 mV above OCP. The scanning rate was 0.1 mV/s. The corrosion current density icorr was calculated based on the following equation: (ASTM standard G3-89):

$$i_{corr} = \frac{b_a b_c}{2.303(b_a + b_c)R_p}$$

where i_{corr} = corrosion current density,

b_a = anodic Tafel slope,

b_c = cathodic Tafel slope,

R_p = linear polarization resistance

A scanning Kelvin probe (SKP), provided by the KP Technology Ltd. (Caithness, UK), was employed to investigate the influence of strain rate on the surface electron work function (EWF). The KP system had three sub-systems, including a digital oscillator, data acquisition, and sample translation, which are controlled by a host PC. A three-axis microstepper positioner permitted high-resolution sample positioning (0.4 μm per step) and the scanning area was 2mm x 2mm. A gold tip with diameter equal to 1mm was used. The oscillation frequency of the Kelvin Probe was 173Hz. Before the KP test, the annealed samples were polished using up to abrasive papers 600 grit and finally finished with 0.05μm alumina. The impact-fractured samples and slow bending-fractured samples were tested with the original fracture surfaces.

Performances of the annealed, impact-fractured and slow bending-fractured surface layer during corrosive wear were evaluated using an electrochemical scratch technique [18]. This technique is briefly described as follows: during the test, a specimen was immersed in a corrosive solution and a potential was applied to the specimen. The surface of a specimen was scratched by a diamond tip under a normal load. The cross-sectional profile of the scratch groove was measured using a profilometer; the dimensions of the profile represented wear loss of the surface caused by scratching in the corrosive solution under a specific potential. In this study, the corrosive medium was a 3.5% NaCl solution (NaCl + H_2O). The scratching tests were all performed under the open circuit potential. Surfaces of all the samples were polished using 600 grit abrasive paper and finally finished with 0.05μm alumina. It should be indicated that the polishing treatment was carefully done to ensure that only a very thin surface layer of about 100~200 μm was removed, which should not affect the evaluation of surface layer's electrochemical properties and its resistance to corrosive wear, since the fractured surface layers were fairly thick (more than 2000 μm, estimated from microindentation tests). Three normal loads were used: 5g, 10g, 30g. The moving speed of the tip was 6mm/s. Sliding distance was 4mm. The cross-sectional profiles of the scratch grooves were measured using an Atomic Force Microscope (Digital Instrument, Santa Barbara, CA, USA). For each sample, 3 scratch tests were made and 12 or more cross-sectional profiles were measured. The wear loss was obtained by averaging 12 measurements, represented by the volume loss per unit length of the scratch groove (mm^3/mm).

3.2 Results and discussion

3.2.1 Surface microstructure and mechanical behavior

Fig.3-2 illustrates fracture surfaces caused by Charpy impact and slow-bending, respectively. The fractographs of the surface resulting from the Charpy impact test shows relatively brittle features, i.e. cleavage facet and river pattern (Fig.3-2 (a) and (b)), while the fracture surface of the slow-bending samples exhibits ductile features, i.e. micro-void coalescence (Fig.3-2 (c) and (d)). Microcracks were observed in surface layers (Fig.3-3), which existed beneath the fracture surface of both types.

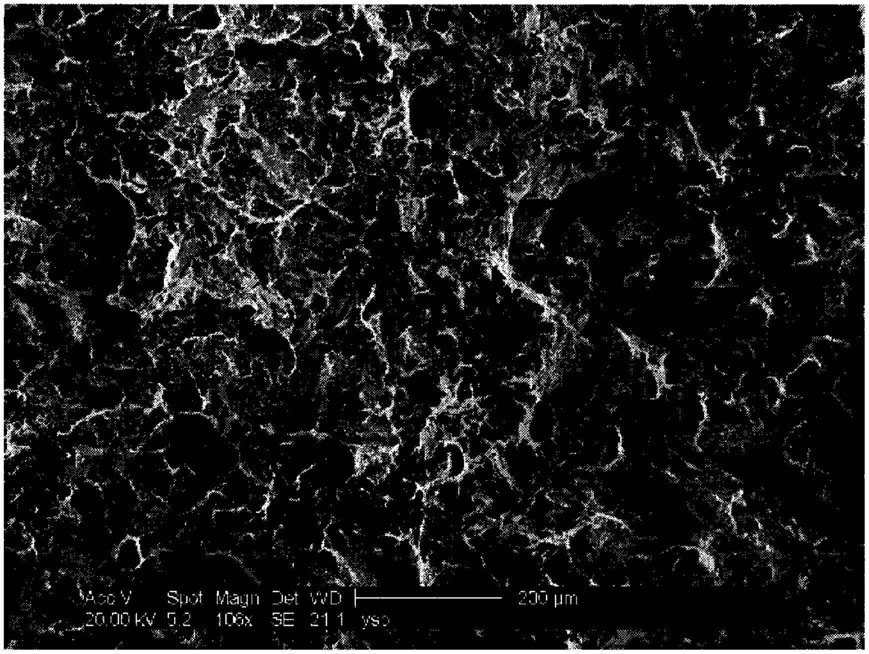

(a) Charpy impact fracture surface

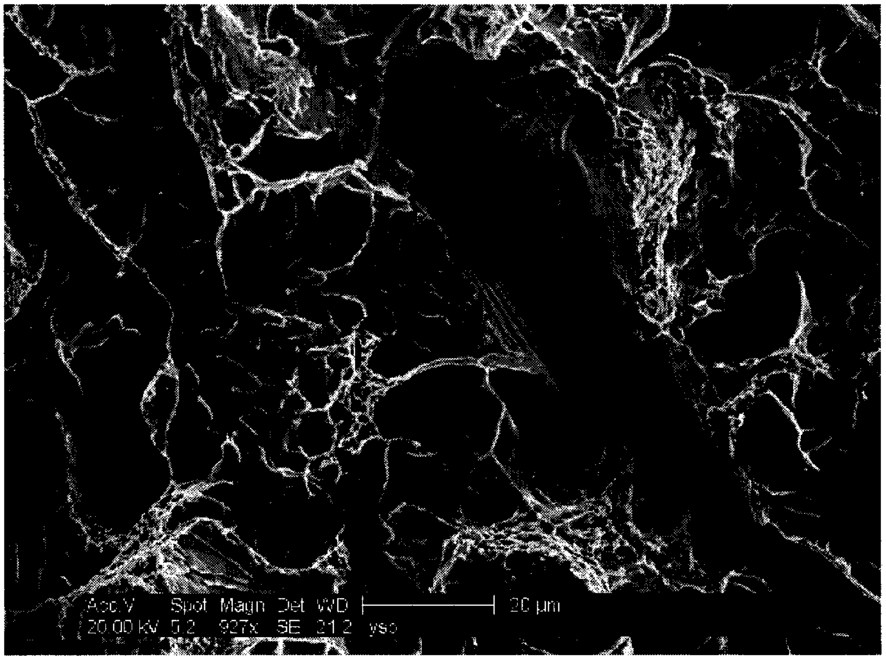

(b) A closer view of the Charpy impact fracture surface

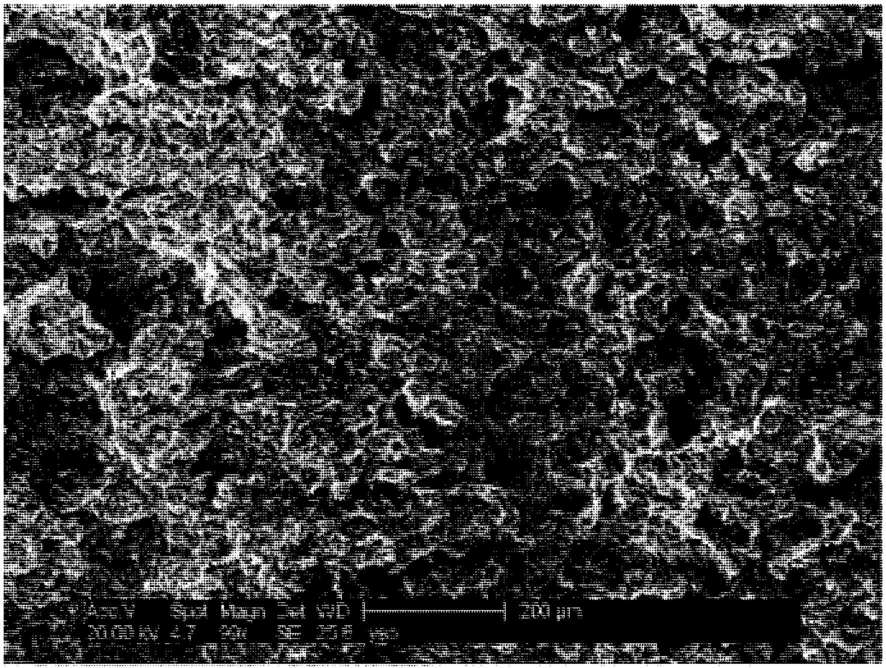

(c) Slow bending fracture surface

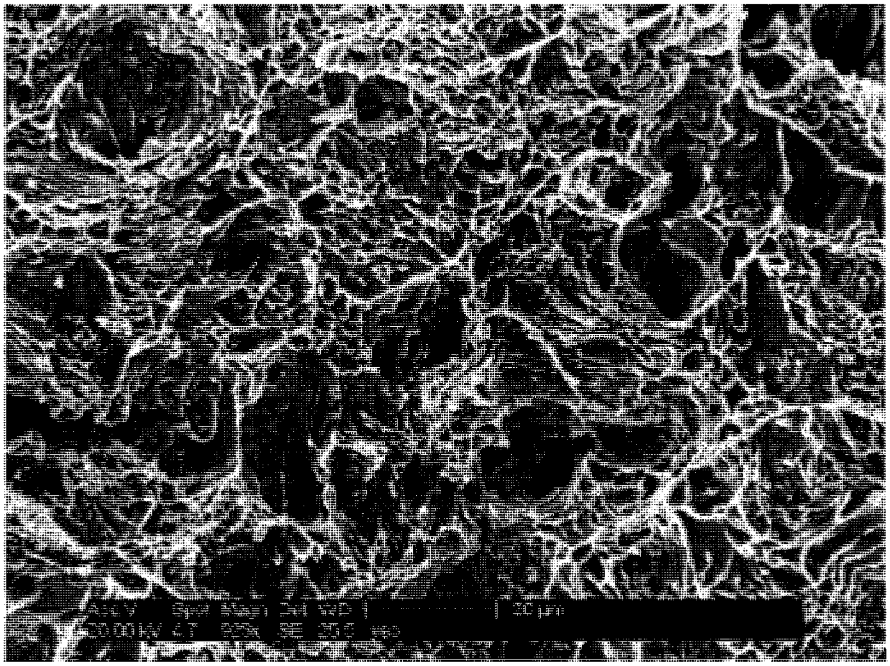

(d) A closer view of the slow bending fracture surface

Fig.3-2 SEM fracture surface morphology

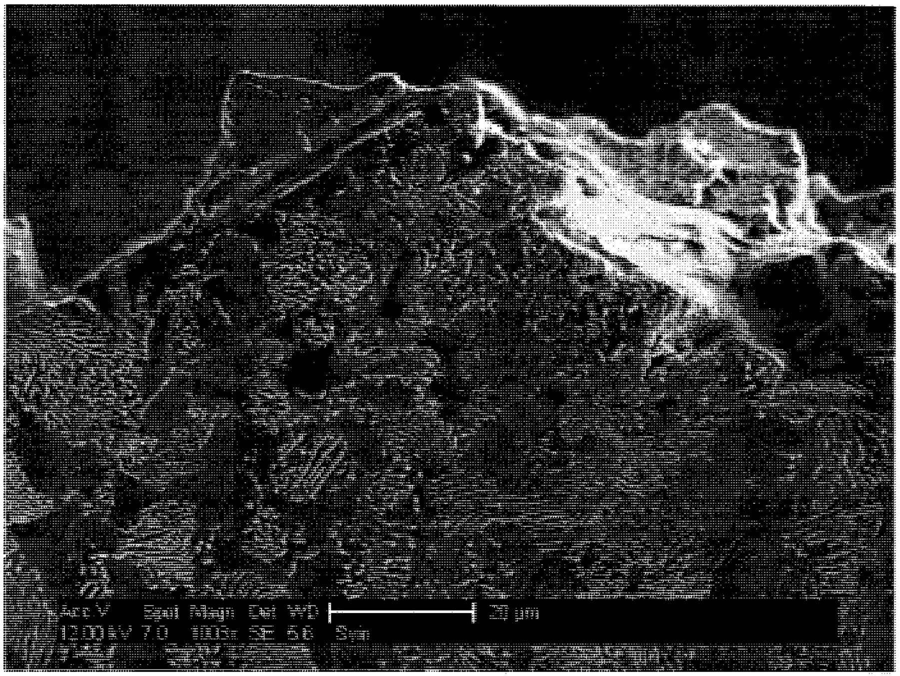

(a) Microcracks in fracture surface layer (cross-section) caused by the Charpy impact test

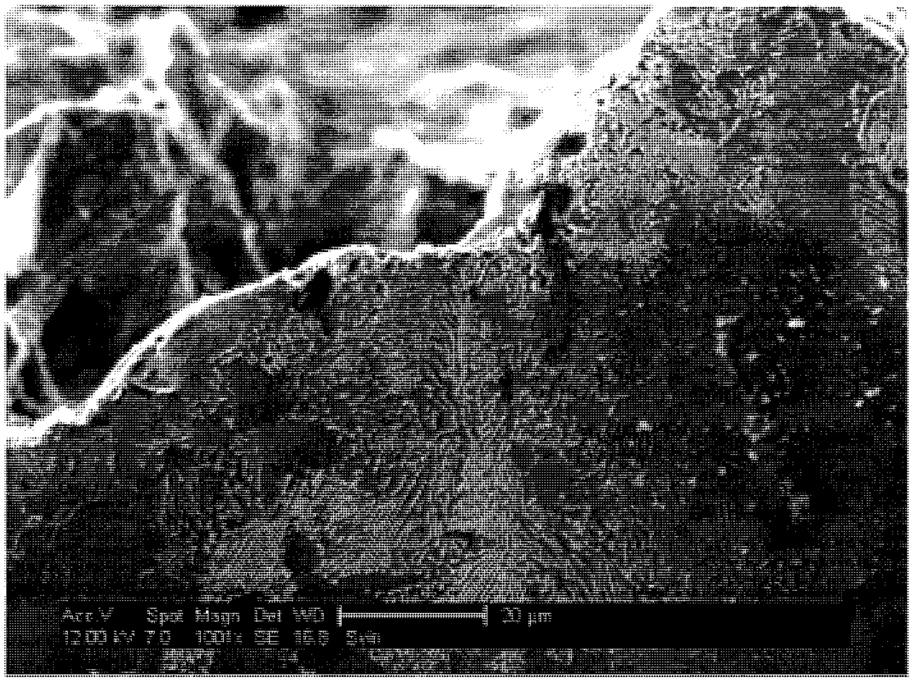

(b) Microcracks in fracture surface layer caused by slow bending test

Fig.3-3 SEM observation of microcracks in fracture surface layers (cross-section)

Absorbed energies of both the Charpy impact and slow-bending samples were measured and are illustrated in Fig.3-4. As shown, the absorbed energy of the former is 32.5 J while that of the latter is 48.6 J. This absorption energy measurement is consistent with results of the SEM fractography examination, in which the impact fracture surface is relatively brittle and therefore consumed less energy during the fracture process.

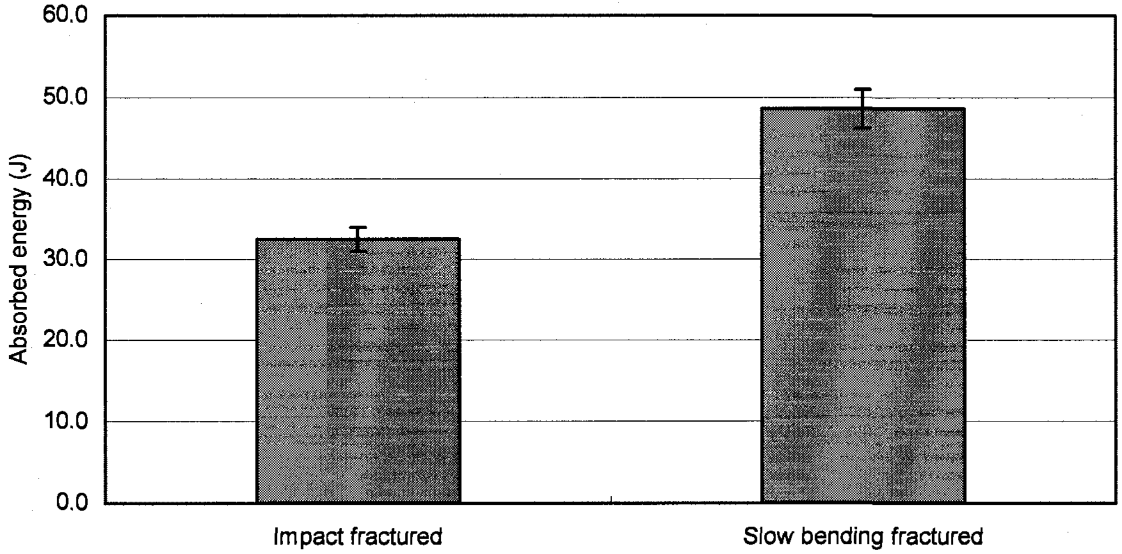

Fig.3-4 Absorbed energies of Charpy impact and slow bending tests

Mechanical properties of the surface layers right beneath the fracture surface were measured using a micro-mechanical probe. Results of the test are shown in Fig.3-5 and Fig.3-6, respectively. As illustrated in Fig. 3-5, slow-bending resulted in the highest hardness (HV 269) followed by the Charpy impact test (HV 254), and the annealed sample had the lowest (HV 147).

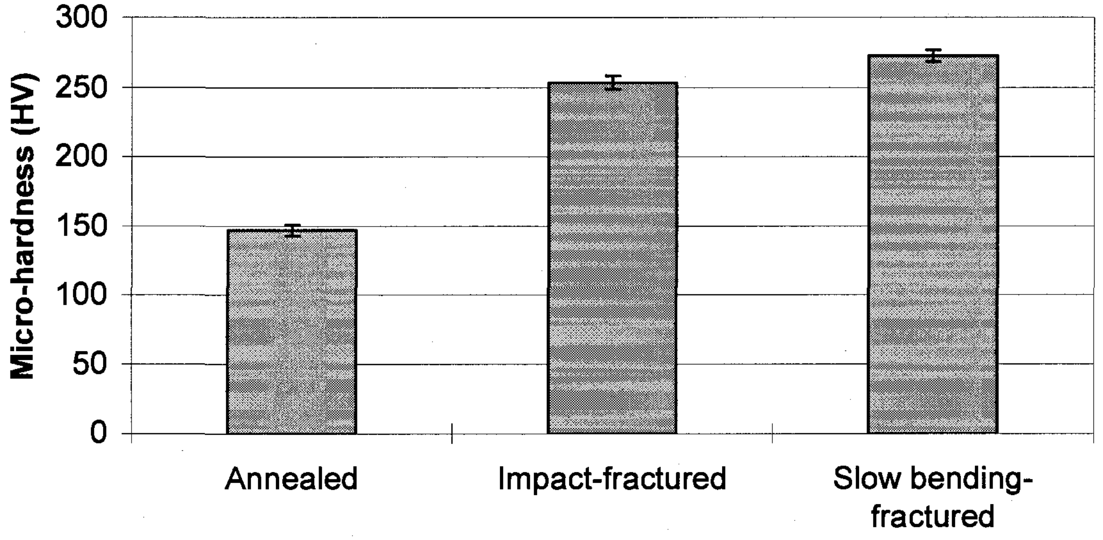

Fig.3-5 Micro-hardness of annealed, impact-fractured and slow bending-fractured sample surface

Fig.3-6 illustrates the variations in micro-hardness as a function of the distance from the fracture surface. As shown, the affected layers are rather thick. The impact-fractured sample has a deformed layer of about 2800 μm while that of the slow bending-fractured sample is 4200 μm thick. The hardness of the very surface is lower than the sub-surface layer. This could be attributed to microcracks in the near surface layer, which could make the layer less resistant to indentation.

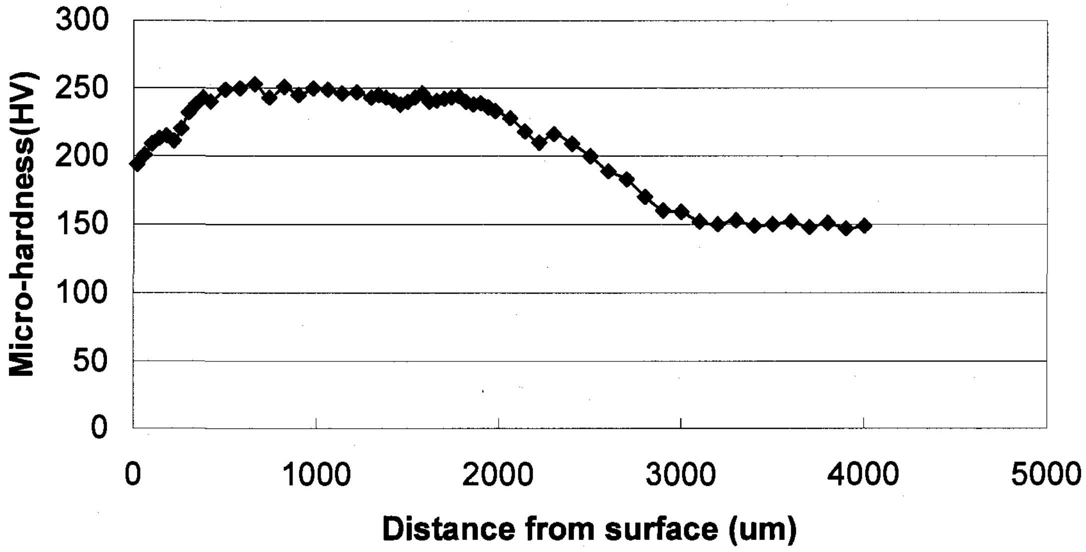

(a) Impact-fractured surface

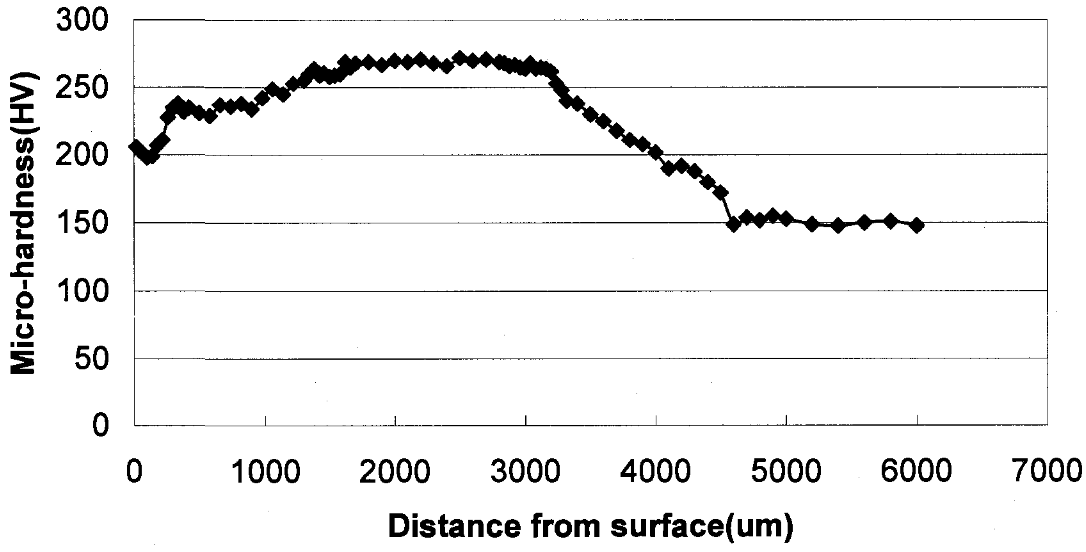

(b) Slow bending-fractured surface

Fig.3-6 Micro-hardness of impact-fractured and slow bending-fractured surface layers

The X-ray diffractograms ((110) peak) of annealed, impact-fractured and slow bending-fractured samples are superimposed in Fig.3-7. (220) peaks were also analysed. The X-ray line profile analysis results are summarized in Table 3-1. It is shown that the slow-bending yielded larger microstrain (0.0401%) than Charpy impact (0.0230%). In addition, the diffraction peaks of both slow bending-fractured and impact-fractured surface layers were found to shift to the left with respect to that of the annealed sample, which indicate the presence of residual tensile stress normal to the fracture surface [117].

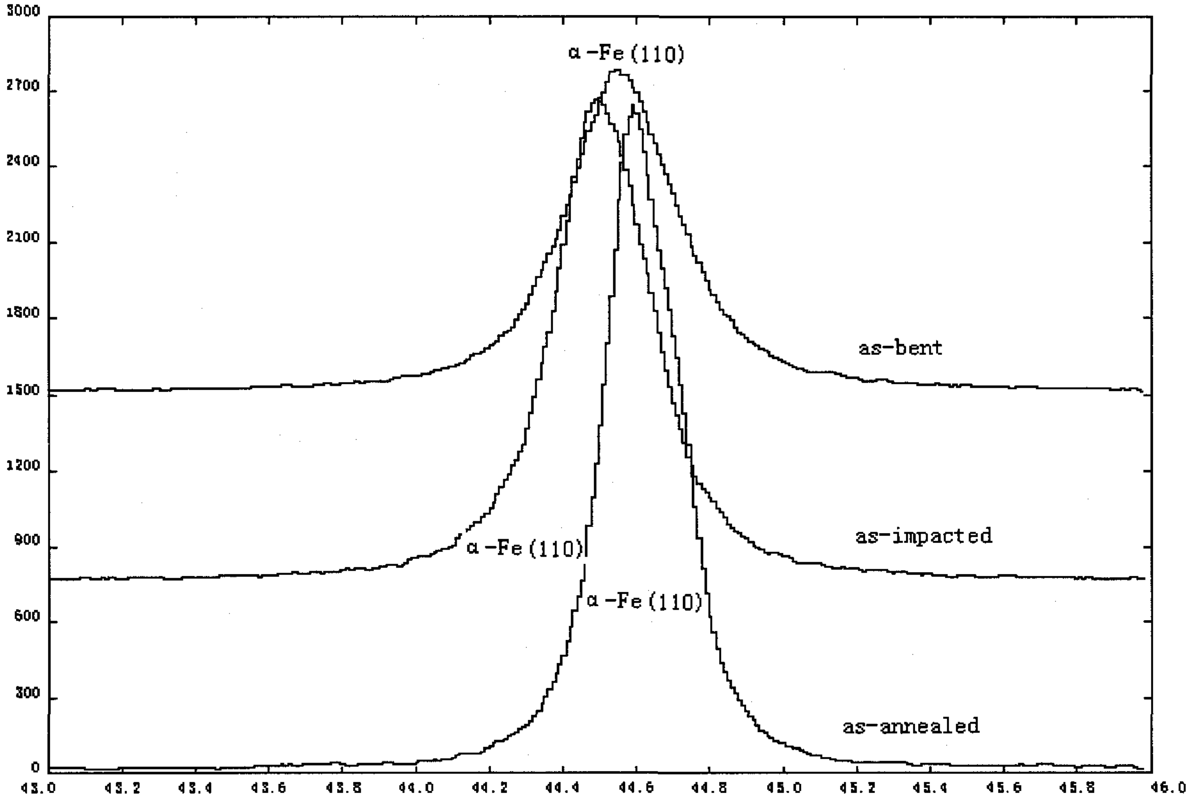

Fig.3-7 X-ray (110) diffractions of full-annealed, impact-fractured and slow bending-fractured surface layers

Table 3-1 Results of the X-ray line profile analysis

	Integral broadening (110)	Integral broadening (220)	Microstrain (%)
Impact-fractured	0.0016	0.0020	0.0230
Bending-fractured	0.0025	0.0032	0.0401

One of our tasks is to investigate the surface microstructure and defect configuration resulting from different loading rates, mainly the dislocation density that strongly influences the electrochemical behaviour of materials. The XRD results indicate that the slow bending-fractured sample may have higher dislocation density than the impact-fractured sample, because its larger residual microstrain should mainly result from higher dislocation density. The XRD result is consistent with that of the micro-indentation test. For instance, the slow-bending sample had a higher microhardness than the impact-fractured sample. This could be mainly attributed to the strain-hardening effect that is dependent on the number of dislocations.

The higher dislocation density of the slow bending-fractured surface layer may also be expected based on the absorption energy measurement. The absorbed energies (E) during fracture can be basically resolved into two components: the plastic strain energy (Wd) and the surface energy (Ws) of the fracture surfaces as well as those of microcracks.

$$E= Wd+Ws \qquad (3.1)$$

The fracture surface and cross-sectional SEM examinations have shown that the impact-fractured and slow bending-fractured surface have similar roughness. Although the former shows more microcracks, the difference in the crack density between the fracture surface layers are not large, at least on the same order of magnitude. Therefore, the higher absorbed energy of the slow bending-fractured sample may imply that it experienced larger plastic deformation than the impact-fractured one. A higher dislocation density is thus expected for the slow bending-fractured sample. However, it should be pointed out that the thicker plastic deformation layer of the slow bending sample also consumed part of the absorbed energy. Nevertheless, the dislocation density of the slow bending-fractured surface layer should be higher, not only supported by all the experimental results but also expected theoretically.

The differences in residual microstrain and dislocation density between slow bending-fractured and impact-fractured surface layers could be explained in terms of dislocation dynamics: the behaviour of dislocations moving at high speeds is quite different from that of quasi-static ones [97]. If we assume that a dislocation has an equivalent mass (m*), the force (F) required to drive the dislocation with a certain acceleration (a) may be determined by Newton's law of motion [97]:

$$F = m^* \cdot a \qquad (3.2)$$

Therefore, there must be a drag force to hold back the dislocation before a certain velocity is reached. The larger the acceleration, the larger the drag force. Thus, when a sample is deformed at a high strain rate, dislocations are relatively difficult to be generated and moved. As a result, the dislocation density would be possibly low and plastic deformation could be restricted to relatively small local regions. Less plastic deformation with lower dislocation density could therefore be expected in samples experienced the Charpy impact test, in which the strain rate at the notch tip was estimated to be in the range of 10^2 to 10^3 s^{-1} [118].

Thus, under the Charpy impact condition, cleavage fracture was the main failure mode with less plastic deformation involved. The deformation caused by the impact force could be accommodated by microcracking. From this point of view, a relatively lower dislocation density can be expected for the impact-fractured sample.

The dynamic behaviour of materials i.e. deformation at high strain rates has been a subject of numerous studies for recent decades, due to its significance to engineering practice [96, 97]. Many investigators have examined the effects of strain rate on the dislocation substructure by means of transmission electron microscopy (TEM) [106-108]. In many cases, a cellular dislocation substructure develops, and the dislocation density increases with strain rate; while the dislocation cell size decreases with the strain rate. As a consequence, microhardness and flow stress have been found to increase with the strain rate. It seems that the results obtained in this study conflict with the previous studies reported in literature. However, it must be pointed out that the previously reported experimental results were obtained using the Split-Hopkinson-pressure-bar technique, in which a specimen was deformed under compressive stress. In a compressive stress state, the number of microcracks could be smaller than that under tensile stress, bearing in mind that compressive stress can not result in cracking. Therefore, more dislocations must be introduced to accommodate deformation under the applied stress. This could be a reason why under compressive stress at high strain rates, more dislocations could be generated but moved in local regions, thus resulting in small dislocation cells. However, in the Charpy impact test, the stress in the vicinity of notch tip is complicated but basically tensile in nature [119,120], which favours the formation of microcracks. Under such a condition, less plastic deformation was involved and cleavage fracture could thus be the main failure mode. All experimental observations in this study are consistent with the theoretical argument.

3.2.2 Corrosion behaviour

The Potentiodynamic polarization curves of the 1045 steel of different states measured in 3.5% NaCl solution at room temperature (~ 22 °C) are shown in Fig.3-8. Table 3-2 summarizes electrochemical properties obtained using Tafel method and linear polarization method. One may see that the slow bending-fractured sample has the highest corrosion rate, followed by the impact-fractured sample, and the annealed sample has the lowest corrosion rate.

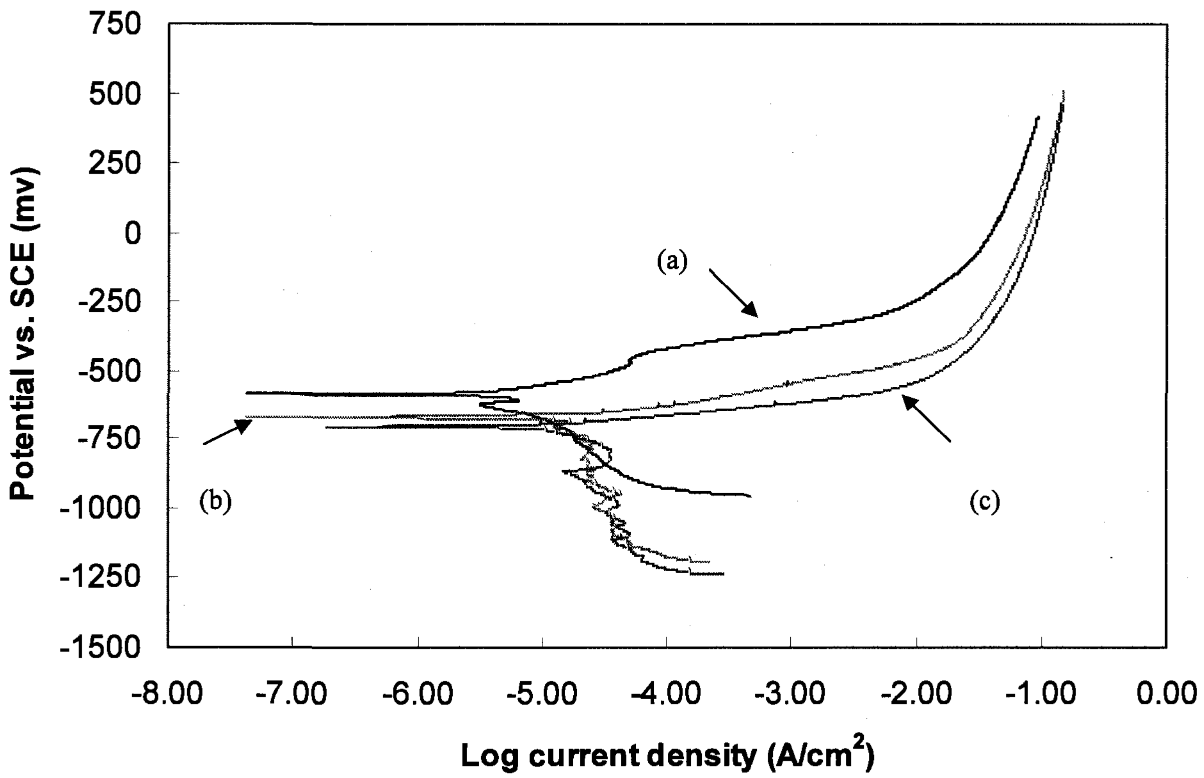

Fig.3-8 Potentiodynamic polarization curves of different surfaces in 3.5% NaCl solution: (a) full annealed; (b) Charpy impact fractured; (c) slow bending-fractured

Table 3-2 Results of the electrochemical test

	Ecorr (mV)	Icorr (μA/cm^2)	Rp (ohm/cm^2)
Annealed	-584±7	6.93±0.23	1266±84
Impact-fractured	-668±10	14.78±0.53	1143±77
Bending-fractured	-695±12	19.19±0.44	934±85

In general, corrosion is an electrochemical reaction in which a metal loses electrons and dissolves in the corrosive solution. The activity of electrons may be reflected by the electron work function (EWF), the minimum energy required to remove electrons from inside a metal to its surface with zero kinetic energy [89]. In order to better understand the above electrochemical results, the electron work functions (EWF) of the three types of sample surface were measured using a scanning Kelvin probe (SKP). Results of the test are shown in Fig. 3-9. As shown, the slow bending-fractured surface has the lowest EWF (4.1-4.3 eV), followed by the impact-fractured surface (4.4-4.6 eV), and the annealed sample has the highest EWF(4.6-4.7 eV).

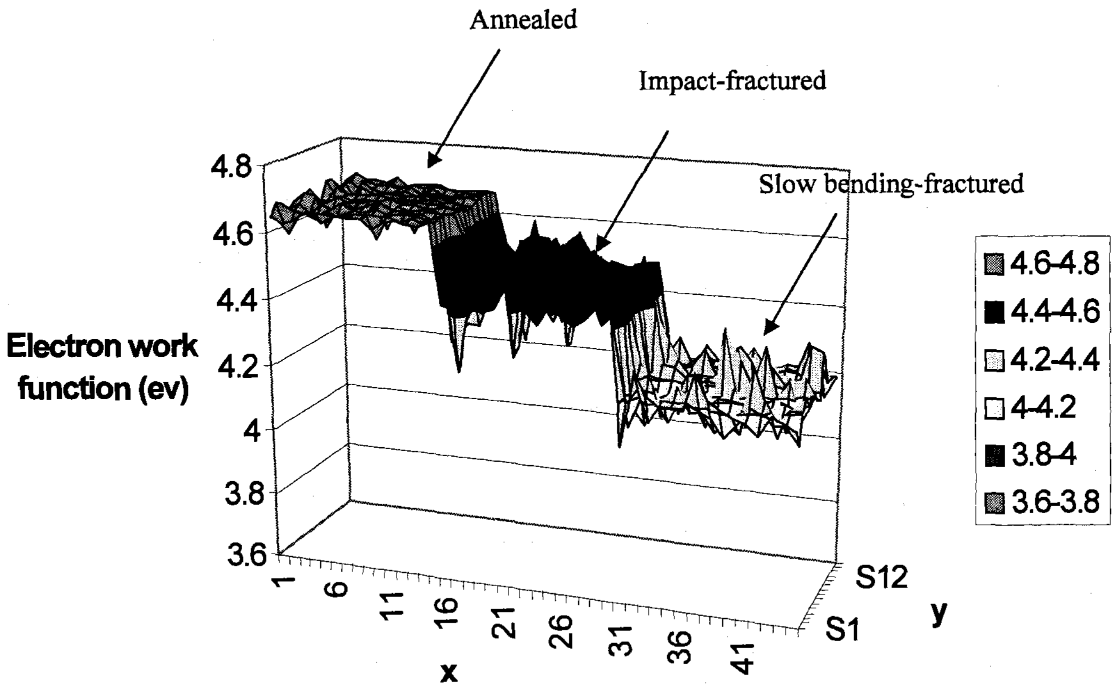

Fig.3-9 Electron work functions of full-annealed, impact-fractured and slow bending-fractured surfaces

It has been demonstrated that the EWF decreases with plastic deformation no matter if it is tensile or compressive [92, 93], which implies that dislocation renders electrons more active and thus increases the driving force for electrochemical reaction. This means that a deformed metal tends to lose electrons more easily than an unreformed one. Consequently, a heavily deformed metal should have a high corrosion rate, since its high-density dislocations provide a large number of active sites at which corrosion is promoted. Previous studies have demonstrated that the corrosion rate of a metal increases with an increase in the amount of plastic deformation [121]. The results of the electrochemical test in this study are consistent with the EWF measurement and also expected based on our previous studies. In summary, since the slow bending-fractured surface layer has a higher dislocation density than the impact-fractured one, the former has a higher corrosion rate. Among the three types of samples, the annealed has the lowest corrosion rate. It should be mentioned that the EWF is also affected by surface roughness. However, since the impact-fractured surface and the slow bending-fractured one have similar roughness, the effect of roughness on EWFs of these two surfaces could be largely minimized or the roughness effect on the difference in EWF between these two surfaces could be negligible. As for the annealed sample, it should have higher EWF than the two fractured surfaces, because of its lower dislocation density or dislocation-free state.

3.2.3 Corrosive wear behaviour

The corrosive wear behavior of the samples was evaluated using scratching test in 3.5% NaCl solution under different loads. After scratching, cross-sectional profiles of the scratch grooves were measured under an atomic force microscope (AFM). The wear rate is represented by the volume loss per unit length of the scratch groove (mm3/mm). As an example, Fig.3-10 illustrates the cross-sectional profiles of grooves scratched under a load of 5g. The wear rate results are summarized in Fig. 3-11.

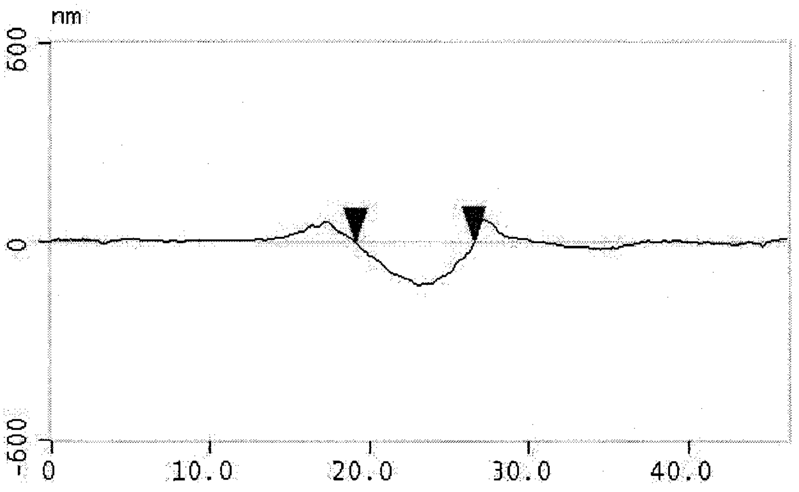

(a)

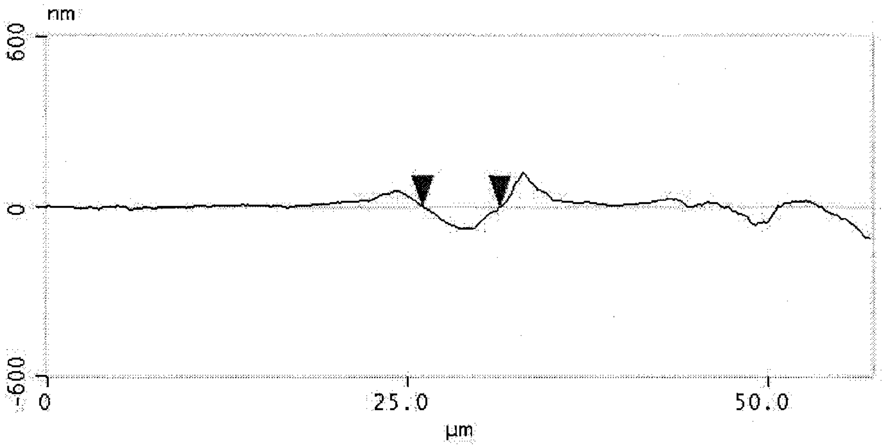

(b)

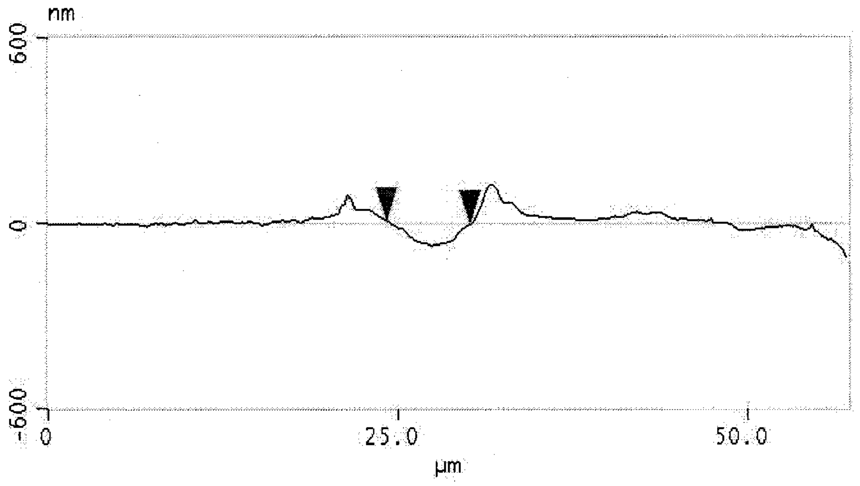

(c)

Fig.3-10 Cross-sectional profiles of scratch grooves generated by scratch in 3.5% NaCl solution at a load of 5g. (a) annealed, (b) impact-fractured, and (c) slow bending-fractured

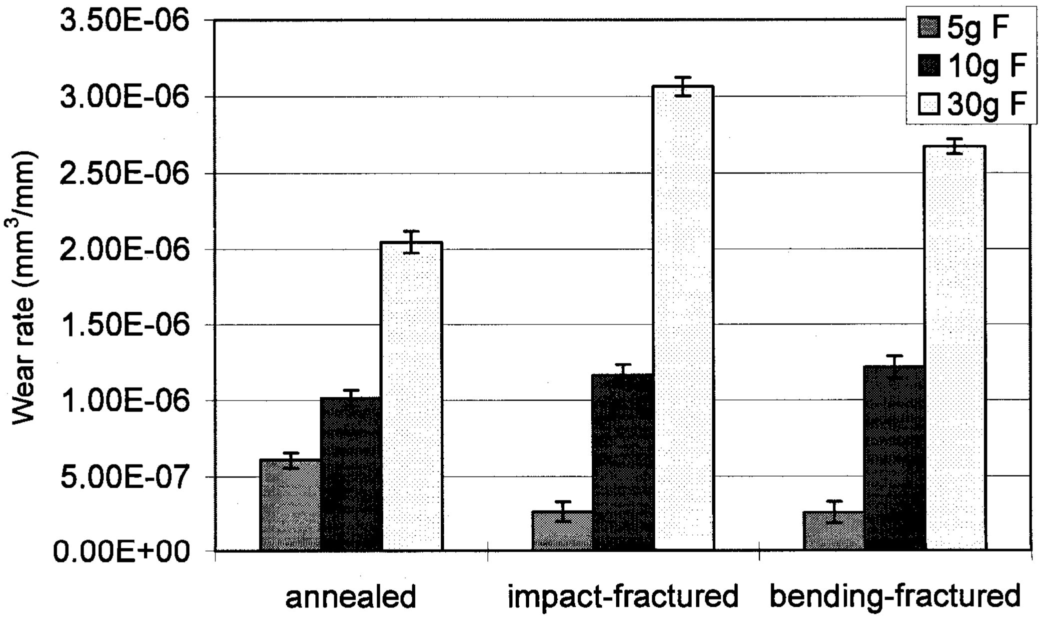

Fig.3-11 Wear rates of annealed, impact-fractured, slow bending-fractured surfaces caused by scratch in the 3.5% NaCl solution.

As illustrated, under different loads, the samples performed differently. At the low load of 5g, the slow bending-fractured and impact-fractured samples have close wear rates that are lower than that of the annealed sample. When the applied load increased, the situation was reversed. At the load of 10g, wear rates of the slow bending-fractured and impact-fractured samples are still close but higher than that of the annealed one. At the load of 30g, the impact-fractured samples have a markedly higher wear rate than the slow bending-fractured samples.

The observed performances of the three types of samples can be explained. It is generally accepted that the wear loss is approximately inversely proportional to the hardness of the target material [34]. The slow bending-fractured and impact-fractured surfaces are harder than the annealed one, due to the strain-hardening effect that more or less benefited the wear resistance [121]. As a result, the slow bending-fractured and impact fractured surfaces, although their toughness was lower, could show higher resistance to wear than the annealed one under low wear force. However, if the wearing force is large, the situation could be different. Under relatively higher loads, the fracture stress might be reached and all the samples would experience relatively severe wear. Under such a condition, the softer sample (annealed) might have improved performance relative to the strain-hardened ones, since it may have larger contact area and thus smaller contact stress, which may decrease the wear damage. In addition, the higher ductility of the annealed sample helps to accommodate deformation and this may reduce nucleation and propagation of cracks.

It must be indicated that the larger volume loss of the fractured surfaces under the load of 30g may be caused by the accelerating effect of corrosion on wear that can be enhanced by defects. The negative effect of defects, e.g., dislocations, on corrosion has been demonstrated by the electrochemical tests and EWF measurements in the present study. In addition, the microcracks and dislocations in the fractured surface layers led to a decrease in toughness, thus reducing the wear resistance under relatively larger wearing forces.

It is interesting to notice that, under the highest load of 30g force, the Charpy impact-fractured sample showed slightly higher volume loss than the bending-fractured sample. This might be ascribed to the surface defect structure. For the impact-fractured surface layer, the dislocation density could be lower than that in the slow bending-fractured surface layer because of the high strain rate as discussed earlier. Instead, the density of microcracks beneath surface could be relatively higher than that of slow bending-fractured sample. The microcracks may act as stress raiser and made the surface vulnerable to wear attack especially under large wearing forces. When immersed in the corrosive solution, material degradation and stress-corrosion cracking at the crack tip could largely accelerate the surface wear failure, leading to a higher wear rate.

3.3 Conclusion

Effects of the loading speed or strain rate on corrosion and corrosive wear of annealed, impact-fractured and slow bending-fractured surface layers of AISI 1045 steel in a 3.5% NaCl solution were investigated. The results showed that the slow bending-fractured surface layer had the highest dislocation density and hardness, followed by the impact-fractured one, and the annealed sample had the lowest dislocation density and hardness. The effect of the strain rate on the dislocation density could be explained based on the dislocation dynamics and fracture mode. Electrochemical tests demonstrated that the slow bending-fractured surface had the highest corrosion rates, followed by the impact-fractured one, and the annealed one had the lowest corrosion rate. Such difference in corrosion rate could be mainly attributed to different dislocation densities, which influence the surface electron activity. Using electrochemical scratching tests, the corrosive wear performances of the three groups of samples were evaluated. It was demonstrated that under a low load of 5g, the slow bending fractured and impact-fractured surfaces had higher wear resistance than the annealed one, while under higher loads, the situation was reversed. Under the highest load of 30g, the impact-fractured surface showed the lowest resistance to corrosive wear.

Chapter 4

Effects of strain rate of prior deformation on corrosion and corrosive wear of AISI 1045 steel in a 3.5% NaCl solution

In Chapter 3, it has been demonstrated that the wear-corrosion synergy can be markedly affected by the strain rate. In this study, effects of strain rate of prior deformation on corrosion and corrosive wear of AISI 1045 steel in a 3.5% NaCl solution were investigated using electrochemical test, scanning Kelvin probing and corrosive sliding wear tests, respectively. Six strain rates of prior deformation, from 7.5×10^{-4} s^{-1} to 2 s^{-1}, were employed for this study. In order to understand the mechanism responsible for the effects of the strain rate on corrosion and corrosive wear, worn surfaces, sub-surface microstructure, microcracks and residual strain were examined with SEM. X-ray line profile analysis. Micro-hardness tests were also carried out to investigate corresponding changes in mechanical properties of surface layers with respect to the strain rate. Based on the effects of prior strain at different rates on surface microstructure and resultant changes in electrochemical and mechanical properties, the corresponding wear behavior of the steel in the 3.5% NaCl solution is discussed.

4.1 Experimental details

AISI 1045 steel (0.43-0.50 wt% C, 0.60-0.90wt% Mn, maximum 0.04wt% P, maximum 0.05wt% S) was selected as a sample material. All specimens were austenized at 810°C for 45 minutes and then quickly cooled down to 640°C and maintained at the temperature for 30 minutes, followed by furnace cooling.

Tensile specimens with a gauge length of 25.4mm and a diameter of 6.35mm were machined. Tensile tests were carried out at strain rates of 0.00075, 0.02, 0.3, 1, 1.5, and 2

s^{-1}, respectively, using a servohydraulic (Instron) testing machine. Scanning electron microscopy (SEM) was used to observe microcracks in layers beneath the fracture surface. The hardness of the subsurface layers was measured using a Mitutoyo AVK-C1 hardness tester. In order to measure the cross-sectional microhardness, a micro-mechanical probe (Fischerscope H100C, made by Fisher Technology Ltd., Windsor, CT, USA) was employed.

Residual microstrains in subsurface layers introduced by deformation at different strain rates were determined by X-ray diffraction line profile analysis [117]. X-ray diffractograms of the subsurface layers experiencing deformation at the different strain rates were obtained using a Rigaku 3014 X-ray diffractometer with CuKα radiation, operated at 40 kV and 35mA in a continuous-scan mode. The scanning speed was 0.2 degree/min. A graphite crystal monochromator was used to obtain monochromatization. Kα1 lines were separated from combined Kα1 and Kα2 lines using a computer program. A full-annealed specimen was used as a reference specimen. (110) and (220) peaks were selected for the line profile analysis.

Electrochemical tests, including potentiodynamic polarization, linear polarization and Tafel plot measurements, were performed at room temperature (~ 22 °C) using a computerized Gamry PC4/750 electrochemical system. All experimental arrangements are the same as those described in Chapter 3.

A scanning Kelvin probe (SKP), provided by the KP Technology Ltd. (Caithness, UK), was employed to investigate the influence of strain rate on the electron work function (EWF) of AISI 1045 steel. All experimental arrangements are the same as those described in Chapter 3.

Corrosive sliding wear tests were performed on a pin-on-disc tribometer (CSEM Instruments, Switzerland). A schematic drawing of the apparatus is shown in Fig. 4-1. In this work, the pin was a ball made of silicon nitride (Si_3N_4) with a diameter of 6mm. During a wear test, the pin was pressed onto a rotating specimen under an applied load. The apparatus was attached with an electrochemical system (connected to a Gamry PC4/750 electrochemical system), which allowed a wear test performed in a plastic cell that contained a corrosive solution under an applied potential. A saturated calomel electrode (SCE) was used as the reference electrode and a platinum plate was used as the counter electrode. A 3.5% NaCl solution was used as the electrolyte.

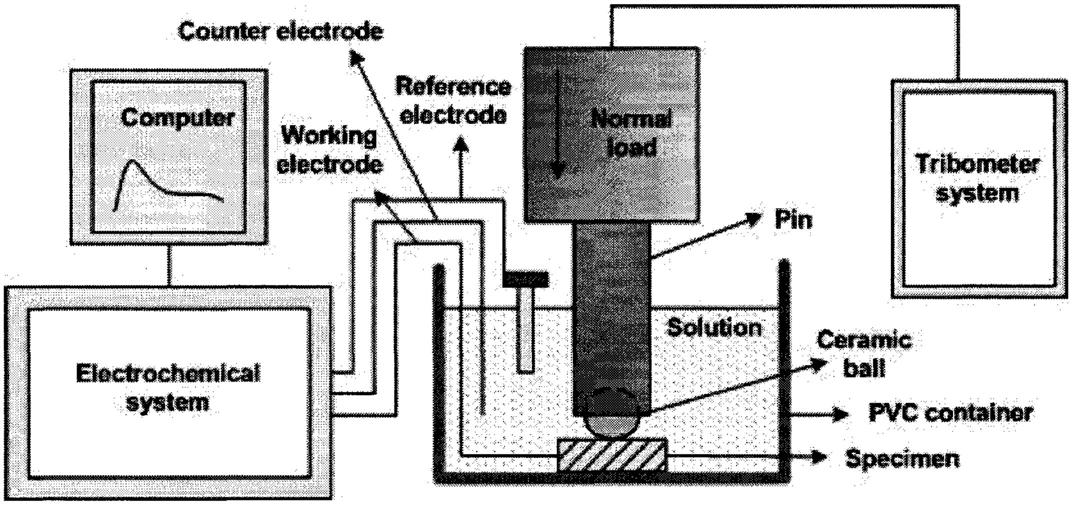

Fig.4-1 Schematic diagram of the apparatus for corrosive sliding wear tests

The corrosive sliding wear tests were carried out under a load of 3N over a sliding distance of 12 m at a sliding speed of 0.5 cm/s. Wear rates (the volume loss per unit length of wear track: mm^3/mm) of all specimens worn in the 3.5 % NaCl solution were determined using the following equation (ASTM Practice G99-04):

$$\text{Volume loss rate} = r^2 \sin^{-1}(d/2r) - (d/4)(4r^2 - d^2)^{1/2} \qquad (4.1)$$

where r is the radius of pin (semi-spherical) and d is the width of wear track. The pin radius, r =3 mm, was kept approximately constant during the tests, confirmed by regularly checking the pin end under an optical microscope. For each wear condition, at least 3 tests were performed. The width of wear track, d, was measured under the optical microscope and averaged over at least 10 measurements at different positions of the track.

Mechanical wear was evaluated by performing sliding wear tests in the 3.5% NaCl solution under full cathodic protection. In order to select an appropriate cathodic potential, variations in the wear rate with respect to applied cathodic potential were measured. The potential at which the wear rate was the minimum was selected for the cathodic protection. The worn surfaces resulting from corrosive sliding wear in 3.5% NaCl solution under a load of 3N were examined using SEM.

4.2 Results and discussion

4.2.1 Microstructure and mechanical properties

Fig.4-2 presents cross-sectional views of microstructures of subsurface layers in which microscopic cracks and voids are visible. As shown, the size and number of the cracks and voids increased with the strain rate.

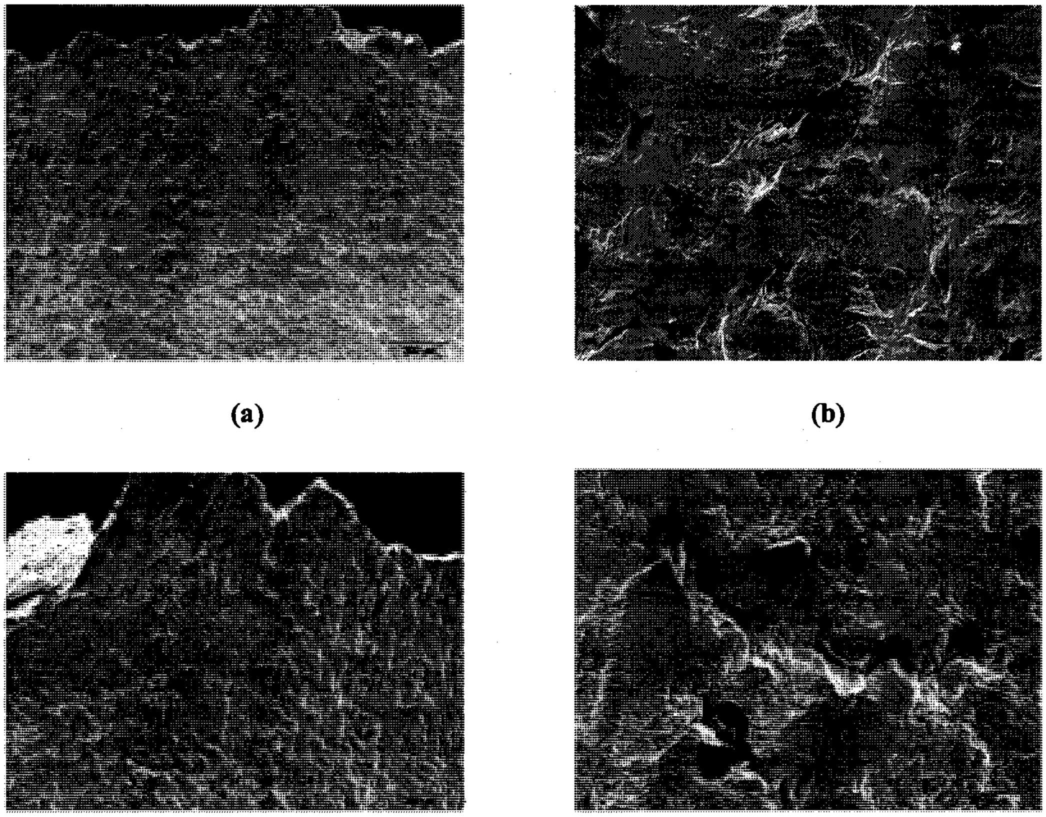

(a) (b) (c) (d)

Fig.4-2 Microscopic cracks and voids in the sub-fracture-surface layer (side view).

(a) Strain rate = 0.00075 s^{-1}.
(b) Strain rate = 0.00075 s^{-1}; a closer view.
(c) Strain rate =2 s^{-1}.
(c) Strain rate = 2 s^{-1}; a closer view.

X-ray diffractograms ((110) and (220) peaks) of all specimens fractured at six different strain rates were analyzed. The microstrain was determined through X-ray diffraction line profile analysis based on approximated profile shape-functions [117]. The X-ray line profile analysis results are summarized in Fig.4-3, which indicates that the microstrain slightly increased initially with the strain rate and then decreased when the strain rate was larger than 0.3 s^{-1}.

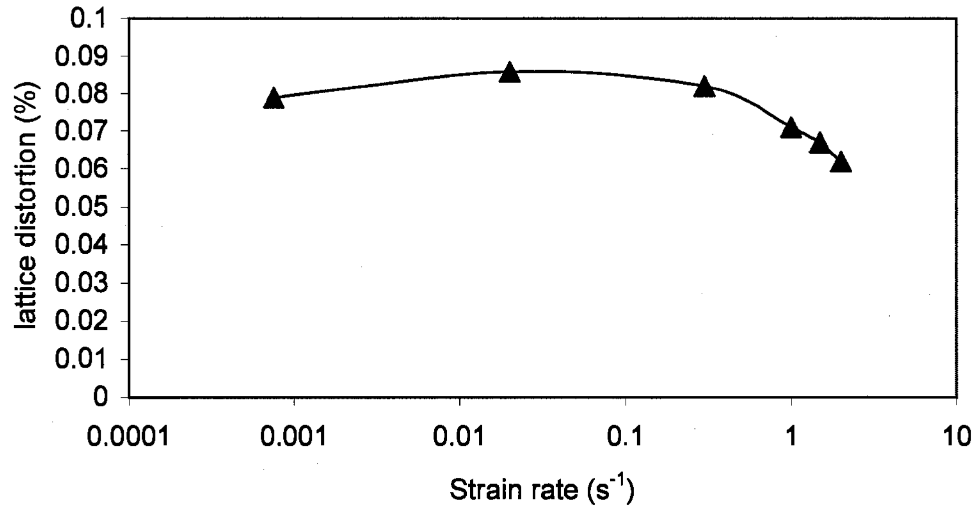

Fig.4-3 Variations in lattice distortion (micro-strain) in the sub-fracture-surface layer with respect to the strain rate of prior deformation.

Variations in the yield strength and fracture strain with respect to the strain rate are illustrated in Fig.4-4. As shown, both the lower and upper yield strengths increased whereas the fracture strain decreased with the strain rate. The upper yield strength increased faster than the lower yield strength.

Fig.4-5 illustrates the variation in hardness of the fracture surface layer with respect to the strain rate. The hardness slightly increased initially with strain rate and then decreased when the strain rate was larger than 0.3 s^{-1}. In order to evaluate the depth of deformation affected zone, variations in microhardness as a function of the distance from the fracture surface were measured. As shown in Fig.4-6, the deformed zone spanned more than 14mm in specimens deformed at both strain rates of 7.5×10^{-4} s^{-1} and 2 s^{-1}, bearing in mind that the hardness of annealed 1045 steel in this study was about 147-152 HV. If we define the deformation zone with microhardness above HV 240 as a "severely deformed zone", one may see that the depths of "severely deformed zone" for $\dot{\varepsilon}=7.5\times10^{-4}$ s^{-1} and $\dot{\varepsilon}=2$ s^{-1} are 8.9 mm and 4.2 mm, respectively. This implies that the deformation zone formed at low strain rates was larger than that formed at higher strain rates. In addition, the microhardness measured throughout the gauge length of the specimen deformed at $\dot{\varepsilon}=7.5\times10^{-4}$ s^{-1} is higher than that of $\dot{\varepsilon}=2$ s^{-1}, which is consistent with the results of the hardness measurement in the sub-fracture-surface layer as shown in Fig. 4-5.

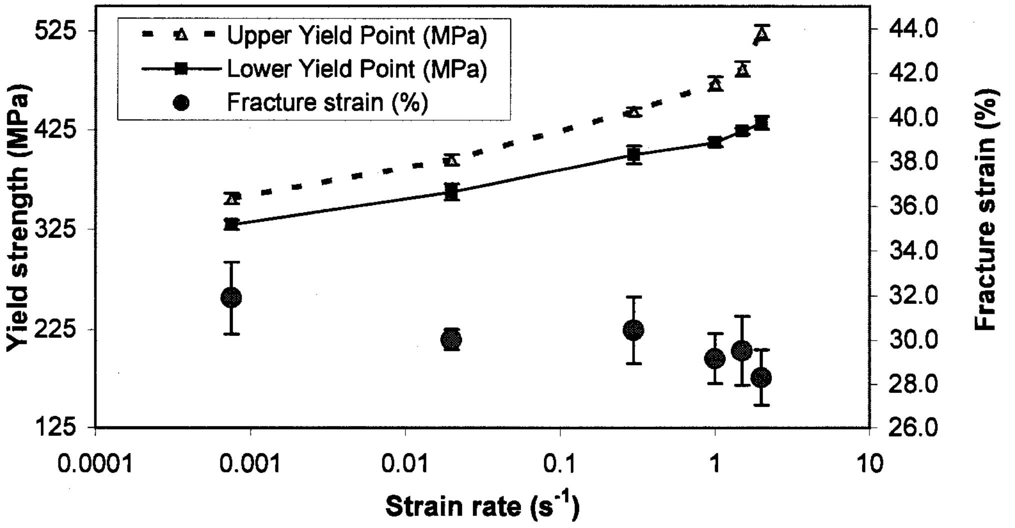

Fig.4-4 Variations in tensile properties of AISI 1045 steel as a function of the strain rate.

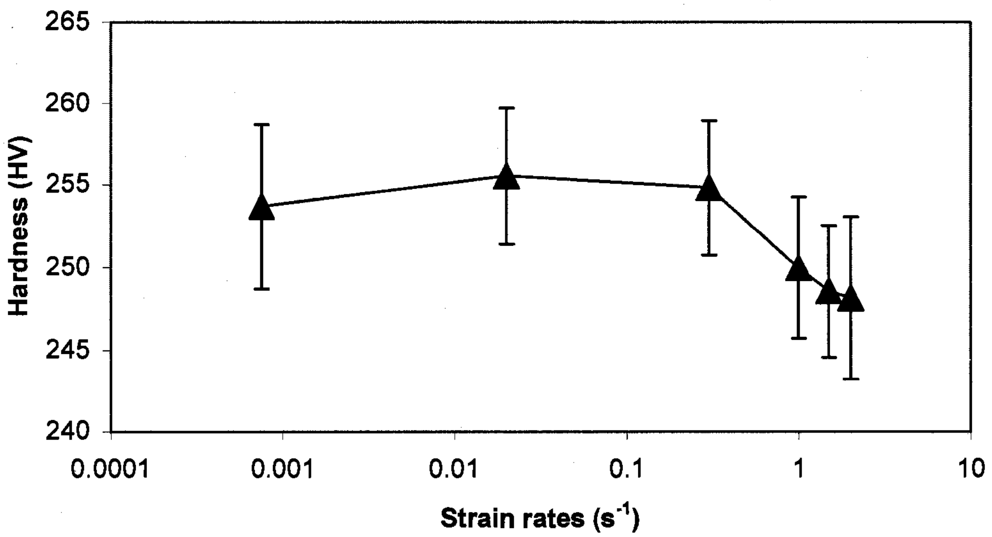

Fig.4-5 Variations in hardness of the sub-fracture-surface layer with respect to the strain rate of prior deformation.

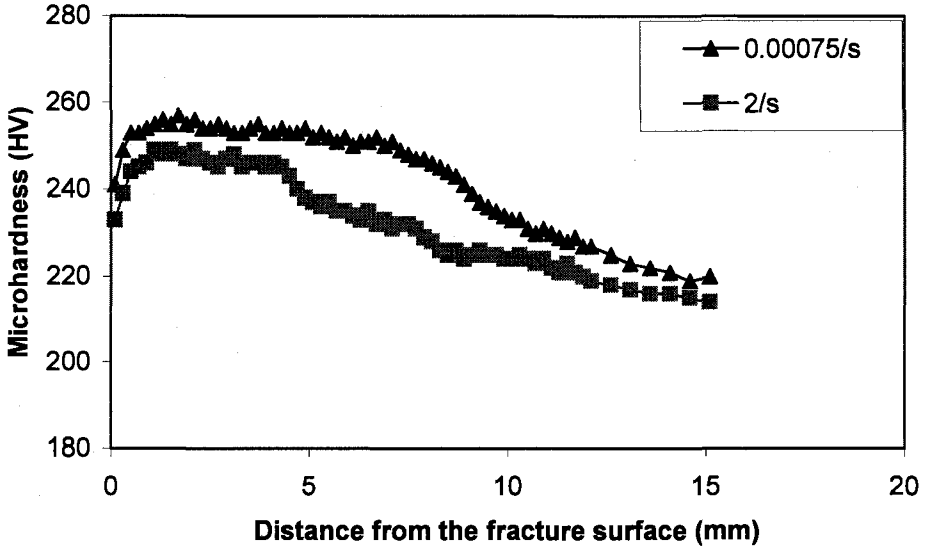

Fig.4-6 Microhardness profiles of the sub-fracture-surface layer for specimens deformed at strain rates of 0.00075 s^{-1} and 2 s^{-1}, respectively.

One of our tasks is to investigate the surface microstructure and defects resulting from prior deformation at various strain rates, mainly the density of dislocations and microcracks that strongly influence the corrosion behavior and corrosive wear of materials. The lattice distortion as a function of strain rate (Fig.4-3) indicates that the dislocation density initially increased with the strain rate and then decreased, bearing in mind that the measured residual microstrain should mainly result from the introduced dislocations. The XRD result is supported by the micro-indentation test (Fig.4-5 and Fig.4-6), since the strain-hardening effect is enhanced with an increase in the density of introduced dislocations.

The observed variations in microstructure and mechanical properties with the strain rate could be explained in terms of dislocation dynamics [96, 97, 122-124]. Dislocations moving in isotropic media at uniform velocities have been theoretically studied [122-124].

As mentioned in the chapter 3, the motion of a dislocation can be regarded as the motion of an equivalent mass around the dislocation. The equivalent mass of a moving dislocation is velocity-dependent, which increases with the velocity as the following equation expresses [122]:

$$m^* = m_0 /[1-(V^2/V_0^2)]^{1/2} \qquad (4.2)$$

where V is the velocity of the dislocation, V0 is the velocity of sound and m0 is the equivalent mass of a screw dislocation at rest. As the velocity increases, the equivalent mass increases correspondingly. Since a dislocation has an equivalent mass, it is reasonable to assume that when the dislocation moves through a crystal lattice, its behavior may obey Newton's law of motion [97]:

$$F = m^* \cdot a \qquad (4.3)$$

where F is the force required to drive the dislocation to move in the crystal lattice, and a is the acceleration to reach a certain speed. There must be a drag force on the dislocation before a certain velocity is reached. The drag force rises as the dislocation moves at a higher velocity, corresponding to a larger equivalent mass.

Under a tensile loading condition, the nominal deformation is accomplished in two ways: motion of dislocations and formation of micro cracks and voids. These are two competitive processes. At relatively low strain rates, i.e. 7.5×10^{-4} s^{-1}, 0.02 s^{-1} and 0.3 s^{-1}, with increasing the strain rate, more dislocations were generated to accommodate the deformation, resulting in an increase in the dislocation density. However, at higher strain rates, the generation and motion of dislocations became difficult as discussed earlier.

Consequently, the plastic deformation was restricted while more micro cracks and voids had to be introduced in order to accommodate deformation generated at high strain rates. As shown in Fig.4-2, when the strain rate was increased, the size and number of microcracks and voids increased at expense of dislocation formation. As a result, the lattice distortion decreased at higher strain rates as illustrated in Fig.4-3. The results are consistent with our previous work published in ref [125] and reported in chapter 3, in which a fractured surface layer (after Charpy impact test) had a lower dislocation density than a slow-bending fractured specimen.

4.2.2 Effect of strain rate on corrosion

Potentiodynamic polarization curves of specimens deformed at different strain rates, measured in a 3.5% NaCl solution at room temperature (22 °C), are shown in Fig.4-7. The variation in the corrosion current density as a function of the strain rate, calculated based on ASTM standard G3-89, is illustrated in Fig.4-8. As shown, the current density initially increased and then decreased with the strain rate, which is consistent with the change in lattice distortion (Fig.4-3.)

In general, corrosion is an electrochemical reaction in which a metal loses its electrons and dissolves in the corrosive solution. The activity of electrons may be reflected by the electron work function (EWF), the minimum energy required to move an electron from inside a metal to its surface with zero kinetic energy [89]. In order to better understand the corrosion - strain rate relationship, variations in electron work function

(EWF) with respect to the strain rate were measured. For complete information, EWFs of both fractured surface and the sub-fracture-surface layer after polishing and etching were measured. Results of the EWF measurement are shown in Fig.4-9. It was observed that the electron work function slightly decreased and then increased with an increase in the strain rate. Such changes in EWF are consistent with the variations in the corrosion current density vs. the strain rate (Fig.4-8). When electrons became more active, the corrosion current was higher. Besides, the EWF of the polished and etched surface was higher than that of the unpolished. This could be attributed to the decrease in surface roughness: the rougher a surface, the lower is its EWF [126].

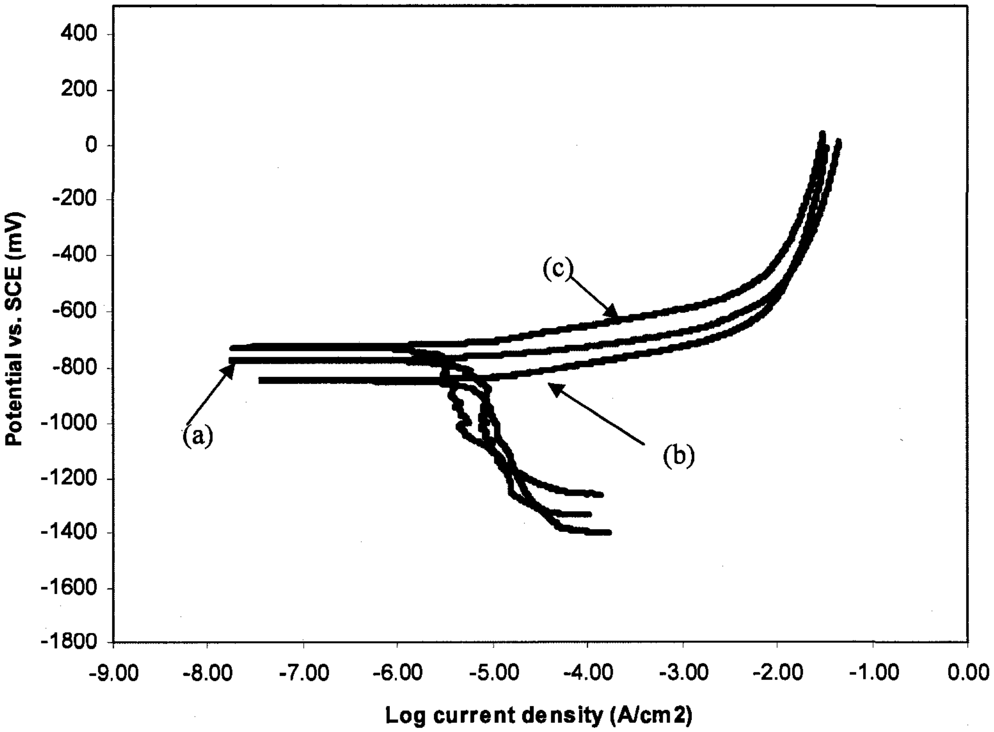

Fig.4-7 Potentiodynamic curves of sub-fracture-surface layers of specimens deformed at strain rates of a) 0.00075 s^{-1}, b) 0.02 s^{-1}, and c) 2 s^{-1}. Solution: 3.5% NaCl.

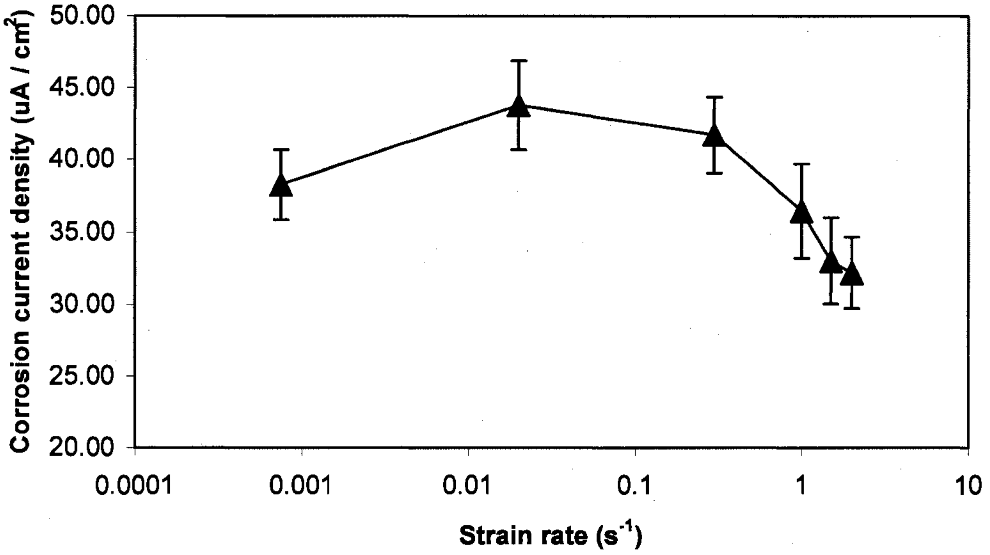

Fig.4-8 Variations in the corrosion current density (i_{corr}) of sub-fracture-surface layers as a function of strain rate. Solution: 3.5% NaCl.

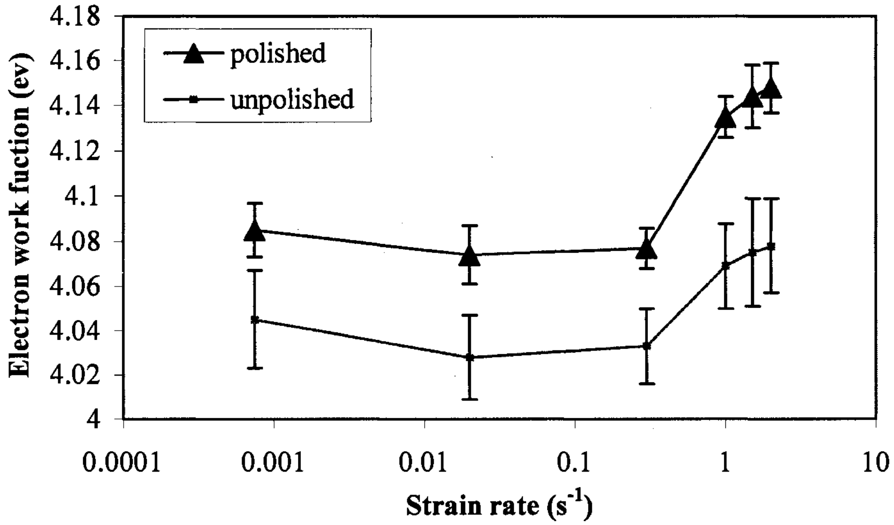

Fig.4-9 Variations in EWF of fracture surfaces with respect to the strain rate of prior deformation.

It has been demonstrated that EWF decreases with plastic deformation no matter if it is tensile or compressive [92], which indicates that dislocation renders electrons more active [93] and thus reduces the energy barrier to electrochemical reactions [127]. Usually, a heavily deformed metal is more anodic and has a higher corrosion rate, since its high-density dislocations provide a larger number of active sites at which corrosion is promoted. Previous experimental studies have confirmed that the corrosion rate of a metal increases with an increase in the amount of plastic deformation [121]. The results of the electrochemical test in this study are consistent with the EWF measurement and expected based on our previous studies. In summary, a fractured surface layer experienced deformation at a higher strain rate, though containing more microcracks and microvoids, had a lower dislocation density and thus a lower corrosion rate, compared to those deformed at lower strain rates (Fig. 4-8).

4.2.3 Effects of the strain rate on corrosive wear

Pin-On-Disc sliding wear tests were performed in a 3.5% NaCl solution to investigate effects of the strain rate of prior deformation on the corrosive wear behavior of AISI 1045 steel. Since depths of entire deformed zones in the specimens under study were larger than 14mm (Fig.4-6), the duration of the wear tests (40 min) should not be too long to touch the undeformed zone.

In this study, the wear loss caused by pure mechanical wear during corrosive wear was evaluated by performing corrosive wear test under cathodic protection. In order to minimize the influence of corrosion on wear, the wear rate of AISI 1045 steel was evaluated under various cathodic potentials. It was found that the wear rate reached the minimum at about –600 mV relative to the open circuit potential (OCP). Therefore, a cathodic protection potential of –600 mV relative to OCP was chosen for evaluating the contribution of pure mechanical wear to corrosive wear.

Effect of the strain rate of prior deformation on the corrosion-wear synergy was also investigated. The total material loss, T, includes the following three contributions (ASTM Practice G119-04):

$$T = W_0 + C_0 + S \tag{4.4}$$

Where W_0 is the volume loss caused by pure mechanical wear and C_0 is the volume loss caused by pure corrosion, which was estimated by multiplying the corrosion rate by the average surface area that was under the corrosive wear attack. S is the additional material loss caused by the corrosion-wear synergy.

Fig.4-10 illustrates effects of the strain rate of prior deformation on pure mechanical wear, total corrosive wear and that caused by the wear-corrosion synergy of 1045 steel in the 3.5% NaCl solution, respectively. As shown, the pure mechanical wear rate (volume loss per unit length of wear track) was relatively stable until $\dot{\varepsilon}=0.3\ s^{-1}$, above which the wear rate markedly increased against the strain rate. For the total corrosive wear and that caused by the wear-corrosion synergy, their variations with the strain rate were similar to that of the mechanical wear.

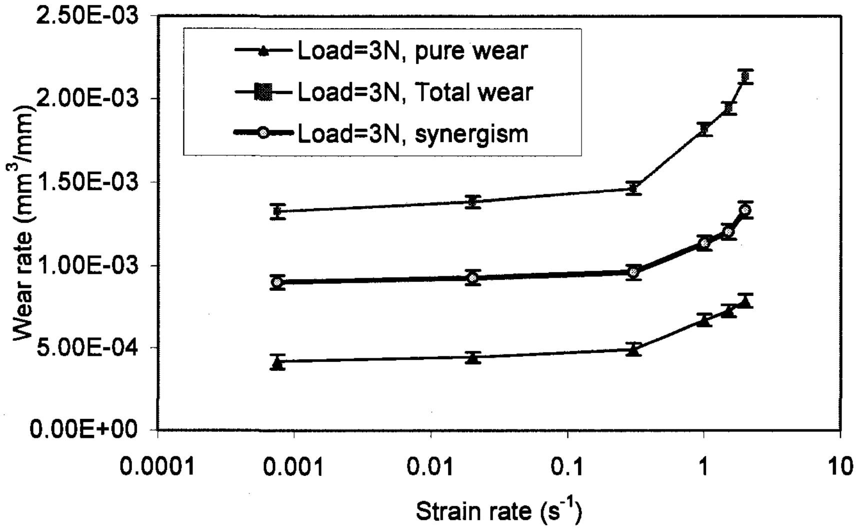

Fig.4-10 Effects of the strain rate of prior deformation on pure wear, wear-corrosion synergism and total corrosive wear of 1045 steel in a 3.5% NaCl solution. (load=3N).

In order to better understand the corrosive wear mechanism, worn surfaces after the wear tests were examined by SEM. Fig.4-11 illustrates wear tracks resulted from corrosive wear at different strain rates under a load of 3N. As shown, microgrooves, corrosion products, and wear debris were visible. More importantly, the number of surface cracks was increased with an increase in the strain rate of prior deformation. At the prior strain rate of 2 s^{-1}, the surface cracking was very severe as Fig.11 (c) shows.

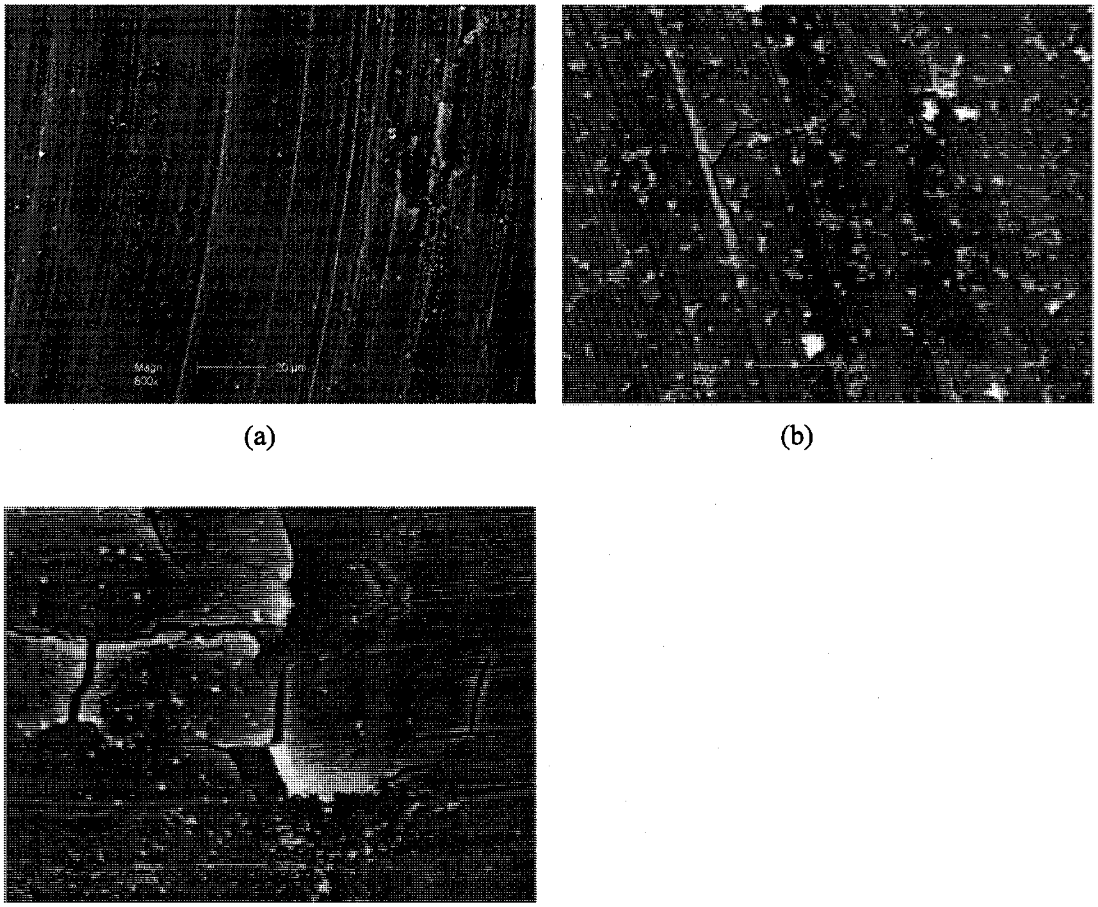

(a) (b)

(c)

Fig.4-11 SEM worn surface morphology (load=3N).

(a) Strain rate = 0.0075 s^{-1}.
(b) Strain rate = 0.3 s^{-1}.
(c) Strain rate = 2 s^{-1}.

The above observations are understandable. The prior deformation has two effects on the corrosive wear: On one hand, the strain hardening caused by prior deformation at low strain rates may benefit the wear resistance [121, 125], since the wear loss is lowered as the hardness of a target material increases [34], although such a benefit could be affected by the dislocation configuration. On the other hand, the increased dislocation density by the prior deformation can increase the corrosion rate [121, 127], which enhances the wear-corrosion synergy and could thus lead to faster material dissolution. Thus, the material loss rate could be relatively stable for specimens that experienced prior deformation at low strain rates. However, when deformed at higher strain rates, other generated defects i.e., the high-density microcracks could significantly deteriorate the mechanical behavior of the target material and thus negatively affect its performance during subsequent corrosive wear. The pre-existed microcracks may act as stress raisers and made the surface vulnerable to wear attack, especially in a corrosive environment. The corrosion-assisted cracking has been extensively investigated [128-132]. A crack could propagate by preferential dissolution at its tip [128-130], which is more anodic due to local plastic deformation and failure of passive film. It has also been suggested that the stress concentration at corrosion pits could reach fracture point and result in crack initiation [131, 132]. The cracks propagate through enhanced dissolution at crack tip and failure of remaining ligaments under applied stress.

In this study, it was observed that at lower strain rates ($\dot{\varepsilon}$ = 0.00075 s^{-1}, 0.02 s^{-1}, 0.3 s^{-1}), the strain hardening more or less benefited wear resistance although it decreased the corrosion resistance, rendering the corrosive wear resistance relatively stable with respect to the strain rate. However, at higher strain rates ($\dot{\varepsilon}$= 1 s^{-1}, 1.5 s^{-1}, 2 s^{-1}), the pure mechanical wear, synergistic attack and total corrosive wear loss all increased with the strain rate, as shown in Fig.4-10. This could be mainly attributed to the increase in the density of microcracks in the subsurface layer (Fig.4-2) as discussed earlier. It was noticed that the number of microcracks increased rapidly with the strain rate when the strain rate was higher than 0.3 s^{-1}. The increase in the density of microcracks could largely deteriorate the surface when subjected to mechanical attack although the corresponding corrosion rate decreased due to fewer dislocations introduced during prior deformation at higher strain rates. Therefore, the reduced resistance to mechanical attack due to the introduced microcracks could be mainly responsible for the increase in corrosive wear loss of those specimens experienced prior deformation at higher strain rates as Fig.4-10 illustrates.

4.2.4. Further discussion

The dynamic mechanical behavior of materials, i.e. deformation at high strain rates has been a subject of many studies for recent decades, due to its significance to engineering practice [96, 97]. Many investigators have examined the effects of strain rate on the dislocation density and configuration by means of transmission electron microscopy (TEM) [106-108]. In these studies, cellular dislocation substructures were observed, and the dislocation density increased with the strain rate; while the size of dislocation cells decreased with the strain rate. As a result, microhardness and flow stress have been found to increase as the strain rate was increased. It appears that the results obtained in this study conflict with the previous observations reported in literature. However, it must be pointed out that the previously reported experimental results were obtained using the Split-Hopkinson-pressure-bar technique, in which a specimen was deformed under compressive stress. In this case, the number of microcracks could be much smaller than that under tensile stress, bearing in mind that compressive stress cannot result in cracking. Therefore, more dislocations should be introduced to accommodate deformation under the compressive stress. This could be a reason why under compressive stress at high strain rates, more dislocations are generated, which move locally and result in smaller dislocation cells. However, in the tensile test, the applied tensile stress favors the formation of microcracks if dislocation cannot be generated timely to accommodate deformation. This may explain why smaller dislocation densities and larger densities of microcracks existed in samples fractured at higher strain rates, as observed in this study.

It should also be indicated that during sliding wear mixed with impact actions, a target surface is under external compressive force. However, wear is largely caused by the local tensile stress behind an asperity as it scratches over a specific region [34]. Besides, when impact actions are involved, a target surface may have no or little lateral constraint so that cracking can be generated by tensile stress components in directions perpendicular to the impact compressive force. Therefore, although the present research was conducted to investigate the effect of prior tensile deformation on subsequent corrosive wear, the obtained information would help to understand the corrosion-wear synergy involving impact actions.

4.3 Conclusion

Effects of the strain rate of prior deformation on corrosion and corrosive wear of AISI 1045 steel in a 3.5% NaCl solution were investigated. The following conclusions were drawn:

1) The strain rate of prior deformation considerably influenced the corrosion behavior of AISI 1045 steel. The corrosion rate initially increased and then decreased with an increase in the strain rate. This may be mainly attributed to the variations in dislocation density with respect to the strain rate. Dislocations make electrons more active and thus decrease the energy barrier to corrosion reactions. At high strain rates, the dislocation density was lower, which led to a lower corrosion rate. At the high strain rates, more microcracks were generated to compensate the decrease in dislocation density in order to accommodate deformation.

2) The strain rate of prior deformation had significant influence on the pure mechanical wear and total corrosive wear of AISI 1045 steel in the 3.5% NaCl solution. Under a load of 3N, the pure mechanical wear and total corrosive wear were relatively stable with respect to the strain rate of prior deformation until $\dot{\varepsilon}=0.3\ s^{-1}$, above which the wear rate increased markedly with respect to the strain rate. The strain rate of prior deformation also strongly affected the wear-corrosion synergy. The wear loss caused by

wear-corrosion synergy increased with the strain rate. The enhanced material loss at higher strain rates may be ascribed to the increased number of microcracks generated by the prior deformation which made the surface vulnerable to wear and corrosive wear attacks.

3) Both the total wear loss and corrosion-wear synergy were enhanced with an increase in the strain rate of prior deformation. Since at higher strain rates the corrosion resistance increased but mechanical properties considerably deteriorated, it appears that the mechanical degradation is mainly responsible for the increase in total wear loss and the enhancement of wear-corrosion synergy for a target material deformed at higher strain rates.

Chapter 5

Development of a modified technique for investigating wear-corrosion synergy

Corrosive wear of materials is a complex surface failure process, which involves both the wear-accelerated corrosion and the corrosion-accelerated wear. Separating contributions of these two processes to the total material loss is of significance for gaining better understanding of the wear-corrosion synergy. Previous studies have generated an electrochemical scratch technique for measuring the wear-accelerated corrosion, based on which other components involved in the corrosion-wear synergy can be determined. In this chapter, a new phenomenon in measuring the wear-accelerated corrosion is reported. It was observed that for non-passivation materials there existed a stirring effect (by pin), which significantly affected the measurement. The resulted mistake was serious. The previous technique was modified accordingly and applied to determine the corrosion-wear synergy of AISI 1045 steel in comparison with that of 304 stainless steel.

5.1. Introduction

Considerable efforts have been made to develop experimental techniques to investigate the wear-corrosion synergy [9-19]. Since the two processes, i.e. additional corrosion due to wear and additional wear due to corrosion, proceed simultaneously, it is difficult to distinguish them and thus to determine the corresponding material losses.

An electrochemical scratch technique was recently proposed and used to separate individual contributions of corrosion and wear to the total material loss caused by corrosive wear [18-19]. During the test, a target surface was scratched by a diamond tip under a certain normal load, and corresponding changes in the corrosion current were recorded. The change in corrosion rate due to wear was calculated using the Faraday Law and the recorded changes in the corrosion current [18]. In the previous studies, it was observed that in most cases the current increased rapidly when the scratch was started and then decreased when scratch was ended, indicating the additional material dissolution caused by wear.

In this chapter, a new phenomenon in measuring the additional corrosion due to wear is reported, which was observed when attempts were made to apply such a methodology to investigate the wear-corrosion synergy using a pin-on-disc sliding wear tester. It was noticed that when moving in a corrosive solution, the pin generated a stirring effect that resulted in negative changes in the corrosion current for non-passive alloys. Such negative changes generated misleading information on the addition corrosion due to wear. Efforts were then made in this study to understand such a phenomenon and accordingly a modified method is proposed to eliminate the stirring effect on the changes in corrosion current caused by wear.

5.2. Experimental details

In this study, two typical passive and non-passive steels, 304 stainless steel and AISI 1045 steel, were selected as sample materials. The former contained 0.08 wt% C, 2.0 wt % Mn, 1.0 wt% Si, 0.04 wt% P, 0.03 wt% S, 19.0 wt% Cr, and 9.0 wt% Ni, while the latter contained 0.43-0.50 wt% C, 0.60-0.90wt% Mn, maximum 0.04wt% P, and maximum 0.05wt% S. Cylinder pins, made of the above two materials, with length of 25.4mm and diameter of 6.35 mm were machined.

In order to determine the corrosion behavior of the materials, linear polarization and Tafel plot measurements were carried out using a Gamry PC4/750 electrochemical system. All experimental arrangements are the same as those described in Chapter 3.

The corrosion current density (icorr) was calculated based on the following equation: (ASTM standard G3-89):

$$i_{corr} = \frac{b_a b_c}{2.303(b_a + b_c)R_p}$$

where icorr = corrosion current density,

ba = anodic Tafel slope,

bc = cathodic Tafel slope,

R_p = linear polarization resistance

The icorr (the corrosion current density) value is converted to a materials loss rate (mm^3 / mm^2 year) according to ASTM Practice G102.

Corrosive sliding wear tests were performed on a pin-on-disc tribometer (CSEM Instruments, Switzerland). A schematic drawing of the apparatus is shown in Fig. 5-1. During a wear test, the pin, which was the tensile specimen, was pressed onto a rotating disc made of SiC under an applied normal load, with the fracture surface facing the counterface. The apparatus was attached with an electrochemical system (connected to Gamry PC4/750), which allowed a wear test performed in a plastic cell that contained a corrosive solution under an applied potential. A saturated calomel electrode (SCE) was used as the reference electrode and a platinum plate was used as the counter electrode. A 3.5% NaCl solution was used as the electrolyte solution.

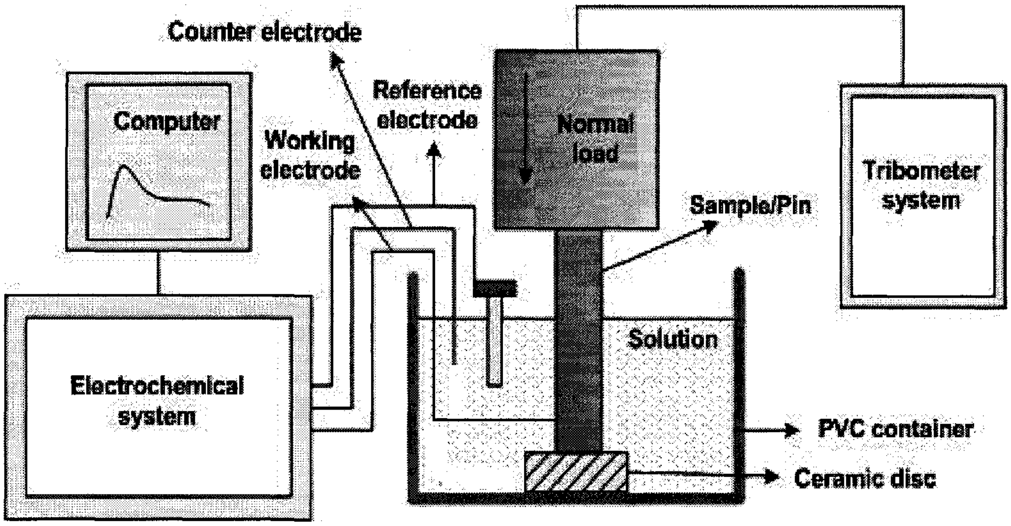

Fig.5-1 Schematic illustration of the tribo-corrosion testing apparatus

The corrosive sliding wear tests were carried out under a normal load of 3N for about 400 s at various sliding speeds (0.1cm/s, 0.5 cm/s and 1cm/s). For measuring the total wear loss rate, the wear tests were performed at open circuit potential. In order to determine the pure mechanical wear rate, the wear test was performed under cathodical protection by applying a certain potential (-600 mV for AISI 1045 Steel [133] and -1000 mV for stainless steel [134]) relative to the open circuit potential. The material loss was determined by measuring the weight, after conversion to the volume loss, the final wear rate was presented as the volume loss per unit exposed area per unit time. In determining the weight loss, a corrosion product removal procedure was used according to ASTM standard G1-03.

In order to investigate the stirring effect on the measured change in corrosion rate due to wear (ΔCw), two groups of test were used: one was a corrosive sliding wear test; the other was a stirring-only test in which the pin was suspending in the solution and rotating without in contact with the disc surface. Various sliding speeds were used (0.1 cm/s, 0.5 cm/s and 1 cm/s) in order to investigate the effect of stirring speed on measured ΔCw.

5.3. Results and Discussion

5.3.1. Background

As suggested (ASTM G119 – 04), corrosive wear rate (T) may be represented a summation of the wear rate in the absence of corrosion (W_0), the corrosion rate in the absence of wear (C_0), and the synergistic component (S):

$$T = W_0 + C_0 + S \qquad (5.1)$$

The synergistic component, S, can be further divided into two components: the change in corrosion rate due to wear (ΔCw) and the change in wear rate due to corrosion (ΔWc).

$$S = \Delta Cw + \Delta Wc \qquad (5.2)$$

According to equation (1), if the additional corrosion due to wear (ΔCw) is determined, the additional wear due to corrosion (ΔWc) can thus be calculated:

$$\Delta Wc = S - \Delta Cw = [T - (W_0 + C_0)] - \Delta Cw \qquad (5.3)$$

T, W_0 and C_0 may be determined by performing corrosive wear test, wear test under cathodic protection, and corrosion measurement, respectively. Consequently, contributions of all individual components to corrosive wear can be determined. Such information is of importance to the design or modification of materials used in corrosive wear environments.

The change in corrosion rate due to wear (ΔCw) may be measured using a potentiostatic method in which a corrosion current vs. time curve is recorded under free potential [18, 19]. When a metal is subject to wear in a corrosive solution, a fresh but deformed metal surface is produced. This will increase the corrosion current due to introduced dislocations in the surface layer and damage to surface films. When sliding contact is ended, the current could restore to the value prior to wear because of the formation of adsorption layer or repassivation of the scratched metal surface [18]. The change in current is schematically illustrated in Fig. 5-2. Such a phenomenon was observed in the previous studies [18, 19].

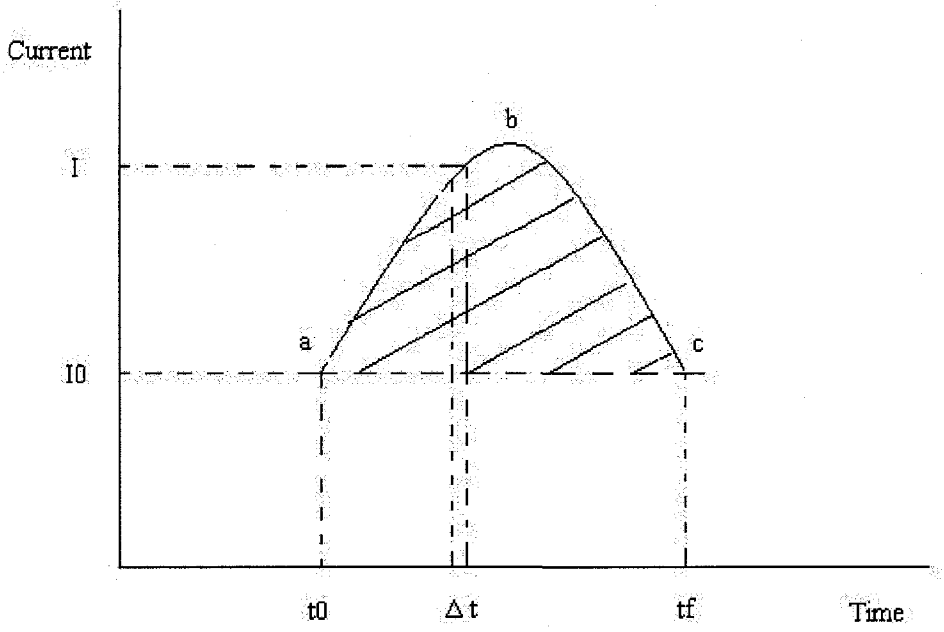

Fig. 5-2 A schematic illustration of the change in current with time during corrosive sliding wear test

During a corrosive sliding wear process, a fresh and deformed metal surface is produced and this results in an increase in the quantity of electric charge (Q), which equals the dashed area under the current-time curve (abc) as Fig.5-2. illustrates, that is

$$Q = \int_{t0}^{tf} (I - I_0)\,dt \tag{5.4}$$

where t_0 is the time when sliding wear starts, and t_f is the time when sliding wear ends. I is the measured current during the sliding contact and I_0 is the current prior to the sliding wear. Q is therefore a measure of additional metal dissolution due to wear. The average increase in corrosion current (ΔI) may thus be calculated as

$$\Delta I = Q / (t_f - t_0) \qquad (5.5)$$

Such an increase in corrosion current (ΔI) can be converted to the material loss rate (ΔCw) represented as the volume loss per unit area per unit time, using the following equation (ASTM Practice G102):

$$\Delta Cw = K \cdot \Delta I \cdot EW / \rho \qquad (5.6)$$

where, $K = 3.27 \times 10^{-3}$ (mm g/μA cm yr), ρ is density of the tested material in g/cm^3, EW is an equivalent weight of the tested material, ΔCw is given in mm^3 / mm^2 year. Two dimensionless factors are used to evaluate the degree of wear-corrosion synergy. The corrosion augmentation factor is defined as:

$$(C_0 + \Delta Cw) / C_0 \qquad (5.7)$$

This factor reflects the effect of wear on corrosion. The wear augmentation factor, which reflects the effect of corrosion on wear, is defined as:

$$(W_0 + \Delta Wc) / W_0 \qquad (5.8)$$

5.3.2 A new phenomenon observed in measuring the change in corrosion rate due to wear (ΔCw)

In this study, corrosive sliding wear tests were performed for 304 stainless steel and AISI 1045 steel in a 3.5% NaCl solution under free corrosion potential. The measured transits of potentiostatic current density are presented in Fig. 5-3 (a) and (b), respectively. As shown, for 304 stainless steel (Fig.5-3(a)), as the sliding wear was started, the corrosion current immediately increased and then gradually rose during the sliding process. When sliding was ended, the current restored to the initial level (approximately zero). This observation is similar to the results reported in a previous paper [18]. Such changes are attributed to the fact that when the wearing force damaged the surface passive film and resulted in a fresh but deformed metal surface, there was a corresponding increase in current, which however disappeared after the sliding action was terminated due to the repassivation of the stainless steel.

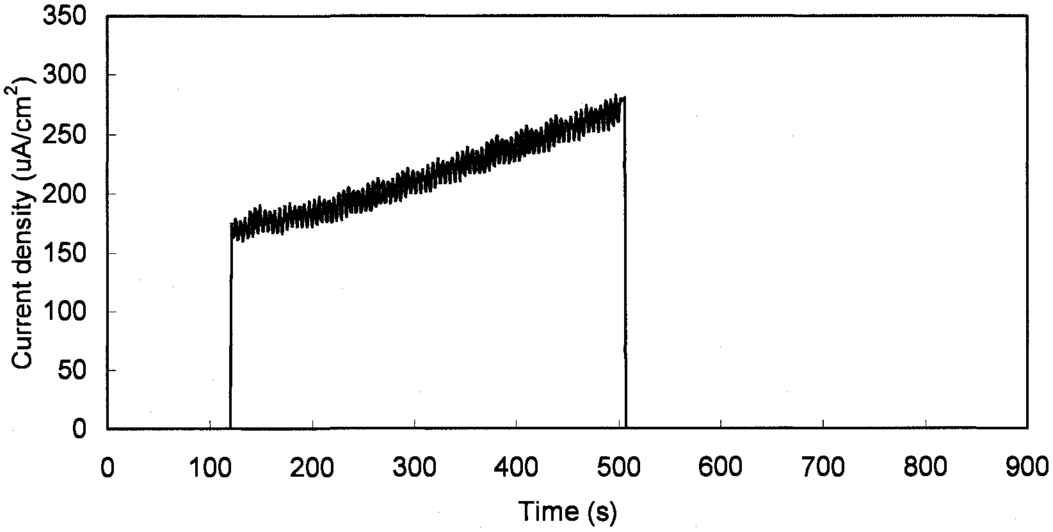

(a)

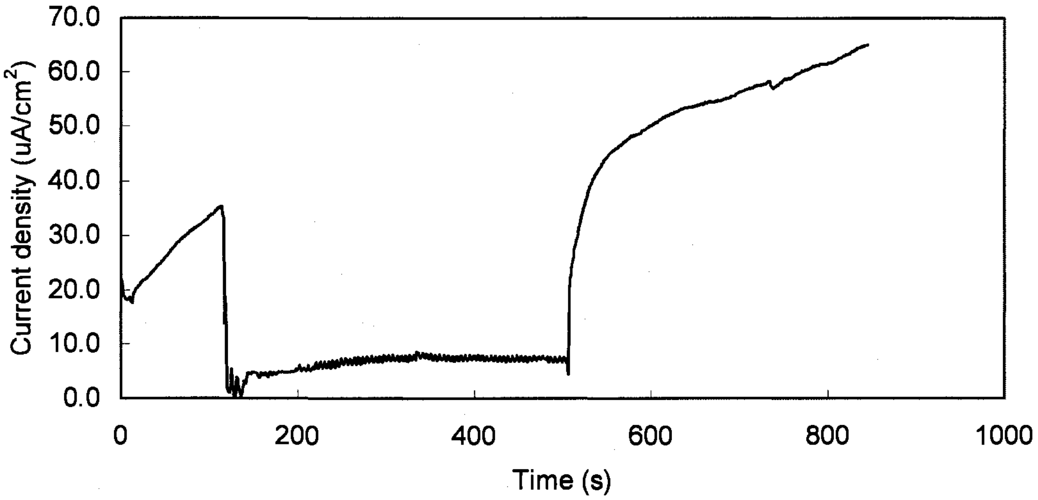

(b)

Fig.5-3 Potentiostatic current density transients measured on a) 304 stainless steel b) AISI 1045 steel during the corrosive sliding wear tests in a 3.5% NaCl solution.

The situation changed in the case of AISI 1045 steel. As illustrated in Fig.5-3 (b), the corrosion current increased when the sample was placed in the solution and it immediately dropped when sliding wear was started. As the sliding wear proceeded, the current was relatively stable. When the sliding process was ended, the initial situation was restored and the current continued to increase following the initial trend. Such changes in current are very different from previous observations during electrochemical scratch tests [11, 12].

In order to understand this new phenomenon, a stirring-only test was performed. During this test, the pin was suspended in the solution and rotated without touching the disc surface. The results are shown in Fig. 5-4 (a) and (b) for 304 stainless steel and AISI

1045 steel, respectively. In the figures, the results obtained from corrosive wear tests, in which the rotating pin was in contact with the disc, are superimposed for comparison.

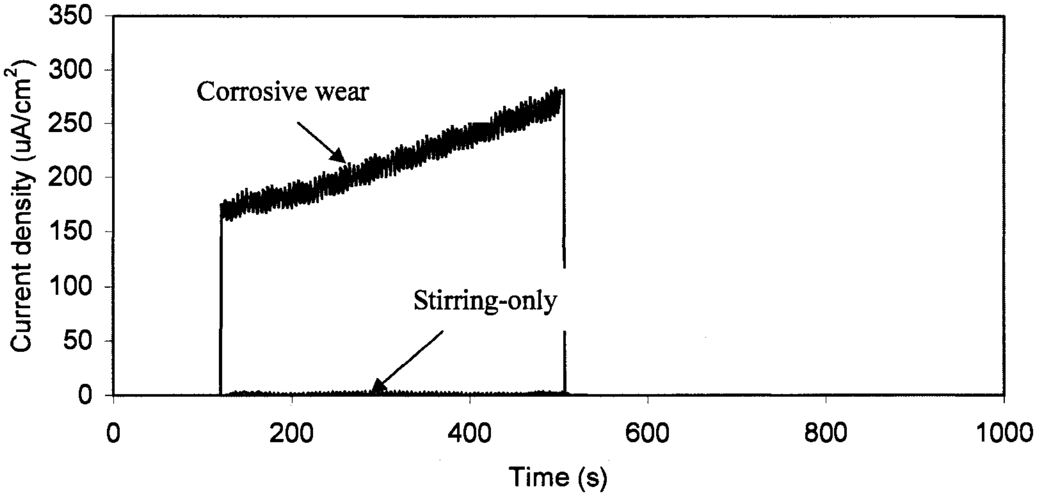

(a)

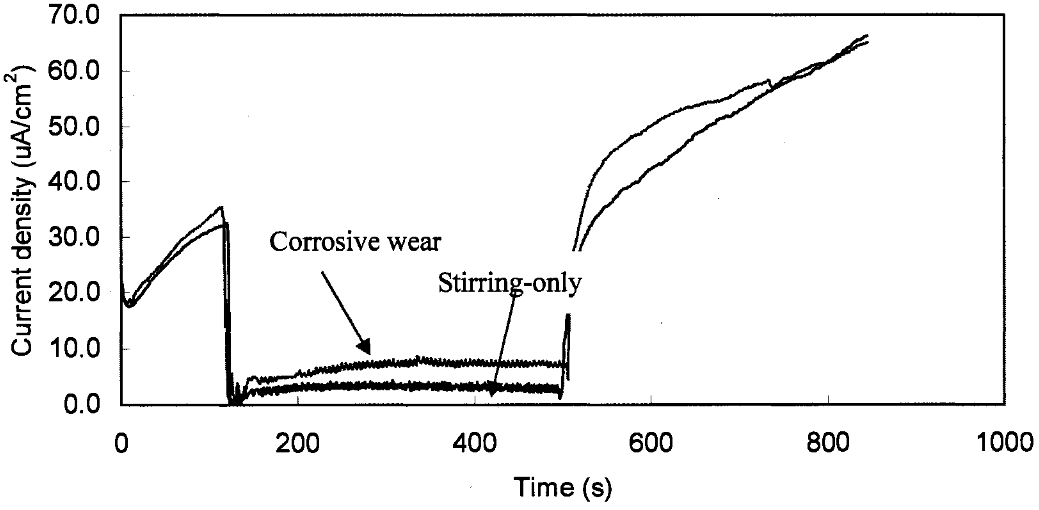

(b)

Fig.5-4 Comparison in potentiostatic current density transients measured on a) 304 stainless steel b) AISI 1045 steel during the stirring-only tests and corrosive wear tests in a 3.5% NaCl solution.

As illustrated in Fig.5-4 (a), under the stirring-only condition, no distinguishable changes in current were observed for the 304 stainless steel. While for the AISI 1045 steel, under the stirring-only condition, a significant drop of current was observed. The amount of the current drop was larger than that caused by sliding contact.

The above results are understandable. During sliding wear tests the motion of the pin provokes stirring the solution and therefore can influence the kinetics of mass transport that is involved in the corrosion electrochemical reactions. At high corrosion rates, electrochemical reactions deplete dissolved species, e.g. dissolved oxygen, in adjacent solution. This makes the mass transport to be a rate-determined process for the electrode reactions, which is so-called concentration polarization [135]. In most cases of corrosion, the concentration polarization is significant for cathodic reduction processes, especially the oxygen reduction. While the concentration polarization for anodic oxidation is usually ignored because a prompt supply of metal atoms is available at the interface and the mass transport of metal ions in the electrolyte is very fast. In the present study, the cathodic process is primarily the reduction of dissolved oxygen:

$$O_2 + 2H_2O + 4e^- \longrightarrow 4\,OH^- \qquad (5.9)$$

The maximum solubility of dissolved oxygen in water is relatively low, about 8ppm at room temperature [135]. In static condition, corrosion is controlled by the diffusion of dissolved oxygen to the steel surface. When the solution is stirred, the cathodic process is greatly facilitated by enhanced oxygen transport and supply.

On the other hand, during an electrochemical test, to meet requirement of charge conservation, the measured current / applied current is equal to [135]:

$$i_{app} = |i_a| - |i_c| \tag{5.10}$$

where i_a is the anodic current and i_c is the cathodic current. As mentioned earlier, stirring can significantly increase the cathodic current while its influence on the anodic current is negligible. As a result, the measured current (i_{app}) can be reduced (or negatively increased) as stirring was introduced, thus leading to a drop of the current as shown in Fig. 5-4 (b) for AISI 1045. However, when the metal surface is covered by a protective oxide film or passive film as that on the 304 stainless steel, the corrosion rate is very low, and the concentration polarization is weak due to the low consumption rate of dissolved oxygen. In this case, the stirring has no significant influence on the cathodic processes. Furthermore, for a passivation metal, stirring could facilitate the passivation process due to the oxidizer concentration effect [135], i.e. more dissolved oxygen was provided to promote passivation. Thus, the anodic current can be suppressed by stirring. The total measured current could be decreased. However, since the measured current prior to wear for 304 stainless steel was very low (0.58 μA/cm^2), stirring has no observable influence on the measured current, as shown in Fig.5-4. (a).

The difference between the current-time curves of sliding test and stirring-only test was plotted in Fig. 5-5 (a) and (b) for 304 stainless steel and AISI 1045 steel, respectively. As shown, in both cases, net current increases were measured, which indicates that corrosion was enhanced by wear regardless if the material is passive or non-passive. By using equation (4) – (6), the change in the current (ΔI) was measured and converted in to change in material loss rate (ΔCw). The results are given in Table 5-1.

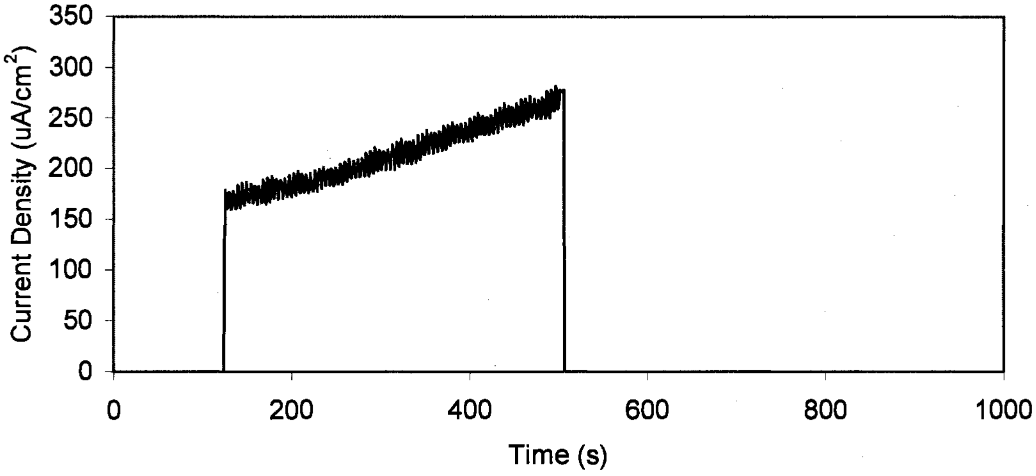

(a)

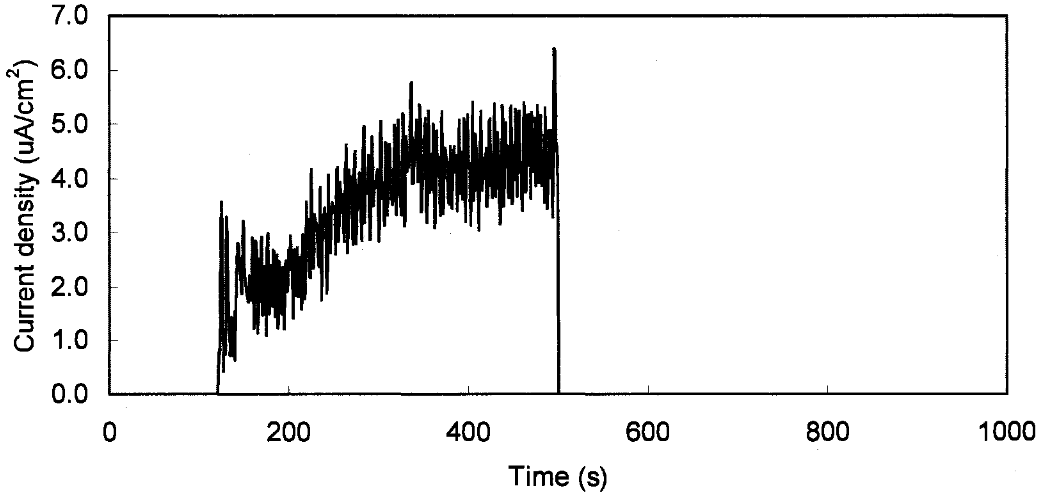

(b)

Fig.5-5 Difference in potentiostatic current density transients measured on a) 304 stainless steel b) AISI 1045 steel during the stirring-only tests and corrosive wear tests in a 3.5% NaCl solution.

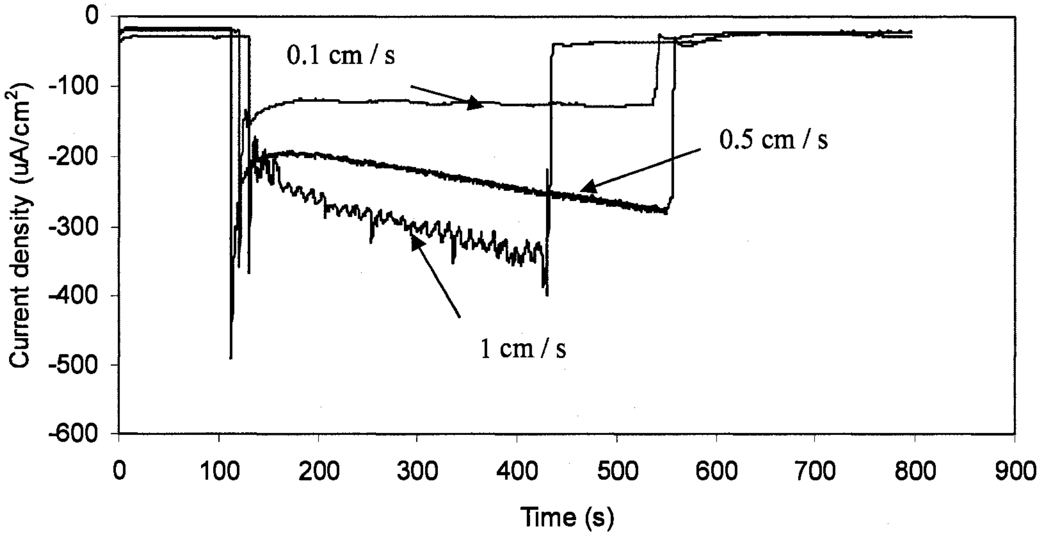

(a)

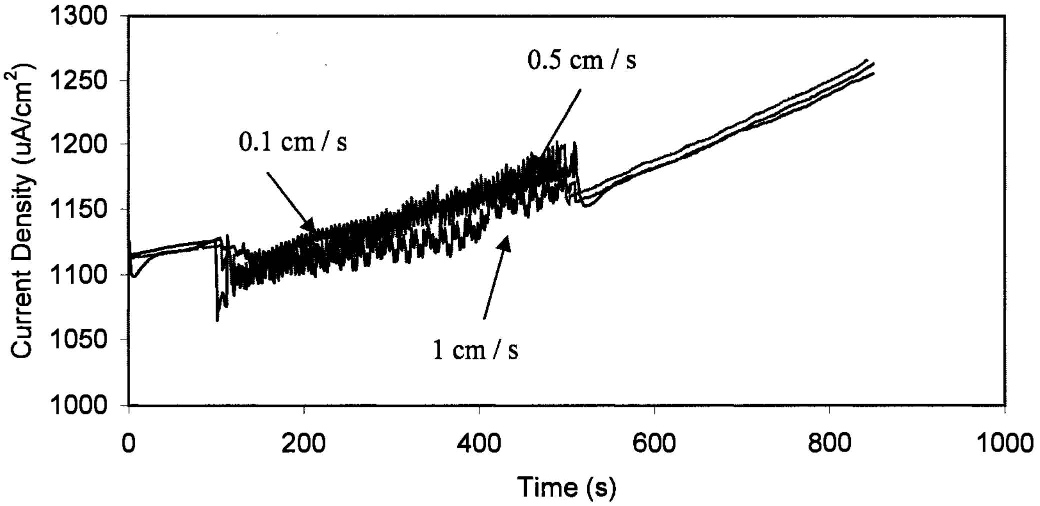

(b)

Fig.5-6 Potentiostatic current density transients measured on AISI 1045 steel during the stirring-only tests in a 3.5% NaCl solution at various stirring speed. (a) at cathodic potential –600mV vs. OCP (b) at anodic potential 200mV vs. OCP.

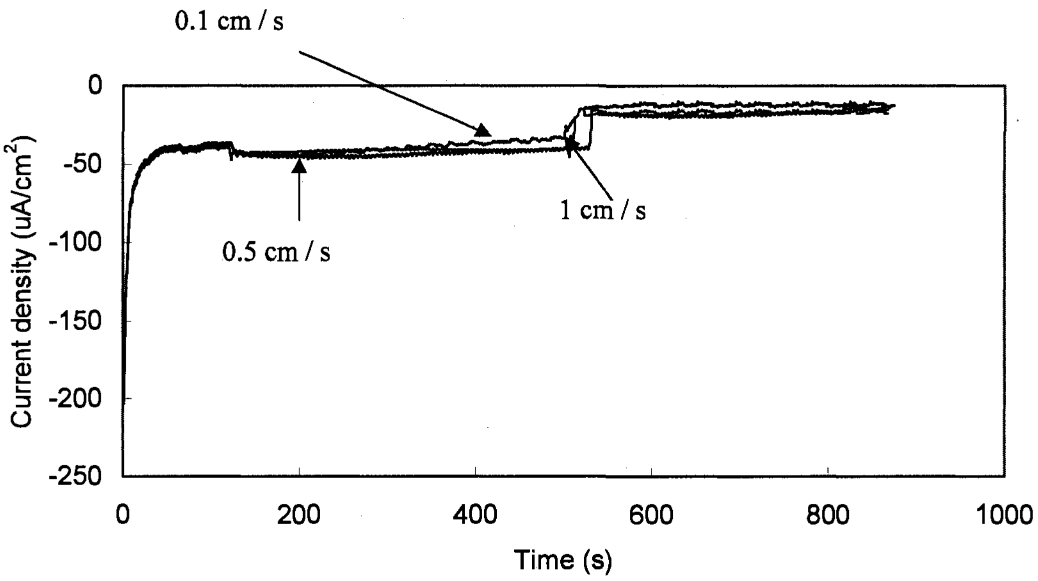
0.1 cm / s
0.5 cm / s
1 cm / s
Current density (uA/cm^2)
0
-50
-100
-150
-200
-250
0
200
400
600
800
1000
Time (s)

(a)

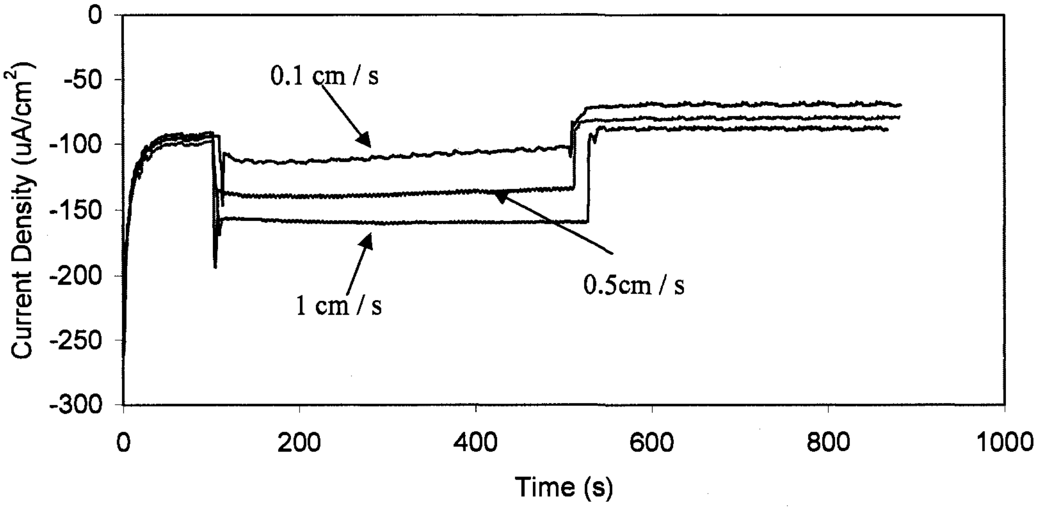
0.1 cm / s
0.5cm / s
1 cm / s
Current Density (uA/cm^2)
0
-50
-100
-150
-200
-250
-300
0
200
400
600
800
1000
Time (s)

(b)

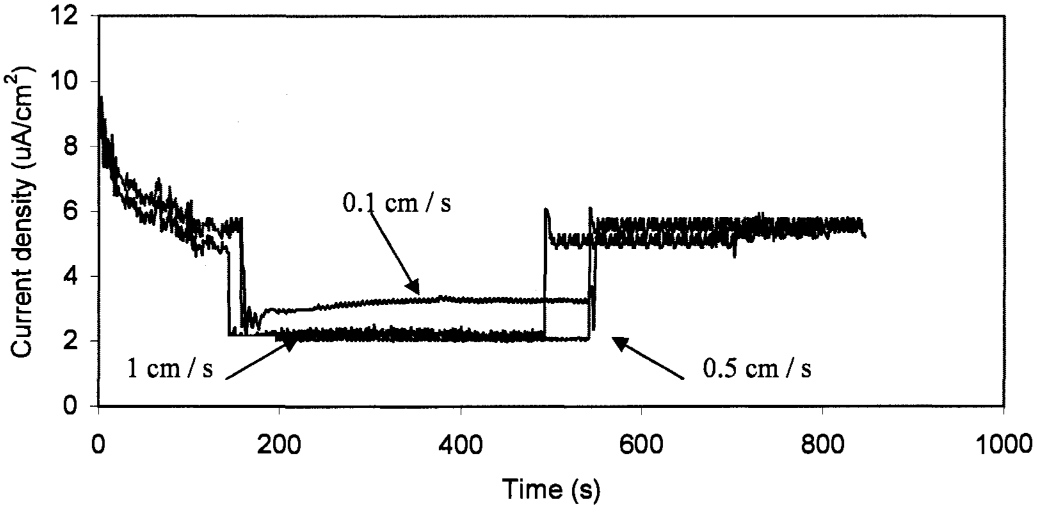

(c)

Fig.5-7 Potentiostatic current density transients measured on 304 stainless steel during the stirring-only tests in a 3.5% NaCl solution at various stirring speed.

(a) at cathodic potential –600mV vs. OCP, with passive pre-treatment

(b) at cathodic potential –600mV vs. OCP, without passive pre-treatment

(c) at anodic potential 200mV vs. OCP.

Table 5-1. Results of measured change in material loss rate due to wear (ΔCw).

Material	ΔI (μA cm^{-2})	ΔCw (mm^3 mm^{-2} year^{-1})
1045 steel	3.1	0.036
304 steel	228	2.359

To confirm the above explanation, stirring-only tests at rotating speed of 0.1cm/s, 0.5 cm/s, 1 cm/s were conducted under applied potentials of -600 mV and 200 mV relative to the open circuit potential, respectively. Potentiostatic current density transients were measured and are shown in Figs. 5-6 and 5-7 for AISI 1045 steel and 304 stainless steel, respectively.

As shown in Fig.5-6 (a) for the AISI 1045 steel under a cathodic potential of –600mV vs. OCP, when cathodic potential was applied, a current drop occurred when sliding wear was started. Because the cathodic current is negative, such a current drop is actually an increase in the absolute value. When the rotating speed was increased, the amount of current change increased, indicating that the stirring effect enhanced the cathodic process. Fig. 5-6 (b) illustrates the effects of stirring on the anodic current of AISI 1045 steel under a potential of 200mV vs. OCP. It was shown that stirring had no significant influence on the anodic process in this case: only a fluctuation in the current was observed.

For 304 stainless steel, in order to investigate the effect of stirring on the cathodic process during stirring-only tests, two types of electrochemical conditions were applied. For the first type, a passivation pre-treatment was made by immersing a polished sample in the NaCl solution for 15 minutes, followed by applying a potential of - 600 mV relative to the open circuit potential, which was maintained throughout the sliding wear tests. The potentiostatic current transient was shown in Fig.5-7 (a). As shown, the stirring had no significant influence on the cathodic process. This may be ascribed to the existence of a protective passive film that isolated the metal from the solution. In the second type of experiment, the cathodic potential (-600mV vs. OCP) was applied to a polished sample (fresh) and maintained from the very beginning. The potentiostatic current transient was shown in Fig.5-7 (b). In this case, an increase in the absolute value of cathodic current was observed when stirring was applied. This may be attributed to the absence of a well developed passive film. When the stirring speed was increased, the amount of current change increased, which is similar to those shown in Fig.5-6 (a).

The effect of stirring on the anodic process of 304 stainless steel is illustrated in Fig.5-7(c). As shown, under the applied anodic potential of 200 mV, stirring caused a current drop of 3-4 $\mu A/cm^2$ and the anodic current was further reduced as the stirring speed was increased. Such a phenomenon could be ascribed to the stirring-accelerated passivation.

5.3.3 Determination of the wear-corrosion synergy

The pure corrosion rate (C0) was measured using potentiodynamic electrochemical method (ASTM standard G3-89). Sample results of the measurements for both 304 stainless steel and AISI 1045 steel are given in Table 5-2. Obtained corrosive sliding wear data are presented in Tables 5-3 and 5-4. The wear-corrosion synergy was evaluated using equations (1) - (8) and the results are presented in Table 5-5.

Table 5-2. Results of polarization measurement for AISI 1045 steel and 304 stainless steel in 3.5% NaCl solution.

Material	Ecorr (mV, SCE)	b_a (mV decade^{-1})	b_c (mV decade^{-1})	Rp (Ω-cm^2)	icorr (μA cm^{-2})	Material loss rate (mm^3 mm^{-2} year^{-1})
1045 steel	-583	84	178	1.28E+03	19.39	0.225
304 steel	-239	276	81	4.68E+04	0.58	0.006

Table 5-3. Sample wear test data for 304 stainless steel

Material	AISI 304 steel					
Density (g cm^{-3})	7.94					
Specimen area (mm^2)	285					
Test condition	Initial weight (g)	Final weight (g)	Weight loss (g)	Time (s)	Material loss rate (mm^3 mm^{-2} year^{-1})	Material loss rate symbol
Corrosive wear test	43.2656	43.2649	0.0007	410	23.793	T
Cathodic protection test	43.0243	43.0237	0.0006	395	21.169	W_0

Table 5-4. Sample wear test data for AISI 1045 steel

Material	AISI 1045 steel					
Density (g cm^{-3})	7.86					
Specimen area (mm^2)	285					
Test condition	Initial weight (g)	Final weight (g)	Weight loss (g)	Time (s)	Material loss rate (mm^3 mm^{-2} year^{-1})	Material loss rate symbol
Corrosive wear test	44.0456	44.0428	0.0028	407	96.851	T
Cathodic protection test	42.5243	42.5225	0.0018	412	61.506	W_0

Table 5-5. Synergy summary for AISI 1045 steel and 304 stainless steel in 3.5% NaCl solution.

	Materials loss rate ($mm^3\ mm^{-2}\ year^{-1}$)						Unitless Factors		
Material	T	W_0	C_0	S	ΔCw	ΔWc	Corrosion augmentation $(C_0+\Delta Cw)/C_0$	Wear augmentation $(W_0+\Delta Wc)/W_0$	Synergy % of Total loss
1045 steel	97.042	61.423	0.225	35.39	0.036	35.36	1.16	1.58	36.5%
304 steel	24.685	20.844	0.006	3.84	2.36	1.48	394.33	1.07	15.5%

As shown in Table 5-5, although the contribution of corrosion alone is very small, from 0.02% (304 stainless steel) to 0.2 % (AISI 1045 steel) of the total material loss, the synergy of wear and corrosion was pronounced. The material loss from the wear-corrosion synergy is significant, ranging from 15% for 304 stainless steel to 36% for AISI 1045 steel (see Table 5-5). This implies that corrosion plays a very important role in the corrosive wear process.

It is also shown that 304 stainless steel has much larger corrosion augmentation factor (394) than AISI 1045 steel (1.16), which is understandable. 304 stainless steel is highly resistant to corrosion due to its strong ability to form a protective passive film on the surface. When the passive film is broken by the wearing force, a fresh metal surface is exposed to the corrosive solution and this could result in a significant increase in the corrosion rate. For AISI 1045 steel, since its surface oxide film is weak or non-protective; when the oxide film is damaged by the wearing force, the corresponding increase in the corrosion rate may not be large relative to its initial corrosion rate, so that a large corrosion augmentation factor is not expected for the carbon steel.

One may see that AISI 1045 steel has a relatively larger wear augmentation factor than the 304 stainless steel. This could be mainly due to the difference in corrosion resistance. During the corrosive wear, the corrosive environment could change the surface structure, e.g., forming a protective passive film or resulting in a degraded surface, and thus affect the surface resistance to mechanical failure. Since 1045 steel has much lower corrosion resistance, the mechanical removal process could be considerably facilitated.

5.4. Conclusions

A new phenomenon was observed during evaluating the wear-corrosion synergy using a corrosive sliding wear test. It was discovered that for non-passivation materials there existed a stirring effect (by pin) which could result in misleading information for determining the additional corrosion due to wear (ΔCw), an important parameter that affects the evaluation of the wear-corrosion synergy. The resulted mistake was serious for non-passive materials but negligible for passive materials, confirmed by the present studies on AISI 1045 steel and 304 stainless steel. The study has led to a correct methodology for investigation of the wear-corrosion synergy.

Chapter 6

Investigation of Effects of the strain rate of prior deformation on the wear-corrosion synergy of carbon steel

In chapter 4, it has been demonstrated that the wear-corrosion synergy can be significantly influenced by the strain rate. In this chapter, using a modified electrochemical sliding wear technique described in Chapter 5, we investigated effects of the strain rate of prior deformation on the wear-corrosion synergy of AISI 1045 steel in a dilute sodium chloride solution. Various strain rates of prior deformation in the range from 7.5×10^{-4} s^{-1} to 2 s^{-1} were chosen for this study. Contributions of individual factors to the total wear loss, including pure wear, pure corrosion, and the corrosion-wear synergy, were determined. In particular, effects of the strain rate of prior deformation on the additional corrosion caused by wear and additional wear caused by corrosion, which are two components of wear-corrosion synergy, were investigated. It was observed that at high strain rates, these two components of the wear-corrosion synergy were markedly enhanced, which was largely attributed to the material deterioration with defects such as microcracks generated by deformation at high strain rates. The experimental results are explained based on changes in surface microstructure and corresponding electrochemical and mechanical properties against the strain rate of prior deformation.

6.1. Introduction

In chapter 4, effects of the prior impact actions (i.e. the prior deformation at high strain rates) on subsequent corrosion and corrosive wear were investigated. However, corrosive wear is a complex process which includes contributions from wear (W_0), corrosion (C_0), and the wear-corrosion synergy (S) that is the summation of additional wear due to corrosion (Δ Wc) and additional corrosion due to wear (ΔCw). Thus, the total corrosive wear is expressed as

$$T = W_0 + C_0 + S = W_0 + C_0 + (\Delta Cw + \Delta Wc) \quad (6.1)$$

In the preliminary studies [125, 133] reported in chapter 4, only the total wear-corrosion synergy (S) was evaluated without further resolving it into ΔCw and ΔWc. Design and selection of effective materials to resist wear in such a mode requires more comprehensive and quantitative information, including the contributions of individual factors to the total wear-corrosion synergy (i.e. ΔCw and ΔWc). Besides, in our earlier studies the corrosive wear was evaluated using a pin-on-disc apparatus, in which a ceramic tip (or pin) was used to scratch a target surface. A drawback of this experimental configuration is that it may not exclude continuous dissolution of a non-passive material after the scratch action is stopped, because the surface defects (such as micro cracks and dislocations) resulting from scratching or sliding could continuously affect the material dissolution. Therefore, the measured wear-corrosion synergistic contribution (S) to the total material loss may not only include the simultaneous corrosion-wear synergy but also extra dissolution due to the post-effect of generated surface defects on corrosion.

In Chapter 5, a new experimental technique was developed to take into account the above-mentioned two issues. This new experimental technique, in which the pin is the target sample while the disc is a ceramic material (see Fig.6-1), allows determining simultaneous ΔCw and ΔWc [134], and the post-effect of surface defects on corrosion can be excluded or minimized. In addition, a potentiostatic current density transient is measured during the corrosive wear test, so that the corrosion component in the wear-corrosion synergy (ΔCw) and the wear component ΔWc = S - ΔCw can be determined.

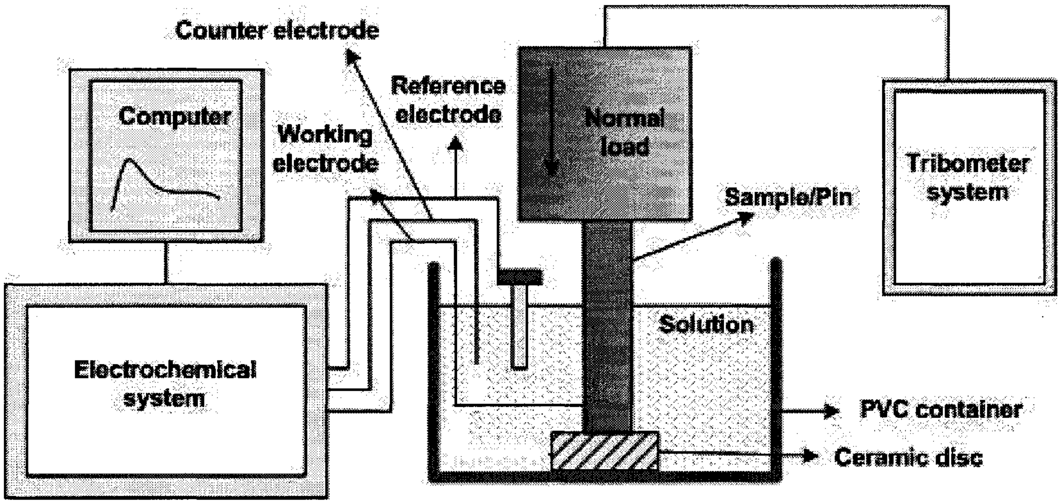

Fig.6-1 Schematic illustration of the tribo-corrosion testing apparatus

In this chapter, using the above-described experimental technique, effects of the strain rate of prior deformation on the wear-corrosion synergy of AISI 1045 steel in a 3.5% NaCl solution were investigated and quantified. In particular, effects of strain rate of prior deformation on the two components of wear-corrosion synergy, ΔCw and ΔWc, were studied. Tensile tests at six strain rates from 7.5×10^{-4} s^{-1} to 2 s^{-1} were employed to generate the prior deformation. Such a range of strain rate could be representative for many industrial wear conditions, such as conveyers, grinding balls, crushers etc. in mining and mineral processing industries. The density of microcracks generated in the sub-fracture-surface layer was measured and quantified using SEM and a digital image analysis system.

6.2. Experimental details

AISI 1045 steel (0.43-0.50 wt% C, 0.60-0.90wt% Mn, maximum 0.04wt% P, maximum 0.05wt% S) was selected as a sample material. All specimens were austenized at 810°C for 45 minutes and then quickly cooled down to 640°C and maintained at the temperature for 30 minutes, followed by furnace cooling.

Tensile specimens with a gauge length of 25.4mm and a diameter of 6.35mm were machined. Tensile tests were carried out at strain rates of 0.00075, 0.02, 0.3, 1, 1.5, and 2 s^{-1}, respectively, using a servohydraulic (Instron) testing machine. For each strain rate, six samples were tested and used for corrosion and corrosive wear tests. Scanning electron microscopy (SEM) was used to observe microcracks in layers beneath the fracture surface. The density of microcracks in the sub-fracture-surface layer was quantitatively analyzed using a digital image analysis system.

In order to quantify the wear-corrosion synergy, the newly developed experimental technique described in detail in chapter 5 was used. The theoretical consideration is presented in chapter 5.

In this study, sliding wear tests in a 3.5% NaCl solution were performed on a pin-on-disc tribometer (CSEM Instruments, Switzerland). A schematic drawing of the apparatus is shown in Fig. 6-1. In this work, the disc was a ceramic material (Si_3N_4) while the pin was the tensile specimen with its fractured surface contacting the disc. Before the tests, fractured surfaces of all tensile specimens were polished using 320 and 600 grit abrasive papers. It should be indicated that the polishing treatment was carefully done to ensure that only a very thin surface layer of about 200-400 μm was removed, which should not affect the evaluation of surface layer's corrosive wear rates, because the fractured surface layers were fairly thick (more than 8mm, estimated from micro-indentation tests [133]). During a wear test, the pin was pressed onto the disc under an applied load. The apparatus was connected to a Gamry PC4/750 electrochemical system, which allowed a wear test performed in a plastic cell that contained a corrosive solution. A saturated calomel electrode (SCE) was used as the reference electrode and a platinum plate was used as the counter electrode.

The corrosive sliding wear tests were carried out under a load of 3N at a sliding speed of 0.5 cm/s for 400 seconds. To measure the total wear loss rate, the wear tests were allowed to proceed at the open circuit potential in the solution. In order to measure the pure mechanical wear loss rate, a wear test was performed under cathodic protection (to eliminate the corrosion influence) by applying a cathodic potential of -600 mV (see Ref [133]) relative to the open circuit potential. The wear loss was determined using weight loss that was converted to the volume loss per unit exposed area per unit time. In measuring the weight loss, a corrosion product removal procedure was used based on ASTM standard G1-03. The resultant worn surfaces were examined by SEM. The pure corrosion rate, reported in this paper, was calculated by converting the corrosion current density ($\mu A/cm^2$) measured earlier [133] into the material loss rate (mm^3/mm^2year) according to ASTM Practice G102.

The additional corrosion due to wear ΔCw may be measured using the developed technique described in Chapter 5. Thus the contributions of individual factors to the total wear-corrosion synergy (i.e. ΔCw and ΔWc) can be determined.

6.3. Results and discussion

Fig.6-2 presents microstructures of subsurface layers (SEM side view) in which microcracks are visible. Through image analysis, the density of microcracks in the sub-fracture-surface layer as a function of the strain rate was determined and summarized in Fig.6-3. As shown, both the density of the microcracks and their total length increased with the strain rate.

In Chapter 4, effects of the strain rate of prior deformation on the residual micro-strain and microhardness in the sub-fracture-surface layer were investigated [133], as shown in figure 4-3 and 4-5. As illustrated, the micro-strain initially increased slightly with the strain rate and then decreased when the strain rate was larger than 0.3 s^{-1}. Changes in hardness with the strain rate showed a similar trend.

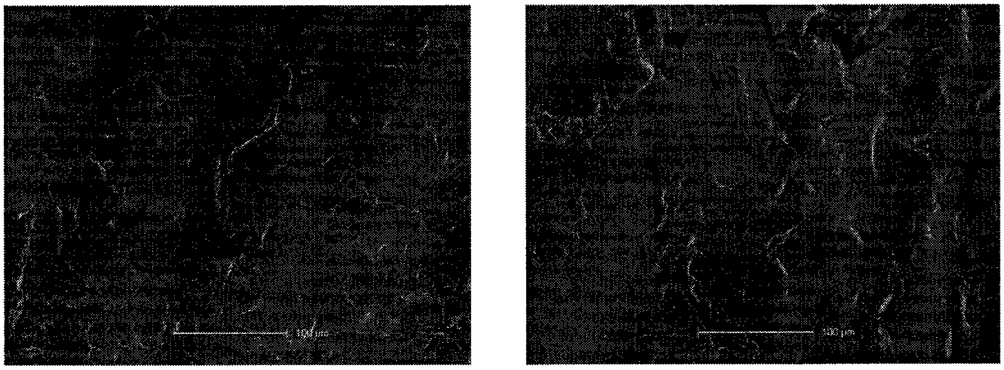

(a) (b)

Fig.6-2 Microscopic cracks in the sub-fracture-surface layer (side view).
(a) Strain rate = 0.00075 s^{-1}.
(b) Strain rate =2 s^{-1}.

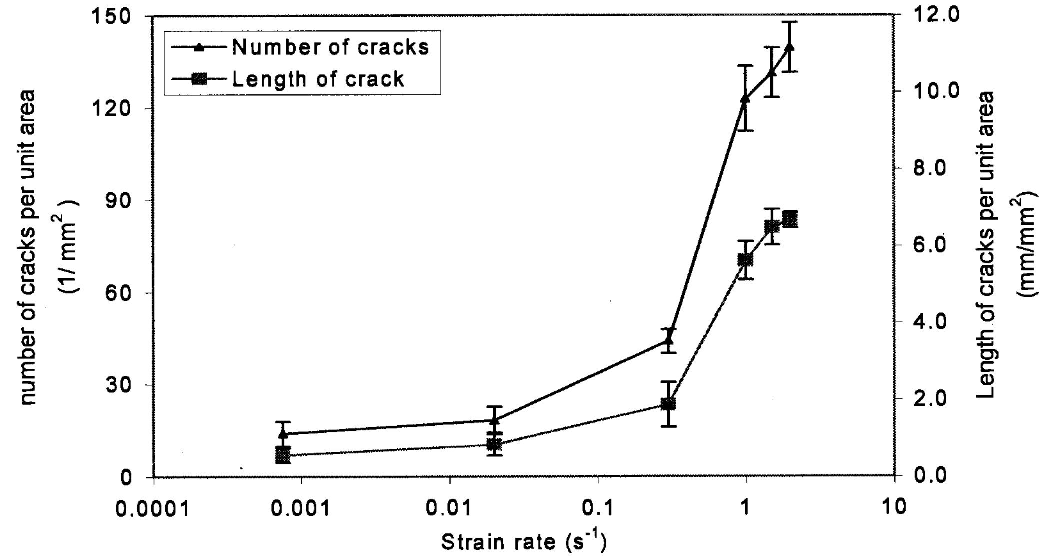

Fig.6-3 Density of microcracks in the sub-fracture-surface layer as a function of the strain rate of prior deformation

The observed variations in surface microstructure and mechanical properties with the strain rate (Fig.6-2, Fig.6-3, Fig.4-3, Fig. 4-5) could be explained based on the dislocation dynamics and energy conservation:

As discussed in Chapter 4, dislocations are more difficult to be generated and moved at higher strain rates. Under a tensile loading condition, the nominal deformation is accomplished in two ways: motion of dislocations and formation of microcracks and voids. These are two competitive processes. At higher strain rates, the motion and generation of dislocations become more difficult so that the plastic deformation was restricted. In order to accommodate deformation under an impact force, more microcracks and voids have to be generated. As shown in Fig.6-2 and Fig.6-3, when the strain rate was increased, the length and number of microcracks increased at expense of dislocation formation.

In Chapter 4, effects of the strain rate of prior deformation on the pure corrosion rate and wear rates including total corrosive wear (T), pure mechanical wear (W_0), and the wear-corrosion synergy (S), were measured and are shown in figure 4-8 and 4-10.

In this chapter, the rate of material loss due to the wear-corrosion synergy (S) was further resolved into two components: additional corrosion caused by wear (ΔCw) and additional wear caused by corrosion (Δ Wc). The results are shown in Fig.6-4. As shown, the additional corrosion rate (ΔCw) was relatively stable until $\dot{\varepsilon}=0.3\ s^{-1}$, above which it increased against the strain rate. The additional wear rate (Δ Wc) showed a similar trend since the latter was equal to S - ΔCw and S had a similar trend to that of ΔCw in terms of its variation with the strain rate. Explanation of the above observed phenomena has been given in later part of this chapter.

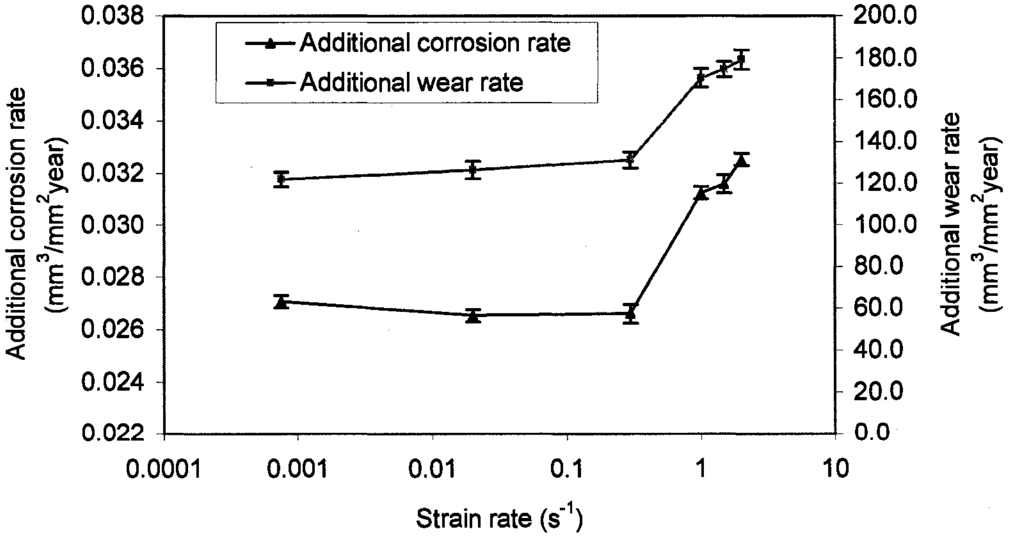

Fig.6-4 Effects of the strain rate of prior deformation on the rates of two component s of wear-corrosion synergy of 1045 steel in a 3.5% NaCl solution. (load=3N).

S/T, ΔCw/S, Δ Wc/S, ΔCw/C_0, Δ Wc/W_0 were calculated and summarized in Table 6-1. It is shown that, first, wear-corrosion synergy took a large portion of the total material loss (i.e. S/T = 62-64%); secondly, the additional wear caused by corrosion dominated the synergy (see Δ Wc/S) while the additional corrosion caused by wear took only a minor portion of the synergy (see ΔCw/S); thirdly, the ratio of additional wear to the pure wear (Δ Wc/W_0) is within the range of (160-180%), which means that in a corrosive environment the effect of mechanical attack on material loss was significantly magnified. However, ΔCw/C_0 was small. It is worth noting that in previous studies on cast iron and high-Cr iron using an electrochemical scratch technique [19], ΔCw/C_0 was very large, while it is not in the present case. The difference in ΔCw/C_0 between the present case and previous one could be attributed to the fact that the measured additional corrosion in the present study using the new technique only represented simultaneous corrosion-wear synergy while the previously measured included extra corrosion occurred after the wear action was completed at wear/scratch track due to scratch-generated defects such as dislocations that made the wear track more anodic with additional materials dissolution. It should also be mentioned that the ratio of ΔCw/C_0 varies, influenced by many factors, including the wearing stress, the corrosivity of the solution, the sliding speed, and the materials involved. Further studies are being conducted for more comprehensive information and understanding. It appears that the strain rate of prior deformation did not have a strong influence on the above ratios, although it affected the absolute value of the material loss rates (T, S, Δ Wc, etc.). Based on results shown in

Table 6-1, the mechanical damage played a predominant role in causing material loss during the corrosive wear process.

Table 6-1. Variations in a few important ratios related to the wear-corrosion synergy

Strain rate (s^{-1})	S / T	ΔCw / S	Δ Wc / S	$\Delta Cw/C_0$	$\Delta Wc/W_0$
0.00075	62.9%	0.0222%	99.97%	5.09%	170.3%
0.02	62.9%	0.0210%	99.97%	5.22%	170.4%
0.3	62.5%	0.0203%	99.97%	5.49%	167.5%
1	64.5%	0.0183%	99.98%	7.38%	182.4%
1.5	64.1%	0.0181%	99.98%	8.23%	179.6%
2	64.2%	0.0181%	99.98%	8.69%	180.0%

It was interesting to observe that the additional corrosion rate (ΔCw) increased with the strain rate when it was above 0.3 s^{-1}, as shown in Fig.6-4, while the rate of pure corrosion showed opposite trend (see Fig.4-8). This could be explained as follows: under the wearing stress, the high stress concentration at the tip of a crack can make the tip more anodic by introducing dislocations and destroying possible protective films on crack surface, thus accelerating the materials dissolution, especially when the density of microcracks is high at high strain rates of prior deformation. However, in the case of pure corrosion this may not happen because there is no external stress.

6.4. Conclusions

Effects of the strain rate of prior deformation on the wear-corrosion synergy of AISI 1045 steel in a 3.5% NaCl solution were investigated. The following conclusions were drawn:

1) The strain rate of prior deformation had significant influence on wear-corrosion synergy of AISI 1045 steel in the 3.5% NaCl solution. Under a load of 3N, both the additional corrosion due to wear and additional wear due to corrosion markedly increased when the strain rate was above $0.3s^{-1}$.

2) Since at higher strain rates the corrosion resistance increased but mechanical properties deteriorated, it appears that the mechanical degradation is more responsible for the increase in total wear loss and enhanced wear-corrosion synergy of the carbon steel experienced prior deformation at higher strain rates.

Chapter 7

Summary and Future Work

7.1 Summary of the research

Effects of strain rate of prior deformation on corrosion and corrosive wear behavior of carbon steel were investigated using electrochemical tests, electron work function measurements, and electrochemical sliding corrosive wear tests. It has been demonstrated that the strain rate of prior deformation strongly affects the wear-corrosion synergy of the material. In order to understand the mechanism responsible for strain rate - corrosive wear behavior relationship, SEM fractography, X-ray line profile analysis and micro-hardness testing were employed to investigate changes in microstructure and corresponding mechanical properties with respect to the strain rate. During the studies, a new experimental technique was developed to quantitatively investigate the corrosion-wear behavior. From the above-mentioned studies, the following conclusions are drawn:

1) The prior cold deformation raised the corrosion rate of copper and had a significant influence on the corrosive wear of the material, depending on the corrosive solution and the applied load. In the 0.1M HNO_3 solution, the ratio of the material loss caused by the corrosion-wear synergy to the total material loss increased with the cold work and became saturated when the cold work reached a certain level. In the 3.5% NaCl solution, however, this ratio decreased initially and then became relatively stable with respect to the deformation.

2) Effects of the loading speed or strain rate on corrosion and corrosive wear of annealed, impact-fractured and slow bending-fractured surface layers of AISI 1045 steel in a 3.5% NaCl solution were investigated. The results showed that the slow bending-fractured surface layer had the highest dislocation density and hardness, followed by the impact-fractured one, and the annealed sample had the lowest dislocation density and hardness. The effect of the strain rate on the dislocation density could be explained based on the dislocation dynamics and fracture mode. Electrochemical tests demonstrated that the slow bending-fractured surface had the highest corrosion rates, followed by the impact-fractured one, and the annealed one had the lowest corrosion rate. Such difference in corrosion rate could be mainly attributed to different dislocation densities, which influence the surface electron activity. Using electrochemical scratching tests, the corrosive wear performances of the three groups of samples were evaluated. It was demonstrated that under a low load of 5g, the slow bending fractured and impact-fractured surfaces had higher wear resistance than the annealed one, while under higher loads, the situation was reversed. Under the highest load of 30g, the impact-fractured surface showed the lowest resistance to corrosive wear.

3) The strain rate of prior deformation considerably influenced the corrosion behavior of AISI 1045 steel. The corrosion rate initially increased and then

decreased with an increase in the strain rate. This may be mainly attributed to the variations in dislocation density with respect to the strain rate. At higher strain rates, the dislocation density decreased due to the fact that the deformation could be accommodated by micro cracking.

4) The strain rate of prior deformation had significant influence on the pure mechanical wear and total corrosive wear of AISI 1045 steel in the 3.5% NaCl solution. Under a load of 3N, the pure mechanical wear and total corrosive wear were relatively stable with respect to the strain rate of prior deformation until $\dot{\varepsilon}$ =0.3 s^{-1}, above which the wear rate increased markedly with respect to the strain rate. The strain rate of prior deformation also strongly affected the wear-corrosion synergy. The wear loss caused by wear-corrosion synergy increased with the strain rate. The enhanced material loss at higher strain rates may be ascribed to the increased number of microcracks generated by the prior deformation which made the surface vulnerable to wear and corrosive wear attacks.

5) The strain rate of prior deformation strongly affected the two components of wear-corrosion synergy. Both the additional corrosion due to wear and additional wear due to corrosion markedly increased when the strain rate was above $0.3s^{-1}$.

6) Both the total wear loss and corrosion-wear synergy were enhanced with an increase in the strain rate of prior deformation. Since at higher strain rates

the corrosion resistance increased but mechanical properties deteriorated, it appears that the mechanical degradation was more responsible for the increase in total wear loss and enhanced wear-corrosion synergy of the carbon steel experienced prior deformation at higher strain rates.

7) A new phenomenon was observed during evaluating the wear-corrosion synergy using a corrosive sliding wear test. It was discovered that for non-passivation materials there existed a stirring effect (by pin) which could result in misleading information for determining the additional corrosion due to wear (ΔCw), an important parameter that affects the evaluation of the wear-corrosion synergy. The resulted mistake was serious for non-passive materials but negligible for passive materials, confirmed by the present studies on AISI 1045 steel and 304 stainless steel. The study has led to a modified methodology for investigation of the wear-corrosion synergy.

7.2 Possible future work

Effects of the strain rate of prior deformation on corrosion and corrosive wear behavior of carbon steel were investigated. It was shown that the strain rate had strong influence on corrosion and corrosive wear processes. In order to further understand the mechanism responsible for strain rate-corrosion-corrosive wear relationship, follow-up studies would be worth conducting:

- Effect of the strain rate of prior deformation on corrosion and corrosive wear of stainless steel. As repassivation is involved during corrosive wear, the response of stainless steel would be quite different as compared to non-passive alloy such as the carbon steel. Such investigations will be beneficial to both fundamental understanding of corrosive impact wear and selection of candidate materials.
- Instantaneous studies on corrosive impact wear. In this study, the impact action or high strain rate deformation was applied before the materials are subject to corrosion and corrosive wear. However, in some real engineering practices, the materials are subject to simultaneously combined attacks of impact, corrosion, and wear. Instantaneous studies on the failure mechanism of such a wear mode would be also helpful to understanding corrosive wear meachanism.

Publications

S.B.Yin and D.Y.Li, Effects of prior cold work on corrosion and corrosive wear of copper in HNO_3 and NaCl solutions, Mater. Sci. Eng. A., 394 (2005) 266-276.

S.B.Yin and D.Y.Li, Corrosion and corrosive wear of annealed, impact-fractured and slow bending-fractured surface layers of AISI 1045 steel in a 3.5% NaCl solution, Wear, 259(2005) 383-390.

S.B.Yin, D.Y.Li, and R.Bouchard, Effects of strain rate of prior deformation on the corrosion and corrosive wear of AISI 1045 steel in a 3.5% NaCl solution, Metallurgical and Materials Transactions A, 38A(2007)1032-1040

S.B.Yin, D.Y.Li, and R.Bouchard, Effects of the strain rate of prior deformation on the wear-corrosion synergy of carbon steel, Wear, 263(2007) 801-807

Songbo Yin, D.Y.Li, A new phenomenon observed in determining the wear-corrosion synergy during a corrosive sliding wear test, Tribology Letters, 29 (2008) 45-52

References

1. M.M.Stack, Int. Mater. Rev., 50 (2005) 1.
2. W.J.Schumacher, Mater. Perform., 23 (1993) 50.
3. D.J. Dunn, in: K.C. Ludema(Eds.), Wear of materials, ASME, 1985.
4. A.M.F. Carter and D. Howarth, "A Literature Review of the Factors that Influence the Wear of Slurry-Handling Systems," Report M319, Council for Mineral Technology, Sept 1987.
5. Comminution and Energy Consumption, National Academy of Sciences, Washington, D.C., 1981, p 27.
6. F.D. DeVaney and M.H. Coghill, Eng. Min. J., 138 (1937) 337–340.
7. A.V. Levy and Y. Man, "Erosion-Corrosion Mechanisms and Rates in Fe-Cr Steels," Paper III, Corrosion 86 (Houston), National Association of Corrosion Engineers, 1986.
8. S. Agarwal and M.A.H. Howes, Erosion-Corrosion of Materials in High-Temperature Environments, Proceedings of AIME Conference on High Temperature Corrosion in Energy Systems (Detroit), American Institute of Mining, Metallurgical, and Petroleum Engineers, Sept 1984.
9. B.W. Madsen, Standard guide for determining amount of synergism between wear and corrosion. In: ASTM G119-93, 1994 Ann. Book ASTM Stand Vol. 03.02, ASTM, Philadelphia, PA (1994), pp. 507–512 Wear and Erosion, Metal Corrosion.

10. B.W. Madsen, Mater. Perform., 26 (1987) 21-27.
11. B.W. Madsen, Wear, 123(1988) 127-142.
12. C.H. Pitt and Y.M. Chang, Miner. Metall. Process., 120(1985)166-172.
13. Y.M. Chang and C.H. Pitt, Corrosion, 43 (1987) 599-605.
14. J. Postlethwaite, M.H. Dobbin, and K. Bergevin, Corrosion, 42 (1986) 514-521.
15. D.C. Kotlyar, C.H Pitt and M.E. Wadsworth, Corrosion, 44 (1988) 221–228.
16. R.L. Pozzo and I. Iwasaki, J. Electrochem. Soc., 136 (1989)1734-1739.
17. R.L. Pozzo, A.S. Malicsi, and I. Iwasaki, Miner. Metall. Process., 143(1990) 16-21.
18. X.Y.Wang, D.Y. Li, Tribology Lett, 11 (2001) 117.
19. X.Y.Wang, D.Y. Li, Wear, 259 (2005) 1490.
20. H.A.Kader and S.M.El-Raghy, Corrosion science, 26 (1986) 647.
21. D. Kotlyar and M.E. Wadsworth, "The Role of Localized Corrosion on Corrosive Abrasive Wear of High Carbon Low Alloy Steel Grinding Media," Paper 246, Corrosion 88 (Houston), National Association of Corrosion Engineers, 1988.
22. S.W. Watson, S.D. Cramer and B.W. Madsen, Corrosion and wear in white cast irons. In: Proc. 12th Int. Corros. Congr. 3A (1993), pp. 1353–1366.
23. S.W.Watson, B.W.Madsen, S.D. Cramer, Wear, 181-183 (1995) 469.
24. E. Wandke and M. Moser, Wear, 121(1988)15-26
25. ASM Handbook, Friction, Lubrication and Wear Technology, Vol. 18, ASM International, USA, 1992
26. J. B. Zu, I. M. Hutchings and G. T. Burstein: Wear, 1990, 140, 333

27. Y. Li, G. T. Burstein and I. M. Hutchings: Wear, 1995, 186–187, 5151

28. M. M. Stack and N. Pungwiwat: Tribol. Int., 2002, 35, 651–660.

29. P. C. Pistorius and G. T. Burstein: Corros. Sci., 1992, 33, 1885.

30. G. T. Burstein and K. Sasaki: Corros. Sci., 2000, 42, 841–860.

31. A. Neville, T. Hodgekiess and H. Xu: Wear, 1999, 233–235, 523–534

32. T. Hodgekiess, A. Neville and S. Shreshta: Wear, 1999, 233–235,623–634.

33. S. Zhou, M. M. Stack and R. C. Newman: Corrosion, 1996, 52, 12, 934–946.

34. I. M. Hutchings, Tribology: friction and wear of engineering materials, 1992, Edward Arnold.

35. S. W. Watson, F. J. Friedersdorf, B. W. Madsen and S. D.Cramer, Wear, 181–183(1995) 476–484.

36. D. Landolt, S. Mischler and M. Stemp, Electrochim. Acta, 46(2001)3913–3929.

37. I. Garcia, D. Drees and J. P. Celis, Wear, 248(2001) 452–460.

38. S. Mischler and P. Ponthiaux, Wear, 248(2001)211–225.

39. S. Mischler, S. Debaud and D. Landolt, J. Electrochem. Soc., 145(1998)750–758.

40. S. Barril, S. Mischler and D. Landolt, Tribology International, 34(2001)599–608.

41. M. M. Stack and H. W. Wang, Wear, 233–235(1999)542–551.

42. M. Stemp, S. Mischler and D. Landolt, Corros. Sci., 45(2003) 625–640.

43. R.E.J. Noël and A. Ball, Wear, 87 (1983) 351–361.

44. A.W. Batchelor and G.W. Stachowiak, Wear, 123 (1988)281–291.

45. I. Iwasaki, J.J. Moore, and L.A. Lindeke, Miner. Metall. Process., 4(1987) 160–166

46. R. I. Trezona, D. N. Alsopp and I. M. Hutchings, Wear, 205(1999) 225-232.

47. K. Adachi and I. M. Hutchings, Wear, 255(2003)23–29.

48. M. M. Stack and M. Mathew, Wear, 255(2003)14–22.

49. A. Gant andM. G. Gee and A. T.May, Wear, 256(2004)954–962.

50. S. Barril, N. Debaud, S. Mischler and D. Landolt, Wear, 252(2002)744–754.

51. S. Barril, S. Mischler and D. Landolt, Wear, 256(2004) 963–972.

52. H. Chen, P. Q. Wu, L Quaeyhagens, K. W. Xu, L. M. Stals, J. W. He and J. P. Celis, Wear, 253(2002) 527–532.

53. A. Sakamoto, H. Funakai and M. Matsumura, Wear, 186(1995)542–547.

54. R. J. K. Wood, Mech. Eng. Sci, 204(1990) 63–65.

55. Z.Gahr, K.H., and Eldis, G.T., Abrasive wear of white cast irons, 1980, wear, Elsevier Sequois S.A., Lausanne, Switzerland.

56. D.J.Dunn, Measurements of Impact Forces In Ball Mills, Mining Engineering, April 1978.

57. T.E.Norman, Wear and energy distribution on grinding balls in ore grinding mills, Northwest Metals and Minerals Conference, Portland, Oregon, 1984

58. E. Rabinowicz, K. Hozaki, Impact wear of ductile metals, in: Proceedings of the JSLE International Tribology Conference, Vol. II, Japan, 1985, pp. 263–268.

59. P.A. Engel, Impact Wear of Materials, Elsevier, The Netherlands, 1978, pp 339

60. N.P.Suh, Wear, 44(1977)1-16.

61. S. Jahanmir and N. P. Suh, Wear, 44(1977)17-38

62. J.R. Fleming and N.P.Suh, Wear, 44(1977)39-56.

63. J.R. Fleming and N.P.Suh, Wear, 44(1977)57-64.

64. B.Zhang,Y.Liu, etal., Wear, 198(1996) 287-292.

65. B.Zhang, W.Shen, Y.Liu, J. Mater. Sci. Lett., 17(1998)765-767.

66. R. Bulpett, T.S. Eyre and B. Ralph, Wear, 162–164 (1993)720-728

67. K.M. Mashloosh and T.S. Eyre, Tribology Int. , 18 (1985) 259–266.

68. S.L. Rice, H. Nowotny and S.F. Wayne, Key Eng. Mater. , 33 (1989) 77–100.

69. A. Molinari, G. Straffelini and B. Tesi et al., Wear 208 (1997) 105–112.

70. R. Osterlund, O. Vingsbo and L. Vincent et al., Scand. J. Metall., 11 (1982) 23–32.

71. Y.Y.Yang, H.S.Fang, et.al., Wear, 185(1995)17-22.

72. E.M.Gutman, Mechanochemistry of Solid Surfaces, World Scientific Publ., New Jersey, Singapore, London (1994)

73. T.P.Hoar and J.C.Scully, J.Electrochem.Soc., 111 (1964) 348

74. Gutman-EM; Solovioff-G; Eliezer-D, Corrosion Science, 38(1996)1141-1145.

75. V.A.C. Haanappel, M.F.Stroosnijder, Corrosion, 57(2001) 557-565.

76. M. Ocampo, Corrosion, 58 (2002) 601-607

77. A.O. Surendranathan, Trans. Indian Inst.Met. , 51(1998) 373-378.

78. R.B. Leggat, Corrosion, 55(1999)984-990.

79. M. Kh. Rabinovich, Materials Science Forum, 243-245(1997) 521-526.

80. T. M. Yue, Journal of Materials Science Letters, 21(2002)1069-1072

81. Z.Szklarska-Smialowska, Corrosion, 27(1971) 223-231.

82. P.Forchhammer, H.J.Engell, Werk, Korros. 20(1969)1-7.

83. A.Randak, F.W.Trautes, Werk, , Korros. 21(1970) 97-104.

84. S.Pednekar, S.Smialowska, Corrosion 36, 10 (1980)565-573.

85. A. Bose, P. K. De, Corrosion 43(1987)624-631.

86. C.L.Briant, A.M.Ritter, Corrosion 38(1982)596-603.

87. C. Garca, Corrosion Science, 43(2001)1519-1539.

88. J. H. Zheng, Corrosion, 49(1993)585-593.

89. R.F.Tinder, J.Appl.Phys., 39(1968)355-362.

90. B.Bhushan and A.V.Goldade, Appl. Surf. Sci., 157 (2000) 373-381.

91. A.L.Zharin and D.A.Rigney, Tribol. Lett., 4(1998)205

92. D. Y. Li, Phys. Stat. Sol. , 191 (2002) 427-430.

93. W. Li and D. Y. Li, Materials Science and Technology, 18(2002)1057-1062.

94. X. C. Lu, Wear, Vol. 225 No.1 1999, p 537-543, Proceedings of the 1999 12th International Conference on Wear of Materials, WOM-99. Atlanta, GA, USA

95. H.Y.Bi, Mocaxue-Xuebao(Tribology), 18(1998)327-331.

96. In: T.Z. Blazynski, Editor, Materials at High Strain rates, Elsevier, New York (1987), p. 243.

97. M.A. Meyers, Dynamic Behaviour of Materials, Wiley, New York (1994).

98. G.R.Johnson, J.M.Hoegfeldt, U.S.Lindholm, and A.Nagy, ASME J. Eng. Mater. Tech., 105(1983)42-53.

99. L. W. Meyer, in Shock-Wave and High-Strain-Rate Phenomena in Materials, eds.

M.A.Meyers, L.E.Murr, and K.P. Staudhammer, Dekker, New York, 1992

100. R. W. Klopp, R.J.Clifton, and T.G. Shawki, Mech.Mater., 4 (1985)375-382.

101. J.D.Campbell, A.M. Eleiche, and M.C.C. Tsao, in Fundamental Aspects of Structural Alloy Design, Plenum, New York, 1977, p.545

102. J.J.Gilman and W.G.Johnston, Dislocation and Mechanical Properties of Crystals, Wiley, New York, 1957, p.116

103. J.J.Gilman and W.G.Johnston, J. Appl. Phys., 33(1959)129-136.

104. D.F. Stein and J.R.Low, Jr., J.Appl.Phys., 32(1960) 362-371.

105. H.Ney, R.Labusch, and P.Haasen, Acta Met., 25(1977)1257-1264.

106. W.S. Lee, H.F.Lam, J. Mater. Processing Tech., 57 (1996) 233-240.

107. K.P.Staudhammer and L.E.Murr, Mater. Sci. Eng., 44(1980) 97-113.

108. C.Y.Chiem and J.Duffy, Mater. Sci. Eng., 57(1983) 233-247.

109. I.D.Baikie and P.J. Estrup, Rev.Sci.Instrum. 69 (1998) 3902-3908.

110. N.W.Ashcroft and N.D.Mermin, Solid State Physics, 1976, New York, Holt, Rinehart, and Winston.

111. J.C.Scully, the Fundamentals of Corrosion, Pergamon Press, 3rd Edition, Oxford, 1990.

112. R.Winston Revie, Uhlig's corrosion handbook, 2nd Edition, electrochemical society series, John Wiley & Sons, Inc. 2000.

113. Copper and copper alloys, ASM specialty handbook.

114. M. Pourbaix, Atlas of Electrochemical Equilibia in Aqueous solution, Pergamon

press, GB, 1996.

115. Y.L. Huang, X.X. Jiang, S.Z. Li, Bull.Mater.Sci., 23 (2000) 539-547.

116. B.A. Kolachev, Hydrogen Embrittlement of Nonferrous Metals, Israel Program for Scientific Translations Ltd., Jerusalem, 1968.

117. H.P.Klug and L.E.Alexander, X-Ray Diffraction Procedures For Polycrystalline and Amorphous Materials, John Wiley & Sons, New York, Second Edition, 1974.

118. S.Xu, G.Shen, R.Bouchard and W.R.Tyson, Effect of excess energy during impact on Charpy absorbed energy, Materials Technology Laboratory Report MTL 2002-6(TR)

119. Standard test methods for notched bar impact testing of metallic materialsd, ASTM E23-02, 2004, Annual Book ASTM Standard, Vol.03.02, Wear and Erosion, Metal Corrosion, ASTM, Philadelphia, PA, 2004, pp.144-169.

120. R.W.Hertzberg, Deformation and Fracture Mechanics of Engineering Materials, 3rd ed., Wiley, 1994.

121. S.B.Yin and D.Y. Li, Mater. Sci. Eng. A., 394 (2005) 266-276.

122. F.C. Frank, Proc. Phys. Soc., London, 1949, A62, pp.131.

123. J.D.Eshelby, Proc. Phys. Soc., London, 1949, A62, pp.307.

124. G.Leibfried and H.D.Dietz, Z.Physik, 126(1949)790-798.

125. S.B.Yin, D.Y.Li, Wear, 259(2005)383-390.

126. W.Li, D.Y.Li, J. of Chemical Physics, 6(2005)122-134.

127. W. Li and D. Y. Li, Appl. Surf. Sci., 240(2005)388-392.

128. H.H.Uhlig: Physical Metallurgy of Stress Corrosion Fracture, T.N.Rhodin, Ed., Interscience Publishers, New York, 1959, pp.1.

129. H.L.Logan, J.Res.Natl.Bur.Stand., 48(1952)99-105.

130. E.N.Pugh, Corrosion, 41(1985)517-522.

131. J.J. Harwood, Stress Corrosion Cracking and Embrittlement, W.D.Robertson, Ed., John Wiley& Sons, New York, 1956, pp.1.

132. P.R.Swann and J.D.Embury: High Strength Materials, John Wiley & Sons, New York, 1965, pp.327.

133. S.Yin, D.Y.Li, and R.Bouchard, Metall. Mater. Trans. A, 38A(2007)1032-1040.

134. S. Akonko, D.Y. Li, M. Ziomek-Moroz, Tribology Letters, 18 (2005) 405-411.

135. D.A. Jones., Principles and Prevention of Corrosion. 2nd ed., Maxwell Macmillan International Pub. Group, New York, 1992.

136. Songbo Yin, D.Y. Li, A new phenomenon observed in determining the wear-corrosion synergy during a corrosive sliding wear test, Tribology Letters, 29 (2008) 45-52.